MOLECULAR DYNAMICS SIMULATIONS OF ELONGATED MOLECULES

A THESIS SUBMITTED TO THE UNIVERSITY OF MANCHESTER
FOR THE DEGREE OF DOCTOR OF PHILOSOPHY
IN THE FACULTY OF ENGINEERING AND PHYSICAL SCIENCES

2012

By
Robert John Sargant
School of Chemical Engineering and Analytical Science

Contents

Word count: 45240

List of Tables

List of Figures

The University of Manchester

Abstract of thesis submitted by **Robert John Sargant** for the degree of **Doctor of Philosophy** and entitled **Molecular Dynamics Simulations of Elongated Molecules** in the year **2012**.

The existence of a thermotropic biaxial nematic liquid crystal phase has been a topic of great interest for almost half a century. Of the various mesogenic shapes suggested as being able to form this phase, theory has suggested that the V-shaped or "bent-core" molecule is one of the most promising candidates. In this thesis we use a simple mesogenic model of a bent-core molecule, constructed from a number of repulsive Weeks-Chandler-Andersen potentials that are assembled into a rigid V shape. Using this model we explore the spontaneous phase behaviour that occurs in a wide array of different systems of mesogens, using molecular dynamics simulations and isotropic initial conditions.

We study the relationship between molecular bend angle and phase behavior for molecules constructed from 11 potentials. We find that the phase behaviour splits into two regions, above and below a critical bend angle. Molecules wider than this angle exhibit isotropic, uniaxial nematic and smectic A phases. Narrower molecules show no uniaxially aligned phases, and instead have a clustered phase with short-range ordering and no global alignment director. Increasing system size improves the smectic layering in the wider molecules, but does not affect the global alignment of the narrower molecules.

Our model is extended to include the effect of the arm length of the molecule by changing the number of potentials from which the mesogens are constructed. As the molecule is reduced in size, the critical bend angle is seen to move slowly towards more linear molecules, reducing the size of the parameter space in which uniaxial nematic alignment is possible. At 5 beads, all mesophases are seen to disappear and systems remain isotropic.

We also study the behaviour of binary mixtures of bent-core molecules, both of differing arm lengths and of differing bend angles. For arm length mixtures, molecules are seen to remain mixed in the isotropic and nematic phases, and phase separate on transition to a smectic phase. In addition, uniaxial nematic phases are induced in systems that have no nematic phase of their own in isolation. For mixtures of different bend angles, systems remain fully mixed in the smectic phases for differences of up to 10°, and beyond this the two components begin to separate at the nematic–smectic transition.

Declaration

No portion of the work referred to in this thesis has been submitted in support of an application for another degree or qualification of this or any other university or other institute of learning.

Copyright

Acknowledgements

Firstly, thanks must go to my supervisor Professor Andrew Masters, whose sustained support and guidance made this thesis possible. I'd also like to thank Professor Mark Wilson, whose insight and ideas were instrumental in getting this project going.

In a roughly chronological order, thank you to Ben, Tom, James, Hugh, Annalaura, Adam, Laura, Linda and all the other residents of C19 and The Mill, past and present, for the helpful discussions, good times and endless mugs of Earl Grey over the years. Special thanks to Alex, my friend and life coach, for his proofreading talents as well as the ongoing motivation and faith.

Finally, the biggest thanks go to my brother and my mum, who have simply always been there for me, through thick and thin, with aid, food and love. Thank you.

Chapter 1

Introduction

Classically, there are just three phases of matter. These phases can be easily described by imagining a simple system of spherical, interacting particles. With enough energy these particles form a gas, moving freely and filling whatever vessel they are contained in. If they are compressed or cooled sufficiently they condense and form a liquid, still free to move around, but now with a fixed volume. If they are cooled further, the free movement of the particles ceases, they solidify and are reduced to vibrating around fixed positions relative to one another. The positions of these molecules can often create long-range ordered structures, forming crystals.

This is the very simple model of matter which most people recognise. Of course, these three phases encompass the states in which the vast majority of matter around us exists. However, there are numerous other phases of matter that can only be described by adding complexity to the model. For example, plasmas and Bose-Einstein condensates can exist at the extremes of the energy spectrum, but require specific knowledge of the subatomic structure of the atom.

If the particles in this simple model are sufficiently distorted from a spherical shape, through being elongated, flattened, or having non-spherical interactions with other particles, then additional phases can exist between the liquid and solid phases. These "intermediate phases", or *mesophases*, occur when the particles in a system align and share a common orientation, similar to a crystal, but retain the ability to move translationally like a liquid. It is from these two characteristics that these mesophases are termed *liquid crystals*.

The initial discovery of liquid crystals was made in the late 19th century by Friedrich Reinitzer while experimenting with cholesteryl benzoate [1]. While melting and freezing these materials, he noted the presence of two different liquid-like phases, one clear and one cloudy, with a distinct phase transition between the two. Under microscopic inspection, it was revealed that this cloudy phase had a crystal-like structure, and that the material also had the ability to interact in unusual ways with polarized light [2]. However, it was the work by Georges Friedel in 1922 that categorized different liquid crystal behaviours into specific classes, and gave credence to the idea that these mesophases were new, distinct phases of matter [3].

1.1 Liquid crystals

There are many different liquid crystal phases, each with their own distinct properties and characteristics. We can explain the major phase categories using a system of rod-like (calamitic) molecules, a simple representation of a liquid crystal mesogen, that is, the solid core of a liquid crystal molecule which gives it its geometric structure. The elongated axis of a calamitic mesogen gives the molecules an orientation vector, along which they will preferentially want to align.

Some of the liquid crystal phases that can be achieved are illustrated in Fig. 1.1. The simplest phase is the isotropic (**I**) state (Fig. 1.1a), in which both the positions and orientations of these molecules are distributed randomly. This is identical to the liquid phase of matter. If, on cooling or compression, the average of the molecular orientation vectors becomes non-isotropic while the molecular motion remains fluid, we have a liquid crystal phase. We can define the net orientation of these vectors as the global system director $\hat{\mathbf{n}}$ and assign a liquid phase according to the following classifications [4]:

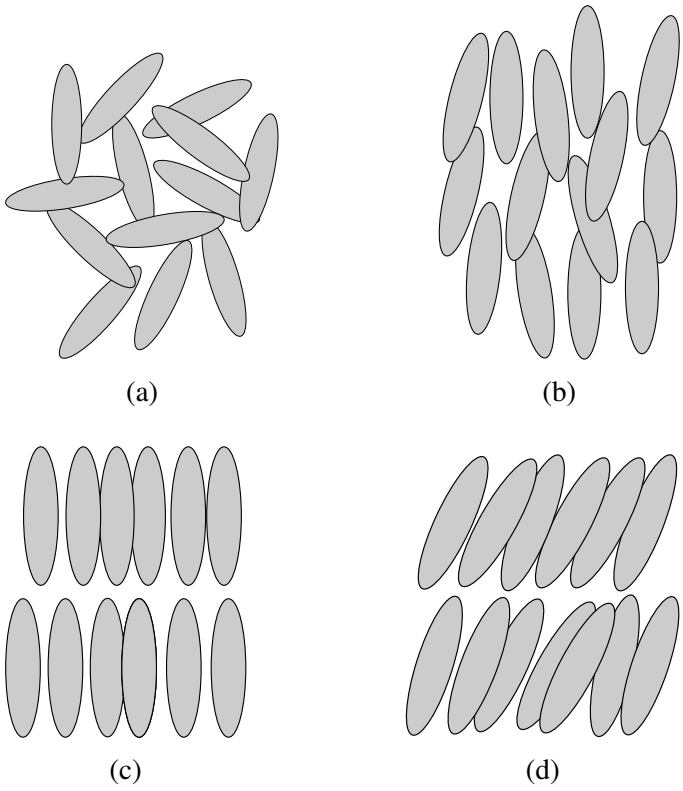

Figure 1.1: Examples of some of the liquid crystal phases achieveable with rod-like molecules. Examples shown include (a) isotropic, with neither orientational nor positional ordering; (b) nematic, with orientational alignment but no positional alignment; (c) smectic A, where the molecules have positional ordering in one dimension; and (d) smectic C, where the orientation director is tilted with respect to the smectic layers.

- If the mesogens have a net alignment along $\widehat{\mathbf{n}}$ but lack any kind of translational ordering, the system is in a *nematic* ($\mathbf{N}$) phase (Fig. 1.1b). The nematic phases can be sub-categorized depending on the geometry of the molecules. These include rod-like nematics, with elongated or calamitic mesogens such as prolate spheroids or spherocylinders; discotic nematics, with "flattened" mesogens such as discs or oblate spheroids; chiral nematics (cholosterics); and biaxial nematics, which will be discussed in more depth later.

- The *smectic* ($\mathbf{Sm}$) phases are characterised by orientationally aligned mesogens, regular translational ordering in one dimension, but a random positional distribution in the other two dimensions. This gives the appearance of repeating, fluid-like layers. There are a number of different types of smectic phases, with the two most common being the smectic A ($\mathbf{SmA}$, Fig. 1.1c) and smectic C ($\mathbf{SmC}$, Fig. 1.1d). In the smectic A phase the director $\widehat{\mathbf{n}}$ is perpendicular to the layers of molecules, while the smectic C phase has a director which is tilted with respect to the layers. Other smectic phases include the smectic B, where the in-layer distribution has a degree of hexagonal packing; and the chiral smectic C ($\mathbf{SmC}^*$), where the director $\widehat{\mathbf{n}}$ is not identical between layers but instead precesses around the layer normal.

- There are many more liquid crystal phases that exist outside of these two primary categories, and are achieveable with different mesogenic shapes. For example, more oblate shapes (such as cut spheres) can form both columnar and cubatic phases [5], both of which are distinct from these groupings.

A change in phase behaviour is generally induced by changing the temperature, pressure or otherwise exerting external forces on a molecular system. The ability to induce

liquid crystal phase behaviour by freezing or melting leads to these phases being classified as *thermotropic* liquid crystals. There is also another family of liquid crystals, termed *lyotropics*, which undergo phase changes based on molecular concentration. These are typically comprised of amphiphilic molecules, consisting of both hydrophilic and hydrophobic components, and are mixed with a solvent such as water. These systems are important in detergents and biological processes, and act as surfactants [6]. The molecules self-assemble in order to shield their hydrophobic components from the solvent, forming micellar phases at low concentrations. As the concentration of these molecules is increased, they can transition to columnar and lamellar layer phases [7].

Today, the most widespread implementation of thermotropic liquid crystals today is in liquid crystal displays (LCDs). These have been primarily based around the *twisted nematic* cell, which takes advantage of the light transmission properties of nematic liquid crystals. An illustration of such a twisted nematic cell is shown in Fig. 1.2.

A nematic liquid crystal is sandwiched between two electrodes, each treated so as to encourage the mesogens to line up with the surfaces in a desired direction. The two surfaces have their preferred directions set perpendicular to each other, which makes the mesogens gradually go through a 90° rotation across the width of the cell. In the "off" state, light passes through a plane polarizer, it is rotated by the twisted nematic, and passes through a second crossed polarizer without effect. In the "on" state, an electric field is applied across the cell, inducing a polarization in the molecules. The director of the nematic phase then aligns along the electric field, rather than to the cell walls. Now that the molecules are parallel to the direction of light transmission, they do not rotate the light as it passes through the cell and the light is extinguished by the second polarizing filter [8].

The types of liquid crystals used in these displays are termed *uniaxial nematics*, as

there is only one axis along which light can be transmitted without a change in its polarization. Typical rod-like molecules which have the necessary shape and polarizability for use in twisted nematic devices include 4-cyano-4'-pentylbiphenyl (5CB, shown in Fig. 1.3) and para-azoxyanisole (PAA) [4, 9].

The nematic phase behaviour exhibited by rod-like mesogens is one of the simplest to manipulate, and it is the most widely-used liquid crystal phase in display technology today. However, more complex mesogenic shapes can give rise to new liquid crystal phases, with unique optical properties, and could form the basis for novel technologies.

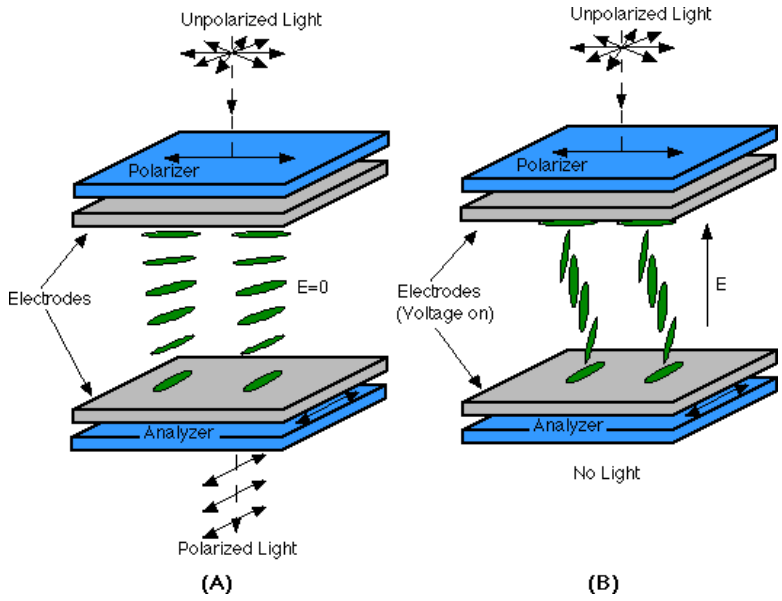

Figure 1.2: A twisted nematic liquid crystal cell, showing the "off" state (A) which allows light transmission; and the "on" state (B), which appears dark. The mesogens, shown in green, reorientates themselves to align along the electric field when it is present. Reproduced from Ref. [10].

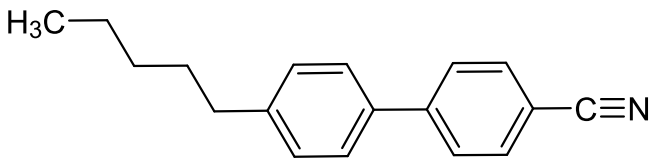

Figure 1.3: 4-cyano-4'-pentylbiphenyl, or 5CB, a commonly used liquid crystal in twisted nematic displays.

1.2 Biaxial nematics

The rod-like molecule used to explain some of the fundamental liquid crystal phases in the previous section has infinite rotational symmetry around its single axis of alignment. Work by Marvin Freiser in 1970 predicted that if a mesogen had less rotational symmetry and instead had a second orthogonal alignment director, a new liquid crystal phase could occur if both directors aligned simultaneously while retaining random positional ordering [11]. This phase was dubbed the *biaxial nematic* phase ($\mathbf{N_B}$), as there would be three separate orthogonal alignment axes, allowing light to pass freely in two directions without affecting its polarization.

An example of a biaxial mesogen is a molecule with a board-like shape, as it has both a "long" and "short" axis along which alignment is possible. A theoretical biaxial nematic phase made from board-like molecules is shown in Fig. 1.4.

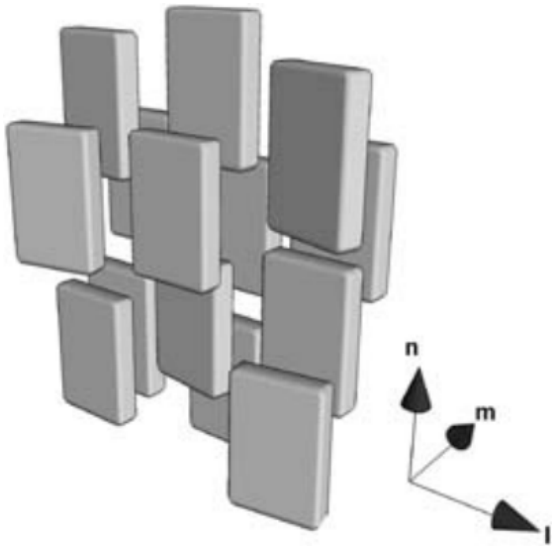

Figure 1.4: A biaxial nematic phase constructed from board-like mesogens, with $\mathbf{l}$, $\mathbf{m}$ and $\mathbf{n}$ indicating the three orthogonal axes of alignment. Reproduced from Ref. [12].

This prediction of the biaxial nematic phase has attracted a lot of research attention over the years [13]. Its special symmetries and multiple alignment axes raise the possibility of novel optoelectronic devices that could make use of these features. One specific proposal is the development of a faster alternative to the twisted nematic cell. In a basic twisted nematic, the realignment of the nematic phase involves rotating the long axis of the mesogens through 90° in order to switch between the "light" and "dark" states. If a nematic could undergo a phase transition between uniaxial and biaxial phases by changing the alignment of just the short axes of the molecules (l in Fig. 1.4), then a reduced level of molecular movement could theoretically lead to much faster display response times [14].

Within ten years of the initial theoretical prediction, Yu and Saupe made the first experimental observation of a biaxial nematic phase in a lyotropic liquid crystal. At a very narrow temperature and concentration window, they were able to create micelles that were board-like in shape [15]. However, the ultimate goal of a thermotropic biaxial nematic liquid crystal phase has presented a somewhat more difficult challenge. In the late 1980s to early 1990s, a number of publications claimed to have discovered thermotropic biaxial nematics using a variety of molecules with board-like shapes [16, 17, 18]. However, macroscopic quantities of bulk nematic liquid crystals rarely have a single system director. Instead they split into large "domains", which interfere with optical analysis techniques and made it difficult to prove that the claimed biaxial nematic phases were real. It was not until the development of non-optical techniques that the presence of a biaxial phase could be reliably examined in bulk samples [19], and it was eventually shown that the claimed phases were instead uniaxial nematics [20, 21, 22].

More recently, V-shaped or "bent-core" mesogens have been suggested as a superior

candidate for the formation of a biaxial nematic phase [23]. As with the the board-like molecules, these mesogens are inherently biaxial with a distinct pair of orthogonal long and short axes. They can be constructed by linking together two rod-like mesogens via a central component which defines a bend angle. An example of such a molecule that has been examined experimentally is shown in Fig. 1.5. The degree of biaxiality of the molecule, i.e. the relative length of the long axis compared to the short axis, is governed by the bend angle of the molecule. The example in Fig. 1.5 has a bend angle of $\sim 140^{\circ}$ between the two arms.

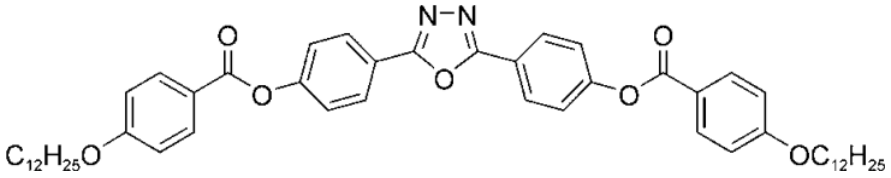

Figure 1.5: An example of the chemical structure of a bent-core mesogenic molecule [24].

Bent-core molecules had long been believed to be a poor choice of liquid crystal mesogen. It was assumed that if the molecules were allowed to rotate freely around their long axis, then the large excluded volume would mean that densities would be too low for reasonable liquid crystal behaviour [25]. The first bent-core mesogens were not synthesized until the early 1990s by Matsunaga and coworkers [26, 27]. In 1996, a bent-core molecule synthesized by Niori *et al.* was shown to have thermotropic phase behaviour [28]. The publication of these findings kick-started a huge surge of research interest into bent-core based liquid crystal phases, and the possibility of their use in liquid crystal devices [29, 30, 31]. In particular, experimental analysis indicated the possibility of an inducable polarity across the short axis of the molecules, suggesting the possibility of phase alignment through the use of external electrical fields [32], similar to how twisted nematic cells are controlled (see Fig. 1.2).

The synthesis and experimental testing of a single bent-core mesogenic compound for the presence of a biaxial nematic phase is a difficult and time-consuming procedure. The systematic testing of a wide range of molecular geometries within a reasonable period of time is virtually impossible. It is therefore important for the synthesis of suitable mesogens to be guided by theoretical predictions, in order to determine which molecular geometries offer the best chance of forming a biaxial nematic phase.

1.3 Molecular simulation

Molecular simulation has proven itself to be an invaluable tool for liquid crystals research over the last fifty years. By directly modelling the interactions of mesogenic shapes, theoretical phase behaviour predictions can be directly tested without the need to synthesize complex molecules. It is especially useful when the techniques for creating specific shapes have not yet been developed. A huge strength of simulation is that the molecular arrangement and statistical properties of a system can be directly inspected, and the phase behaviour can be examined without the need to rely on the sometimes indirect observations that are necessary with experimental systems. Results from simulations can be fed back into theory to validate or improve their predictions and provide a more robust insight into which properties are important in achieving desired liquid crystal phase behaviours.

As liquid crystal phase behaviour is reliant on the collective motion and alignment of many mesogens, relatively large quantities of molecules must be simulated for meaningful results. Full atomistic simulation of sufficient quantities of molecules is therefore impossible without vast quantities of computational power. By simplifying

the molecules down to the interactions between their mesogenic cores, we can obtain a strong understanding of which properties are most important to the fundamental physics of these systems, while remaining simple enough to calculate in a reasonable time.

1.4 Thesis outline

In this thesis we aim to extensively explore the available parameter space of bent-core mesogens using molecular dynamics simulations of a highly simplified molecular model. The goal of this work is to provide insight into which structural properties are important to the phase behaviour of bent-core systems, particularly with the goal of achieving a biaxial nematic phase.

In Chapter 2, we detail the molecular simulation concepts used for the simulation of liquid crystals in this thesis, as well as the main analysis methods used for determing the phase behavior that occurs. In Chapter 3 we investigate how the liquid crystal phase behaviour of bent-core mesogens is related to the bend angle between the two arms of the molecules. Chapter 4 focuses on how the length of the mesogenic arms is influential in the liquid crystal phase behaviour of these systems. The phase behaviour of binary mixtures of mesogens is studied in Chapter 5, in order to determine their ability to alter the monocomponent phase behaviour and potentially form new phases. Chapter 6 then concludes this thesis with a discussion and summary of the results, and possible avenues for further research.

Chapter 2

Molecular simulation of liquid crystals

When computing resources first became available to the public, one of their earliest applications was in the simulation of complex multi-body dynamical systems. It was in 1953 that Metropolis *et al.* published the first ever computer study of a liquid of hard discs in two dimensions [33], and this was rapidly followed by the first study of a three dimensional liquid [34]. These papers established the basis of the Monte Carlo method (MC) for studying the behaviour of multi-body systems. Within a few years, Alder and Wainwright had published the first results of computer simulations that modelled the interactions between hard spheres using classical mechanics [35] – the first implementation of a molecular dynamics (MD) simulation.

These breakthrough works were essentially proof-of-concepts, and were verified by calculating the equations of state and comparing them to values obtained through other theoretical techniques. The first actual novel discovery made using molecular simulation was presented in a pair of papers by Alder and Wainright [36] and Wood and Jacobson [37]. They suggested that a system of spheres with purely repulsive interactions and no attractive forces could undergo a phase transition from a liquid into an

ordered crystal. This was one of the first "experimental" results that supported the idea that the repulsive interactions between molecules are the most important property that defines the behaviour of simple liquids [38].

The last fifty years have seen these two simulation methods of MC and MD substantially developed, refined and improved, but their fundamental methods remain absolutely central to molecular simulation today. In this chapter we will outline the methods involved in MC and MD simulation, and their application in the simulation of liquid crystal mesogens. We will also detail some of the methods used for analysing the data generated by our simulations.

2.1 Monte Carlo simulations

In statistical mechanics, a thermodynamic ensemble is defined through a choice of values for three macroscopic system properties – a value for internal system energy or temperature (E or T); a value for the pressure or volume of the system (P or V); and the number of molecules or chemical potential (N or μ). The type of ensemble is often abbreviated as the combination of these three letters – for example, a constant-volume, constant-energy system can be referred to as an NVE ensemble, while an isobaric-isothermal system is an NPT ensemble.

On the microscopic level, the instantaneous configuration (microstate) of a system comprised of N rigid, aspherical molecules can be fully described by the complete set of position vectors $\mathbf{r}_N = r_i \dots r_N$ and orientation vectors $\mathbf{u}_N = u_i \dots u_N$. For a specific choice of values for the macroscopic thermodynamic variables, there can be infinitely many microstates in which the molecular configuration matches these values.

An ensemble can be defined as a probability distribution for finding the system in any one of the possible microstates at a specific time.

Some thermodynamic properties of an ensemble can be calculated by measuring the value of the property in every microstate and then integrating across all possible microstates, weighting each microstate by its probability of occuring. The *ensemble average* of some property A in the NVT ensemble can be written as

$$\langle A \rangle = \int d\mathbf{r}_N \, d\mathbf{u}_N \, A(\mathbf{r}_N, \mathbf{u}_N) \, P(\mathbf{r}_N, \mathbf{u}_N), \tag{2.1}$$

where the probability of the configuration occuring, $P(\mathbf{r}_N, \mathbf{u}_N)$, is given by

$$P(\mathbf{r}_N, \mathbf{u}_N) = \frac{\exp(-\beta E(\mathbf{r}_N, \mathbf{u}_N))}{\int d\mathbf{r}_M \, d\mathbf{u}_M \, \exp(-\beta E(\mathbf{r}_M, \mathbf{u}_M))}, \tag{2.2}$$

where E is the total internal energy of the system, the numerator is the Boltzmann factor, and the denominator is the partition function of the complete ensemble [38].

In anything but the smallest of systems where N is very close to 1, the calculation of these integrals is impossible to achieve either analytically or numerically. The strategy behind Monte Carlo simulations is that the values of these integrals can be estimated through random sampling of a large number of microstates. In the most basic approach this can be done by generating a random set of positions and orientations $\mathbf{r}_N$ and $\mathbf{u}_N$ for a set of N molecules, measuring the value of the property A and its Boltzmann weight in that microstate, and repeating for a very large number of possible configurations.

Used naïvely, this strategy rapidly runs into trouble. The distribution of probable configurations in the large parameter space is very inhomogeneous. In a dense molecular system, the vast majority of randomly generated configurations will result in at least

two molecules overlapping. If a pair of molecules have a large repulsive force at short separations, then each overlapping pair adds a huge contribution to the internal energy of the system, and as a consequence the Boltzmann factor assigns the configuration a very low probability of occuring. The high probability configurations without overlapping molecules occupy a relatively tiny amount of the parameter space, such that random sampling will generate vastly more unimportant than important configurations by many orders of magnitude, wasting simulation time and failing to properly sample the parameter space corresponding to probable configurations.

2.1.1 Metropolis algorithm

The Metropolis algorithm avoids this pitfall by using a technique called importance sampling. Instead of generating configurations entirely at random and weighting them by their Boltzmann factor, the Metropolis method performs a series of random pertubations on an initially probable microstate. The Boltzmann factor is used to decide whether or not to accept the new configuration, and the measured values from all accepted microstates are averaged with equal weight.

The Metropolis method biases the simulation towards microstates that are more likely to occur by only introducing small pertubations from a known acceptable microstate. However, it is still important to ensure that the parameter space is sampled randomly. This is done by establishing a Markov chain: a sequence of configurations in which a newly perturbed configuration depends only on the configuration before it, and has no memory of the configurations that came before [39]. The steps of a Metropolis Monte Carlo algorithm that achieve this in an NVT ensemble of rigid, anisotropic particles are:

1. A molecule from the system is selected at random (if molecules are selected sequentially, then the steps are not independent of one another)

2. The molecule is perturbed in some way through a random translation or rotation

3. The change in internal energy of the entire system due to the pertubation is determined

4. The move is accepted or rejected based on the new microstate's probability, as given by its Boltzmann factor.

For rigid anisotropic molecules, the pertubations are typically a small randomly generated translation or rotation up to a maximum pertubation size. In more complex systems, the pertubations can be more varied – for example, a pertubation might consist of a bond rotation in a system of molecules with increased degrees of freedom, or a system in the NPT ensemble can modify the pressure by scaling the size of the simulation cell and the intermolecular separations by a random amount to simulate volume fluctuations. Regardless of which pertubation is undertaken, the initial choice of which parameter to modify is chosen at random so as not to break the Markov chain.

The Boltzmann factor is used in the decision of whether or not to accept the newly perturbed configuration. If the change in energy from the current configuration c to the new configuration p is less than zero, then the total internal energy of the system has been reduced by making the pertubation and the move is automatically accepted. Otherwise, the move is accepted according to the probability

$$P(c \to p) = \exp(-\beta \Delta E). \tag{2.3}$$

In hard body systems where the energy barrier is infinite, ΔE is infinite when two

molecules overlap and the probability is zero. For soft potentials there is a finite probability that the system can exist in a higher energy configuration, allowing energy barriers to be overcome due to thermal fluctuations.

2.2 Molecular dynamics simulations

In contrast to the stochastic nature of Monte Carlo simulations which calculate system properties based on ensemble averages, molecular dynamics simulations are fully deterministic, and properties of systems are calculated using time averages. Molecular dynamics techniques aim to solve the classical equations of motion for a system of N interacting bodies such that the individual trajectories of each body can be traced as a function of time.

In order to simulate the motion of a particle i within a system, we need to solve the second law of motion

$$\frac{d^2}{dt^2}\,\mathbf{r}_i(t) = \frac{d}{dt}\mathbf{v}_i(t) = \mathbf{a}_i(t) = \frac{\mathbf{F}_i(t)}{m_i}, \tag{2.4}$$

where $\mathbf{r}_i(t)$ is the position of particle i at time t, $\mathbf{v}_i(t)$ is its velocity, m_i is the mass of particle i and $\mathbf{F}_i$ is the force acting on particle i at time t. The force acting on a particle arises from its interactions with the potentials of every other particle in the system at that instant, that is

$$\mathbf{F}_i(t) = -\nabla \mathbf{U}_i(\mathbf{r}_1(t) \ldots \mathbf{r}_N(t)). \tag{2.5}$$

In dense systems where there are many particles with soft potentials interacting simultaneously, these equations of motion take the form of a complex multi-body interaction

and are impossible to solve analytically. In time-driven molecular dynamics, the equations of motion are solved using a *finite difference* method of numerical integration. In knowing the full set of positions of the particles at a time t, we attempt to resolve the positions of every particle at a later time $t + \delta t$, where δt is the timestep of the simulation. Once the full set of particle positions are known at the time $t + \delta t$, they are used as the new input and the system configuration at $t + 2\delta t$ can be computed. In this manner, the trajectory of an entire system over time can be found iteratively.

In time-driven molecular dynamics simulations, the timestep δt has a constant value for the duration of the simulation. Sensible selection of a value for δt is very important – a small value will increase the accuracy of the calculations, but will also increase the number of iterations required to move the system forwards through time, slowing the speed of the simulation. If the timestep is too large, the simulation loses accuracy – a large timestep can leave two potentials in a highly improbable configuration, or even miss interactions entirely. It is therefore better to be cautious where possible and use as small a timestep as is reasonable, while still being able to simulate sufficiently small motions and obtain good time averages for any measured properties.

2.2.1 Integration algorithms

There are a number of choices available for performing the numerical integration of the equations of motion. The most straightforward of these is the Verlet method [40], obtained by performing a Taylor expansion for the position of a particle $\mathbf{r}_i$ around t and $t + \delta t$, such that

$$\begin{aligned} \mathbf{r}_i(t + \delta t) &= \mathbf{r}_i + \mathbf{v}_i \delta t + \frac{1}{2}\mathbf{a}_i^2 \delta t^2 + \ldots, \\ \mathbf{r}_i(t - \delta t) &= \mathbf{r}_i - \mathbf{v}_i \delta t + \frac{1}{2}\mathbf{a}_i^2 \delta t^2 + \ldots. \end{aligned} \tag{2.6}$$

By adding together these two equations, we can eliminate the velocity and get

$$\mathbf{r}_i(t+\delta t) = 2\mathbf{r}_i - \mathbf{r}_i(t-\delta t) + \mathbf{a}_i^2\delta t^2 + \ldots, \tag{2.7}$$

which gives the new position of a particle at time $t+\delta t$ knowing only the current force on it, $\mathbf{F}_i(t)$, its current position $\mathbf{r}_i(t)$ and its prior position $\mathbf{r}_i(t-\delta t)$.

While straightforward, the standard Verlet algorithm has a couple of significant flaws. Firstly, the addition of a $\mathcal{O}(\delta t^2)$ term to an $\mathcal{O}(\delta t^0)$ term can lead to the summation of two numbers many orders of magnitude apart, which can give rise to significant problems with numerical accuracy as the simulation proceeds [41]. Secondly, velocities are not calculated explicitly and are instead obtained by taking the average velocity over neighbouring timesteps, i.e.

$$\mathbf{v}_i(t) = \frac{\mathbf{r}_i(t+\delta t) - \mathbf{r}_i(t-\delta t)}{2\delta t}. \tag{2.8}$$

As the velocities are not calculated directly from the forces and are instead averaged, they may not be well-behaved and system properties which depend on them (e.g. kinetic energy) can be inaccurate.

There are two main improvements to the Verlet algorithm. The first is Verlet leapfrog [42], where instead velocity is calculated at a half timestep $t+\frac{1}{2}\delta t$, given by

$$\mathbf{v}_i(t+\frac{1}{2}\delta t) = \mathbf{v}_i(t-\frac{1}{2}\delta t) + \mathbf{a}_i\delta t, \tag{2.9}$$

and then the positions of the particles are updated using these mid-timestep velocities, i.e.

$$\mathbf{r}_i(t+\delta t) = \mathbf{r}_i(t) + \mathbf{v}_i(t+\frac{1}{2}\delta t)\delta t. \tag{2.10}$$

This resolves the problems with adding together two values of different magnitudes, and the velocities are calculated directly from the interacting forces. However, the velocities are not known at the same time as the particle positions, and again an average of two timesteps must be taken to find their mid-point value.

The second algorithm, velocity Verlet, uses a two-step procedure to resolve this issue [43]. Firstly, the half-step velocity is obtained via

$$\mathbf{v}_i(t + \frac{1}{2}\delta t) = \mathbf{v}_i + \frac{1}{2}\ \delta t\ \mathbf{a}_i(t), \tag{2.11}$$

and the position at the full timestep is calculated via

$$\mathbf{r}_i(t + \delta t) = \mathbf{r}_i(t) + \mathbf{v}_i(t + \frac{1}{2}\delta t)\delta t. \tag{2.12}$$

As the positions of the particles at $t + \delta t$ are now known, so are the forces between them, and so the velocities can be brought up to date in the second step, using

$$\mathbf{v}_i(t + \delta t) = \mathbf{v}_i(t + \frac{1}{2}\delta t) + \frac{1}{2}\mathbf{a}_i(t + \delta t). \tag{2.13}$$

Although this method requires an additional step and a second set of redundant velocities need to be calculated, both velocities and positions at $t+\delta t$ are determined directly from the interacting forces. The two values are continuously tracked as adjustments to the positions and velocities from the previous steps.

The choice between Verlet leapfrog and velocity Verlet depends primarily on the computational cost of calculating the second set of velocities, versus the necessity to know precise values for the velocities of the particles. With molecules more complex than

simple spherical potentials in an NVE ensemble, the cost is multiplied with the effects of molecular rotation, barostats and thermostats.

2.2.2 Motion of non-spherical particles

The algorithms for the integration of the equations of motion given in the previous section can be used to obtain the linear positions and velocities of particles in a many-body system. However, liquid crystal mesogens gain their phase behaviour from being nonspherical, and thus the orientation and angular velocity of the molecules must also be considered.

The orientation of a rigid nonspherical body can be defined in a number of ways. One of these is through a set of Euler angles. These are the three angles that define a set of rotations from which an initially aligned molecule can be rotated into an arbitrary orientation. If we have a molecule with a set of orthogonal axes $\hat{\mathbf{x}}, \hat{\mathbf{y}}$ and $\hat{\mathbf{z}}$, we can define its orientation as a rotation around its own $\hat{\mathbf{z}}$ axis by an angle of ϕ, followed by a rotation of θ around its $\hat{\mathbf{x}}$ axis, then a third rotation of ψ around its new $\hat{\mathbf{z}}$ axis [44].

An alternative representation of rotation is through the use of quaternions, four dimensional unit vectors of the form $\mathbf{Q} = (q_0, q_1, q_2, q_3)$. These have the advantage in that there is no way a rotation can become "locked" unlike Euler angles, and the computation of rotation matrices are a lot more straightforward [45]. A quaternion can be

calculated from a set of Euler angles using the definitions

$$\begin{aligned} q_0 &= \cos\left(\frac{\theta}{2}\right)\cos\left(\frac{\phi+\psi}{2}\right), \\ q_1 &= \sin\left(\frac{\theta}{2}\right)\cos\left(\frac{\phi-\psi}{2}\right), \\ q_2 &= \sin\left(\frac{\theta}{2}\right)\sin\left(\frac{\phi-\psi}{2}\right), \\ q_3 &= \cos\left(\frac{\theta}{2}\right)\sin\left(\frac{\phi+\psi}{2}\right), \end{aligned} \tag{2.14}$$

and can be ensured they form a unit quaternion through the check that [45]

$$q_0^2 + q_1^2 + q_2^2 + q_3^2 = 1. \tag{2.15}$$

The motion of a fully rigid molecule can be described by calculating linear and rotational motion separately. The linear motion of its center of mass can be found through the use of one of the Verlet integration techniques detailed in the previous section, and its orientation and angular velocity can be derived in parallel using quaternions. A modification to the Verlet leapfrog algorithm can be used to model this [46], where the angular momentum of a molecule at half and whole timesteps can be calculated from

$$\mathbf{I}_i(t) = \mathbf{I}_i(t - \frac{1}{2}\delta t) + \frac{1}{2}\delta t \boldsymbol{\tau}_i(t) \tag{2.16}$$

and

$$\mathbf{I}_i(t + \frac{1}{2}\delta t) = \mathbf{I}_i(t - \frac{1}{2}\delta t) + \delta t \boldsymbol{\tau}_i(t) \tag{2.17}$$

where $\boldsymbol{\tau}_i(t)$ is the torque on the molecule at time t around its center of mass $\mathbf{r}_i(t)$. The current time derivative of the quaternion, $\dot{\mathbf{Q}}_i(t)$, can be calculated through a simple matrix multiplication of $\mathbf{Q}_i(t)$ and the angular velocity at t [45], and the quaternions

at the half-timestep found through

$$\mathbf{Q}_i(t + \frac{1}{2}\delta t) = \mathbf{Q}_i(t) + \frac{1}{2}\delta t\dot{\mathbf{Q}}_i(t). \tag{2.18}$$

By combining $\mathbf{I}_i(t + \frac{1}{2}\delta t)$ and $\mathbf{Q}_i(t + \frac{1}{2}\delta t)$, $\dot{\mathbf{Q}}$ can be found at the half timestep, and the final quaternion at the full timestep found through

$$\mathbf{Q}_i(t + \delta t) = \mathbf{Q}_i(t) + \delta t\dot{\mathbf{Q}}_i(t + \frac{1}{2}\delta t) \tag{2.19}$$

which is analogous to Eq. (2.10). A more complex implementation also exists for velocity Verlet integration [47].

For non-rigid molecules the procedure of updating positions is much more complex, due to the degrees of freedom in the flexing and stretching of molecular bonds. A common way to resolve this is to model the movement of every non-rigid component without bond constraints, and then reintroduce the bonds by iteratively applying small deviations to the components according to the restoring forces of the bonds. Two commonly used methods include the SHAKE algorithm [48] based on Verlet leapfrog, and the RATTLE algorithm [49] based on velocity Verlet. The presence of non-rigid bonds in a molecule can also add intramolecular motions which are faster than the motion of the center of mass motion of the molecule, e.g. bond oscillations. The selection of a timestep δt must be considered such that the effects of these extra degrees of freedom are not ignored, and to ensure that the system does not move into an unphysical configuration.

2.2.3 Ensembles

Using the method described in Sec. 2.1.1, Monte Carlo simulations are typically performed in the NVT ensemble. Molecule moves do not attempt to conserve the energy of the system, and instead act to bring the system into equilibrium with an external temperature. With the addition of box volume change moves, the NPT ensemble can also be simulated.

As molecular dynamics simulations are based on the classical equations of motion, energy is strictly conserved and simulations are performed in the NVE ensemble by default – in fact, testing for a drift in internal energy of the system is one way of detecting whether the simulations are accurate and the timestep is sufficiently small. To simulate systems in the NVT or NPT ensembles, a thermostat and barostat need to be implemented. These ensembles are required for our work as thermotropic liquid crystal phase transitions are only induced experimentally by a change in the pressure or temperature of the system.

2.2.3.1 Thermostats

The temperature of a molecular system is a property of the average kinetic energy of the constituent molecules, which in turn is related to the linear and angular velocities of the molecules. A thermostat can be implemented by directly altering the velocities of the molecules, such that their kinetic energy is brought in line with the distribution of energies expected at the desired temperature.

There are several different methods for scaling the linear velocities of the molecules

within a molecular dynamics simulation. Among these are the Berendsen [50], Gaussian [51] and Nosé-Hoover [52, 53] thermostats. The simplest of these to implement is the Berendsen, which is a simple scaling of the velocities of the molecules between each timestep, given by

$$\mathbf{v'}_i(t) = \mathcal{X}_B(t)\mathbf{v}_i(t), \tag{2.20}$$

where $\mathbf{v}'_i(t)$ is the new velocity of particle i after scaling, and $\mathcal{X}_B$ is a system-wide velocity rescaling factor. It is defined as

$$\mathcal{X}_B(t) = \left[1 + \frac{\delta t}{\tau}\left(\frac{T_{ext}}{T(t)} - 1\right)\right]^{1/2}, \tag{2.21}$$

where T_{ext} is the desired barostat temperature, $T(t)$ is the current instantaneous temperature of the system, and τ is a time constant that defines how quickly the thermostat reacts.

The scalings of the Berendsen thermostat are decoupled from the equations of motion and are conducted between timesteps. This is a rather crude way of adjusting the temperature, as energy is simply added or removed without a physical explanation. The Nosé-Hoover method instead modifies the equations of motion themselves to add a friction coefficient, as if the molecules are continuously interacting with a heat bath. The equations of motion under this thermostat are given by

$$\frac{d^2}{dt^2}\,\mathbf{r}_i(t) = \frac{d}{dt}\mathbf{v}_i(t) = \frac{\mathbf{F}_i(t)}{m_i} - \mathcal{X}(t), \tag{2.22}$$

where the friction coefficient $\mathcal{X}$ is given by the first order differential equation

$$\frac{d}{dt}\mathcal{X}(t) = \frac{1}{\tau^2}\left[\frac{T(t)}{T_{ext}} - 1\right]. \tag{2.23}$$

As the friction coefficient is a time-based derivative, its trajectory through the life of a simulation is also tracked using the same half-step method used to track velocity in Verlet leapfrog (Eq. 2.9) or velocity Verlet (Eq. 2.13).

2.2.3.2 Barostats

As with Monte Carlo simulations, the pressure of a system can be controlled by scaling the volume of the simulation cell and the distances between the molecules. There are barostat equivalents for both the Berendsen and Nosé-Hoover thermostats that follow the same concepts. The Berendsen barostat is implemented by scaling the volume of the simulation cell between timesteps by a factor

$$\eta_B(t) = 1 - \frac{\delta t}{\tau}(P_{ext} - P(t)), \tag{2.24}$$

where P_{ext} is the desired barostat pressure. The simulation cell vectors and distances between each molecule and the system center of mass are scaled in each dimension by $(\eta_B)^{1/3}$.

The equations of motion given by the Nosé-Hoover thermostat can modified to add a term that compresses or decompresses the system and scales particle positions continuously using a piston-like effect, as formulated by Melchonnia [54]. The modified

equations of motion to incoroporate both the thermostat and the barostat are given by

$$\begin{aligned}
\frac{d}{dt}\mathbf{r}_i(t) &= \mathbf{v}_i(t) + \eta(\mathbf{r}_i(t) - \mathbf{r}_{COM}), \\
\frac{d}{dt}\mathbf{v}_i(t) &= \frac{\mathbf{F}_i(t)}{m_i} - \mathbf{v}_i(t)\left[\eta(t) + \mathcal{X}(t)\right], \\
\frac{d}{dt}\mathcal{X}(t) &= \frac{1}{\tau_T^2}\left[\frac{T(t)}{T_{ext}} - 1\right], \\
\frac{d}{dt}\eta(t) &= \frac{P(t) - P_{ext}}{\rho N k_B T_{ext}\tau_P^2}, \\
\frac{d}{dt}V(t) &= 3\eta(t)V(t),
\end{aligned} \tag{2.25}$$

where $\mathbf{r}_{COM}$ is the center of mass of the entire system, η is the piston-like barostat friction and τ_P and τ_T are the response times of the barostat and thermostat respectively. A full implementation of the Nosé-Hoover barostat using the Verlet leapfrog and velocity Verlet integration techniques can be found in the `DL_POLY_2` user manual [55].

2.2.4 Event-driven molecular dynamics

In Monte Carlo simulations, it is possible to model "hard" potentials, e.g. a solid sphere potential of the form

$$U(r_{ij}) = \begin{cases} \infty & r_{ij} \leq \sigma, \\ 0 & r_{ij} > \sigma, \end{cases} \tag{2.26}$$

where σ is the radius of the sphere and r_{ij} is the separation between the two interacting spheres. This leads to acceptance probabilities of either 0 or 1 depending on whether two spheres are overlapping.

Due to the discrete changes in energy, these types of potentials cannot be simulated using normal molecular dynamics techniques. With a fixed time step, the simulation

will overshoot the step changes in the potential and, in the case of infinitely repulsive potentials such as the hard sphere case, enter impossible configurations. One solution to this is to use a variable-sized timestep which will fast-forward the system to the exact time of the next particle interaction. This technique is known as event-driven molecular dynamics.

In an event-driven simulation, the size of the next timestep is chosen by comparing the trajectories of every possible pairing of particles and calculating the time until their next collision, if at all. The smallest value of all these collision times system-wide is the time of the next event, and is used as the value of δt for the current molecular dynamics timestep. Every particle in the system is fast-forwarded to the new time, and the velocities of the two particles that have collided are updated using simple conservation of momentum laws. The process is then repeated to find the next pairing of particles which will collide, and so forth.

In order for the time to the next event to be calculated, all the equations of motion in the system must be able to be determined analytically, at least until the time of the next collision. Therefore there cannot be any continuously varying potentials in the system, and all motion is ballistic between collisions. This also means that no Verlet-style integration algorithms are required to evolve the system.

At low densities, or in systems where the check to see if two particles will collide is simple to compute, event-driven molecular dynamics can be very fast and systems in excess of 10^6 particles have been successfully simulated for long timespans with relatively little computational time [56]. However, at high densities the values of δt can become very small and the overall speed of the simulation can drop below that of using a soft-potential equivalent due to the extra step of comparing all future collision times. In addition, detecting the time of next collision of two non-spherical particles is

far more computationally expensive to calculate than the simple ballistic behaviour of spherical particles.

There are a number of techniques that can be used to reduce the number of collision time checks required and speed up event-driven molecular dynamics simulations. One of these is "neighbour lists", where the system is subdivided into small cells and only pairs of particles in the same or neighbouring cells are checked for their collision times [35]. Another is the use of asynchronous algorithms, where the trajectories of particles are only updated when they are in the vicinity of a colliding pair or are themselves tested for collision against another particle [57, 58]. Each particle keeps track of its own current time in the simulation, and their ballistic motion means that particles can be independently updated to the current "global" time as needed. Using these techniques, it is feasibly possible to simulate liquid crystal systems of mesogens with hard potentials using deterministic molecular dynamics methods [59].

2.3 Periodic boundary conditions

Regardless of which simulation techniques are used, current computational power typically restricts us to $\lesssim 10^6$ interacting potentials. If these potentials are within a simulation cell that has solid walls, a significant fraction of the interactions will be between the molecules and the edges of the cell. These boundary effects can strongly influence the behaviour of the system and provide simulation results that are not indicative of true behaviour in bulk systems.

These finite-size effects can be reduced through the use of periodic boundary conditions [60]. Under these conditions, the main simulation cell is assumed to be a small

portion of a much larger bulk material. Exact replicas of the main cell are placed on each of its edges, termed *image cells*. When a particle moves within the main cell, all of its replicas in the image cells move in an identical fashion. When a particle reaches the boundary of a cell, it "wraps around" the edges of the cell and reappears on the other side – effectively the same as the particle moving into an image cell, and a replica particle entering the main cell. A two dimensional illustration of this is shown in Fig. 2.1. As well as particle movement wrapping around the cell boundaries, the presence of image particles allows for two particles on opposite sides of the main cell to interact with each other via their image replicas.

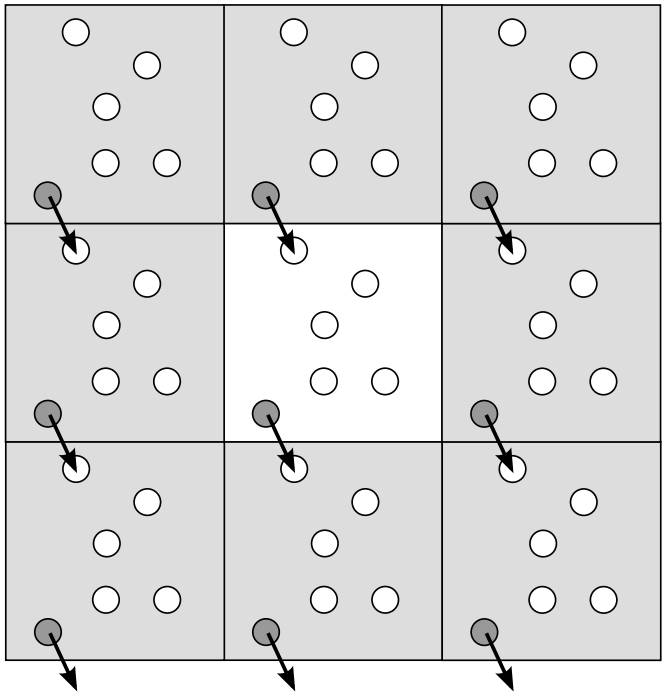

Figure 2.1: A two-dimensional example of periodic boundary conditions. The white cell is the real simulation cell, and the shaded cells are the image cells.

Using periodic boundary conditions can introduce new finite size effects which must be accounted for. If the range of a potential is greater than half the length of the shortest edge of the main cell, then a particle may interact with itself via its own image, and can introduce artificial periodicity to the system [61]. This is especially important to consider in liquid crystal simulations, as elongated mesogens can span a significant length of a simulation cell and self-interact if not simulated in large enough quantities, where the artificial periodicity can be mistaken for the formation of liquid crystal phases.

2.4 Choice of simulation technique

In this thesis, we will be using molecular dynamics simulation techniques exclusively. To date, Monte Carlo methods been widely used due to the relative simplcity in which they can be implemented, compared to the complexity of the full equations of motion of molecular dynamics techniques. However, the ongoing exponential growth in available computer power means that it is now feasible to perform molecular dynamics simulations on reasonably large sample sizes (tens of thousands of potentials) and obtain bulk properties of simulated systems in a reasonable amount of time.

As liquid crystal phases require the simulation of high density liquids, Monte Carlo techniques can sometimes suffer from a large number of rejected trial moves due to overlapping molecules. In addition, the collective motion of all molecules simultaneously in molecular dynamics can lead to faster and clearer system equilibration following a barostat or thermostat parameter change. These collective motions can be important in the formation of liquid crystal phases, which involve the mutual alignment of

large numbers of molecules simultaneously. Some properties of a system (e.g. compressibility) can also be more efficiently calculated using molecular dynamics [60], while some dynamical properties (e.g. transport coefficients) cannot be directly calculated at all using Monte Carlo techniques.

2.5 Results analysis

In order to analyse the phase behaviour that occurs within our simulations, it is necessary to determine both what the phases are and where the transitions occur. In this section we describe a number of tools used for identifying the properties of our results that are indicative of liquid crystal phases.

2.5.1 Equation of state

In all simulations, the equation of state of a simulation run was traced by plotting the pressure of the system against the number density of the molecules. In a single phase, the equation of state will describe a smooth curve of density increasing as pressure increases. At the mesophase transitions, the collective re-ordering of the molecules causes a discontinuity in the system density. In practice, this is observed as separate "branches" in the equation of state, with each branch corresponding to a separate phase [62]. The locations of these branches can accurately tell us the pressure windows for each mesophase, but very little about the actual molecular arrangement of the phase.

There are a number of theories which can successfully predict the equation of state for different molecular systems in the isotropic liquid phase. By selecting a suitable

theory, we can check that our simulations are representative of a true isotropic liquid before the simulation runs begin, and to identify the point at which the liquid phase ends and the mesophases begin. For ideal gases, the equation of state is given by

$$Z = \frac{\beta P}{\rho} = 1, \tag{2.27}$$

where ρ is the molecular density and Z is the compressibility of the gas. In the ideal gas limit, the molecules have no volume and the compressibility is invariant. For a system comprised of hard spheres, the compressibility can be accurately described by the Carnahan-Starling equation [63]

$$Z = \frac{1 + \eta + \eta^2 - \eta^3}{(1 - \eta)^3}, \tag{2.28}$$

where η, the packing fraction, is given by

$$\eta = \rho \frac{\pi \sigma^3}{6}, \tag{2.29}$$

where σ is the hard-sphere diameter. It has recently been shown that repulsive soft potentials that approximate hard sphere behaviour can have their compressibility expressed by a modified form of the Carnahan-Starling equation, given by

$$Z = \frac{1 + \eta + a\eta^2 - b\eta^3}{(1 - \eta)^3}, \tag{2.30}$$

where a and b are fitting parameters that can be determined empirically depending on the potential used [64].

If we have molecules which are composed of a number of soft potentials linked together, we can combine Eq. (2.30) with the SAFT theory of polymerization [65] and

Wertheim pertubation theory of polymerization [66] and derive an equation for the compressibility for these molecules. The full derivation is given in Appendix A, and the final-line equation is

$$\begin{aligned} Z =& 1 + m \left[\frac{4\eta + (a-3)\eta^2 + (1-b)\eta^3}{(1-\eta)^3} \right] \\ & - (m-1)\eta \left[\frac{a - 3 + 2\eta(1-b)}{4 + (a-3)\eta + (1-b)\eta^2} + \frac{3}{1-\eta} \right], \end{aligned} \tag{2.31}$$

where a and b are the same fitting parameters from Eq. (2.30), η is the same packing fraction as Eq. (2.29) and m is the average number of potentials per polymer.

In order to select appropriate fitting values for a and b, Eqn. (2.31) was tested against a number of datasets obtained from simulation results. This is detailed in the appendix section A.2. From these tests, we determined that the fitting parameters of $a = 1$ and $b = 1$ (equivalent to the hard-sphere Carnahan-Starling equation of state) were the most appropriate in describing the densities of our soft potential systems in the isotropic liquid phase.

2.5.2 Order parameters

As liquid crystal phases are characterised by the way in which mesogens are mutually aligned, quantifying this level of alignment is a useful tool for the identification of phases. Different order parameters can be used to quantify different kinds of mutual alignment, and together can be combined to identify specific types of phase behaviour. In our case, it is useful to define a pair of uniaxial nematic and biaxial nematic order parameters, which will indicate when molecules have aligned along a common primary and secondary axis respectively.

We define a set of three orthogonal axes $\hat{\mathbf{a}}$, $\hat{\mathbf{b}}$ and $\hat{\mathbf{c}}$ within the frame of reference of a single bent-core mesogen, and assume that these are the axes along which the mesogen will preferentially align. We can then define the uniaxial nematic order parameter Q_{00}^2 and biaxial nematic order parameter Q_{22}^2 using the equations

$$\begin{aligned} Q_{00}^2 &= \frac{1}{2}\left(3\cos^2\theta - 1\right), \\ Q_{22}^2 &= \frac{1}{2}(1+\cos^2\theta)\cos 2\phi\cos 2\psi - \cos\theta\sin 2\phi\sin 2\psi, \end{aligned} \tag{2.32}$$

where θ, ϕ and ψ are the Euler angles mentioned in Sec. 2.2.2. When a system is perfectly isotropic, $Q_{00}^2 = Q_{22}^2 = 0$. In a perfect uniaxial nematic phase $Q_{00}^2 = 1$ while $Q_{22}^2 = 0$, and in a perfect biaxial nematic phase $Q_{00}^2 = Q_{22}^2 = 1$ [67].

In the absence of an external field or force encouraging molecules to arrange in a specific direction, we do not know which set of laboratory axes the molecules will be aligning themselves to. Therefore, we need to use the directions of the molecules themselves to define our set of lab axes.

For each of the three orthogonal molecular unit axes, we define an order tensor given by

$$\mathbf{Q}_{\alpha\alpha} = \frac{1}{2N}\sum_{i=1}^{N}(3\alpha_i \otimes \alpha_i - \mathbf{I}) \tag{2.33}$$

where N is the number of molecules, $\mathbf{I}$ is the second-order, unit tensor and $\alpha \in \{\widehat{\mathbf{a}}, \widehat{\mathbf{b}}, \widehat{\mathbf{c}}\}$ for each molecule [45]. We then diagonalize each of these order tensors to obtain three sets of eigenvalues, which are sorted from largest to smallest and labelled λ_α^+, λ_α^0 and λ_α^-. Whichever of the three λ^+ eigenvalues is the largest indicates the molecular axis that is the most strongly aligned. Its corresponding eigenvector is taken as being our laboratory Z-axis, $\hat{\mathbf{z}}$. In turn, the eigenvector corresponding to the second largest value of λ^+ gives the laboratory Y-axis, $\hat{\mathbf{y}}$. The final corresponding

eigenvector defines our X-axis, $\hat{\mathbf{x}}$.

With these axes defined, the order parameters Q_{00}^2 and Q_{22}^2 can be redefined as

$$Q_{00}^2 = \hat{\mathbf{z}} \cdot \mathbf{Q}_{zz} \cdot \hat{\mathbf{z}}, \tag{2.34}$$

$$Q_{22}^2 = \frac{1}{3}\left(\hat{\mathbf{x}} \cdot \mathbf{Q}_{xx} \cdot \hat{\mathbf{x}} + \hat{\mathbf{y}} \cdot \mathbf{Q}_{yy} \cdot \hat{\mathbf{y}} - \hat{\mathbf{y}} \cdot \mathbf{Q}_{xx} \cdot \hat{\mathbf{y}} - \hat{\mathbf{x}} \cdot \mathbf{Q}_{yy} \cdot \hat{\mathbf{x}}\right), \tag{2.35}$$

which are equivalent to the definitions given in Eqn. (2.32).

2.5.3 Pair correlation function

The pair correlation function $g(r_{ij})$ can be used to detect regular structure and ordering within a liquid system, and is useful for detecting phases that are otherwise indistinct when using order parameters alone, e.g. smectic A and uniaxial nematic. It is defined as the distribution of all pairwise intermolecular distances in the system, normalized by the equivalent distribution of distances in an ideal gas. The pair correlation function can therefore be given by the equation

$$g(r) = \frac{V}{N^2}\left\langle \sum_{i}^{N} \sum_{i \neq j}^{N} \delta(\mathbf{r} - \mathbf{r}_{ij}) \right\rangle \tag{2.36}$$

where δ is the Dirac delta function [60]. The resulting distribution gives the probability that for a given molecule, another molecule will be a distance r away. If regular structure between molecular centers is present in the system (e.g. smectic phases), $g(r)$ will have peaks at repeating intervals.

2.5.4 Visual inspection

As mentioned in Chapter 1, one of the great strengths of molecular simulation is the ability to directly inspect the positions and orientations of molecules within a system. We can have a clearer understanding of the values obtained through pair correlation functions and order parameters if we know what kind of phase behaviour they correspond to. Therefore, it is very useful to obtain qualitative information about the current phase of a simulated system by visualizing it.

Throughout this thesis, we make extensive use of QMGA [68], a molecular visualization package designed specifically for rendering the configuration of molecular systems of arbitrary objects. One of the strengths of QMGA is that molecules can be coloured based on their alignment to a pre-speficied system director, on a spectrum from blue (for fully aligned) to red (for 90° out of phase). By combining the coordinate data of our systems with the global alignment director determined through the order parameter calculations in Sec. 2.5.2, we can visualize areas of common alignment within a system based on colour. We can also use QMGA to highlight specific parts of a molecule in order to inspect layered phases, such as smectics. By pairing these visualizations with quantitative data from other analysis techniques, we can categorize and identify phase behaviour more successfully.

2.6 Summary

In this chapter we have described the theory behind the two main methods used for simulating the phase behaviour of liquid crystal mesogens, and defined a number of

the tools we will be using to identify any phases which are formed during our simulations. As we will be using molecular dynamics simulations for the modelling of our mesogens, in the next chapter we will build a model of a bent-core molecule suitable for use with this simulation technique. We will then test the validity of our model against existing theoretical predictions and compare to Monte Carlo-based results, and analyse the effect of bend angle and system size on the overall phase behaviour.

Chapter 3

Phase behaviour of 11-bead bent-core molecules

In this chapter, we begin by creating a simple model of a bent-core mesogen. We conduct molecular dynamics simulations with this model in order to test its validity, and the suitability of our simulation methods are compared to existing theories. The spontaneous phase behaviour occuring in monocomponent systems of these mesogens is explored as they are compressed from an initially isotropic state, and the parameter space of bend angle and pressure is investigated with respect to the resulting liquid crystal phase behaviour.

3.1 Background

There have been two different important theoretical treatments used for predicting the phase behaviour of simple bent-core molecular systems. Teixeira *et al.* [69] used excluded volume calculations of hard spherocylinder dimers to derive a phase diagram of bend angle against density for bent-core molecules in the Onsager limit, where the ratio of molecular arm length L to arm diameter D is $L \gg D$. A reproduction of their phase diagram is shown in Fig. 3.1, which indicates four distinct regions. These consist of the isotropic phase, the uniaxial nematic phase for long molecules with a large internal bend angle, the discotic nematic phase for molecules with a much smaller bend angle, and the biaxial nematic, where both types of nematic alignment are present. Prior mean-field theory calculations by Luckhurst *et al.* on more general biaxial particles without cylindrical symmetry [70] have also been re-applied specifically to bent-core molecules, and a similar phase diagram derived [22]. Both works show a very narrow biaxial phase that exists between the two nematic phases, with all four phases meeting at a critical point located at $\theta \approx 110^\circ$. The span of internal bend angles that are accessible by the biaxial nematic phase in these diagrams is small, with a range of only $\sim 4^\circ$ between the two uniaxial phases.

Following these theoretical treatments in the ideal limit, a wide variety of molecular simulations have been used to identify the phase behaviour of models of bent-core mesogens with finite values of L/D. In addition, they have also explored the further phase behaviour at densities beyond the nematic phases. The earliest of these simulations was by Camp *et al.*, who modelled a bent-core molecule using two hard spherocylinders with $L/D = 2$, joined together at a fixed angle to form a dimer [67]. MC simulations from initial low-density disordered and high-density ordered configurations found isotropic, nematic, smectic and solid phases for internal bend angles

of $\theta = 180°$ (linear), $170°$ and $160°$, with the smectic phase disappearing at $150°$. At much narrower angles of $120°$ and $90°$ they found no evidence of spontaneous ordering from initially isotropic conditions.

Further work on hard spherocylinder dimers was performed by Lansac *et al.* [71]. From initally ordered high-density systems, MC simulations were used to map out the complete phase behaviour for dimers with $L/D = 5$ in the range $90° < \theta < 180°$. Their phase diagram is reproduced in Fig. 3.2. Away from the area of the phase diagram where $\theta > 165°$ and the biaxiality of the molecules is low, they found systems

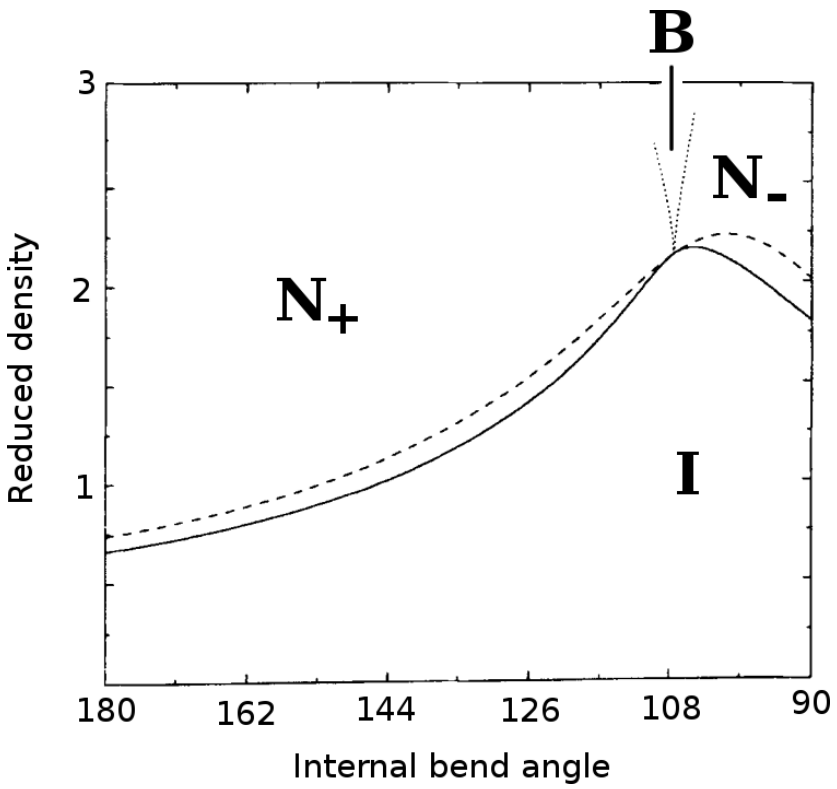

Figure 3.1: A reproduction of the phase diagram of reduced density against bend angle, calculated for bent-core molecules in the Onsager limit by Teixeira *et al* [69]. Labelled regions are, clockwise from top left, rod-like uniaxial nematic ($\mathbf{N}_+$), biaxial nematic ($\mathbf{B}$), plate-like uniaxial nematic ($\mathbf{N}_-$) and isotropic ($\mathbf{I}$). The vertical axis indicates the relative numerical density of the system.

exhibiting polar crystal, polar smectic A (whereby the short axes of the molecules are pointing in parallel similar to a biaxial nematic, but the molecules are still separated into smectic layers), uniaxial nematic and isotropic phase behaviour. In addition, they also saw the loss of the uniaxial nematic phase for bend angles of $\theta < 135°$.

Simulations utilizing soft potentials have also been performed, resulting in more exotic phase behaviour. Memmer used a bent-core model consisting of two Gay-Berne ellipsoids joined at a bend angle of $140°$, and used MC tecnhiques to cool an isotropic system with independently-varying simulation cell dimensions [72]. As well as uniaxial nematic and smectic A phases, large helical superstructures were seen. However, it was not seen in all instances and was described as potentially being an artefact of the

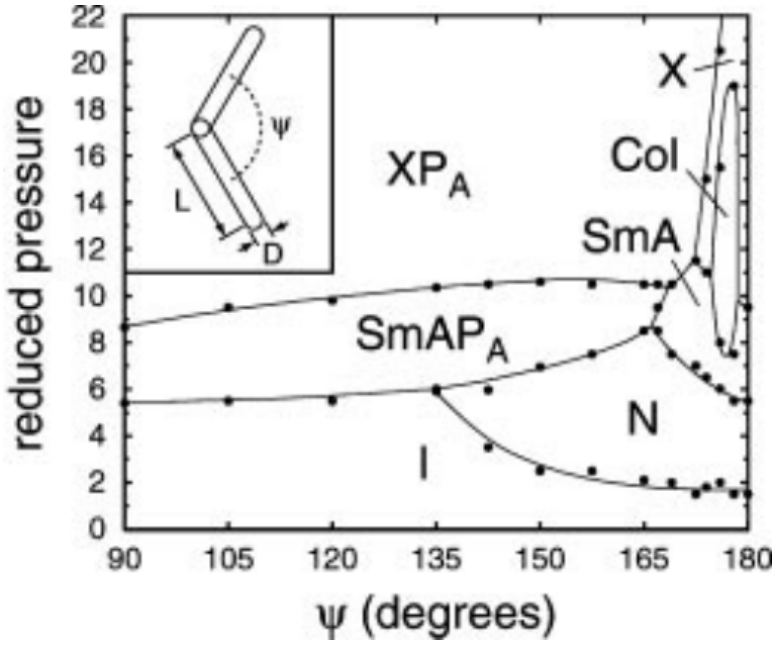

Figure 3.2: A reproduction of the phase diagram of reduced pressure against bend angle, calculated for bent-core molecules made from hard spherocylinder dimers with $L/D = 5$ by Lansac *et al* [71]. Their definition of reduced pressure is $P^* = \beta v_0 P$, where v_0 is the volume of the entire spherocylinder dimer. Labelled regions are isotropic (**I**), rod-like nematic (**N**), smectic A ($\mathbf{SmA}$), polar smectic A ($\mathbf{SmAP_A}$), columnar ($\mathbf{Col}$), crystal ($\mathbf{X}$) and polar crystal ($\mathbf{XP_A}$).

simulation technique. Similar work was conducted by Johnston *et al.* for Gay-Berne molecules with bend angles $180^\circ \leq \theta \leq 110$, in an elongated cuboidal cell with fixed box length ratios [73]. They too found a strong dependence of the phase behaviour on the bend angle, with tilted smectic B phases at around 160°.

More recently, Józefowicz and Longa have used a similar Gay-Berne-based molecule. In their model a harmonic bond was used to link the two arms, allowing a degree of molecular flexibility [74, 75]. Through MC simulations, they found that adding flexibility reduced the melting temperatures for the crystal phases. In further work [75] they propose the existence of a biaxial nematic phase for a molecule with a harmonic bend angle around $\theta \approx 140^\circ$, but this was only observed on cooling runs, with the phase being absent when melting ordered crystal phases.

There has also been work making use of molecules comprised of multiple soft potentials linked together rigidly. Paolini *et al.* were among the first to use such a model to simulate liquid crystal phases [76] by melting a crystal of molecules comprised of eleven repulsive spherical potentials, linked to form a rod. Dewar and Camp have used a similar model to perform MC simulations on the thawing of initially ordered systems of molecules comprised of seven spherical Lennard-Jones potentials [77]. For bend angles of $\theta = 160^\circ$ they found smectic B and uniaxial nematic liquid crystal phases, while at $\theta = 140^\circ$ the nematic phase is lost, resulting in tilted and untilted smectic phases.

Finally, Peláez and Wilson have performed the most detailed simulations to date [78], using fully atomistic molecular dynamics to model a real bent-core molecule which has been proposed to exhibit biaxial nematic behaviour experimentally [79, 24]. The existence of the biaxial nematic phase is reported, but with a low degree of biaxial system ordering.

3.2 Simulation method

With the exception of the recent work by Peláez and Wilson [78], almost all modelling of bent-core molecules has been performed using Monte Carlo techniques, often from an initially ordered crystal lattice. We will use molecular dynamics techniques with systems in isotropic initial conditions, in the hope of achieving previously reported phase behaviour directly and spontaneously. In this section we will outline the design of mesogenic model we chose, as well as the methods used for conducting the simulation runs.

3.2.1 Molecular model

Figure 3.3 is an illustration of the molecular model used within the simulations conducted in this chapter. The overall geometry of the molecule is defined by two intersecting vectors $\hat{\mathbf{e}}_1$ and $\hat{\mathbf{e}}_2$, delineating the arms of the molecule. The angle between

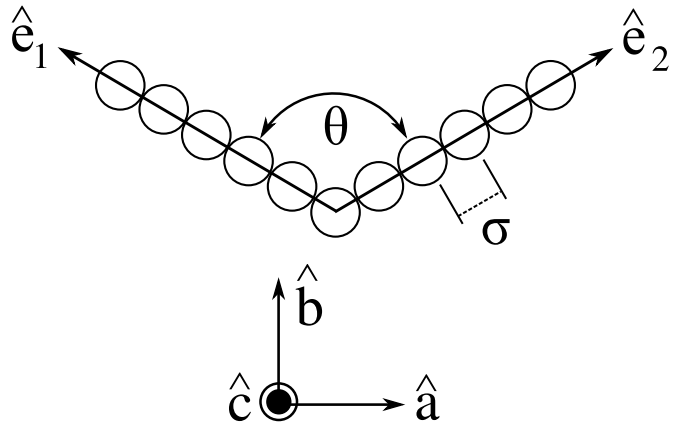

Figure 3.3: A representation of an 11-bead bent-core molecule and a set of orthogonal frame vectors. The centres of the spherical potentials along an arm vector are separated by a distance σ.

these two vectors is the internal bend angle θ. Spherical potentials are placed symmetrically along both arms, with a shared potential at the point of intersection between $\widehat{\mathbf{e}}_\mathbf{1}$ and $\widehat{\mathbf{e}}_\mathbf{2}$. Each of these "beads" is placed a distance σ from its neighbours. Each bead is fixed in place relative to the defining vectors, producing a fully rigid molecule with no bending or flexing in the arms, or any variation in the internal bend angle. It should be noted that the placement of a bead at the vector intersection means that the values of L/D for the spherocylinder dimers in other works [67, 71] are not exactly the same as $(n-1)/2$, where n is the number of beads, but that the equivalent L/D values for the molecules used here are slightly smaller.

We also define a set of orthogonal vectors, representing the molecular frame of reference along which liquid crystal alignment is most likely to manifest itself. These are given as

$$\begin{aligned} \widehat{\mathbf{a}} &= \frac{\widehat{\mathbf{e}}_\mathbf{1} - \widehat{\mathbf{e}}_\mathbf{2}}{|\widehat{\mathbf{e}}_\mathbf{1} - \widehat{\mathbf{e}}_\mathbf{2}|}\,, \\ \widehat{\mathbf{b}} &= \frac{\widehat{\mathbf{e}}_\mathbf{1} + \widehat{\mathbf{e}}_\mathbf{2}}{|\widehat{\mathbf{e}}_\mathbf{1} + \widehat{\mathbf{e}}_\mathbf{2}|}\,, \\ \widehat{\mathbf{c}} &= \widehat{\mathbf{a}} \times \widehat{\mathbf{b}}\,. \end{aligned} \tag{3.1}$$

For convenience, the vectors $\widehat{\mathbf{a}}$ and $\widehat{\mathbf{b}}$ will be referred to as the "long" axis and the "short" axis of the molecule respectively.

In order to simplify the model and examine the effects of shape and bend angle alone, we chose a purely repulsive isotropic potential to represent the sphere-sphere interaction between the beads of neighbouring molecules. We use the Weeks-Chandler-Andersen (WCA) potential [80], which is defined as

$$U(r_{ij}) = \begin{cases} 4\epsilon\left[(\frac{\sigma}{r_{ij}})^{12} - (\frac{\sigma}{r_{ij}})^{6}\right] + \epsilon & r_{ij} < 2^{1/6}\sigma \\ 0 & r_{ij} \geq 2^{1/6}\sigma \end{cases} \tag{3.2}$$

The upper part of Eqn. (3.2) is based on the Lennard-Jones potential, but with the addition of ϵ, which is equal to the attractive well depth in the regular Lennard-Jones interaction. This added term upshifts the entire potential such that there are no attractive interactions. As the minimum of the attractive well lies at $2^{1/6}\sigma$, the interaction is now exactly zero at this point. The lower part of the potential acts to truncate it at this minimum, removing all long-range interactions. The resulting WCA potential is a function which goes asymptotically towards $+\infty$ at $r_{ij} = 0$, smoothly decreasing non-asymptotically to zero at a finite separation of $r_{ij} = 2^{1/6}\sigma$.

The steepness of the WCA potential means it can be treated as a continuous potential analogue for hard spheres – the equation of state for the WCA monomer fluid can be expressed as a simple correction to the Carnahan-Starling expression for hard sphere fluids [64], where the effective hard-sphere diameter of the WCA potential can be expressed as

$$\sigma_{\text{eff}} = \frac{2^{1/6}}{(1+\sqrt{T*})^{1/6}}\,\sigma, \tag{3.3}$$

where T^* is the reduced temperature [81], defined in the next section in Eqn. (3.4). Therefore, when the temperature of the system is $T^* = 1$, the effective hard sphere diameter is the same as σ.

The finite cutoff is also beneficial to the speed of the molecular dynamics simulations, as the majority of potential pairings in a system have a separation of $r_{ij} \gg 2^{1/6}\sigma$ and the interaction strength does not need to be calculated. In systems with long-range interactions such as the Lennard-Jones potential, the long interaction tail is normally ignored beyond a certain cutoff in order to provide similar efficiencies [38].

3.2.2 Reduced units

The numerical values chosen for ϵ and σ in Eqn. (3.2) define the fundamental energy and length scales of the simulations. Therefore, any specific choice of values for temperatures, pressures and so forth in SI units is relatively arbitrary, as such values are entirely dependent on the values chosen for ϵ and σ [38]. Given the non-atomistic nature of the molecular model being used, it is convenient to use dimensionless quantities relative to these fundamental parameters for all values that would otherwise have units. This also allows for straightforward comparison of results with other works, regardless of what choices have been made for the actual simulation parameters implemented.

In this work, the basis for our reduced units was set by defining the fundamental energy and length scales of the interactions as $\epsilon = 1$ and $\sigma = 1$ respectively. In addition, a single bead is used as the fundamental unit of mass, $m = 1$. The conversions between SI units and reduced units for pressure P^*, temperature T^*, time t^* and number density ρ^* are therefore defined as

$$\begin{aligned} P^* &= P\,\frac{\sigma^3}{\epsilon}\,, \\ T^* &= T\,\frac{k_B}{\epsilon}\,, \\ t^* &= t\left(\sigma\sqrt{\frac{m^*}{\epsilon}}\right)^{-1}\,, \\ \rho^* &= \rho\,\sigma^3 \end{aligned} \tag{3.4}$$

respectively, where k_B is the Boltzmann constant.

3.2.3 Simulation procedure

All simulations in this chapter were implemented and conducted using DL_POLY_2 [82], a general multipurpose molecular dynamics simulation package using velocity Verlet integration algorithms. Starting configurations were generated within a cubic simulation cell with periodic boundary conditions. The required number of molecules were placed on the sites of a primitive cubic lattice, with lattice spacings chosen such that the number density of the system was $\rho^* \approx 0.001$ – sufficiently large such that the intermolecular spacing was much greater than σ. This ensured that the molecules would not initially be overlapping, and that free rotations about their initial positions would not cause them to initally collide with any other molecules and restrict their movement.

Using a timestep of $t^* = 0.01$, the system was then allowed to run under constant-volume, constant-energy conditions (NVE ensemble) for 10^5 steps in order to create an isotropic, gaseous configuration, with with DL_POLY_2 generating initial velocities based on an initial system temperature of $T^* = 1$. Due to the fully deterministic nature of DL_POLY_2 and the inability to provide a different generator seed to the initial assignment of molecular velocities, distinct molecular trajectories were generated by repeating this step multiple times, with the configuration after each sequence of 10^5 timesteps recorded. Each of these configurations were used to provide a different isotropic arrangement for use as a starting state for a subsequent simulation trajectory.

To perform a simulation run, we switched a low-density isotropic configuration to to constant-pressure, constant-temperature conditions (NPT ensemble) at a pressure of $P^* = 0.15$ and a temperature of $T^* = 1$, using a Nosé-Hoover thermostat and barostat. This compressed the system into an isotropic liquid phase below any onset

of liquid crystal behaviour. Systems were then equilibrated under these conditions for 10^6 timesteps.

Compression runs were performed by increasing the system barostat pressure in discrete steps. At each interval the pressure was increased by a fixed amount and the system allowed to re-equilibrate under the new pressure for 10^6 timesteps. The number density of the system was monitored to ensure that the system volume had equilibrated and any occuring phase transitions had finished. If the value had not settled, another 10^6 timesteps were performed until the value fluctuated around a constant value. A production run was then performed over the next 10^6 timesteps. Due to the potentially vast amount of data generated in a simulation run, the trajectory was sampled every 10^4 timesteps and the entire molecular configuration of bead position and velocities recorded, providing 100 samples per production run for analysis. Each resulting molecular configuration was used as the initial configuration for the next increase in pressure, and the procedure repeated until all the desired phase behaviour had been observed or the system had crystallized.

3.3 Results for $N = 512$ molecules

To begin, initial simulations were performed using systems of 512 11-bead molecules. This is the closest approximation to $L/D = 5$ possible using a molecule composed of beads – this value being used by Lansac *et al.* in the generation of their comprehensive phase diagram in Ref. [71]. This allows us to test the validity of our choice of mesogenic model.

Simulation runs were conducted for ten different types of 11-bead molecule, each with

a different bend angle in the interval $170^\circ \leq \theta \leq 110^\circ$, all at a constant temperature of $T^* = 1$. In each instance, a minimum of five different starting configurations were used to ensure that any phase behaviour exhibited was not specific to a unique molecular configuration. This also provides error estimates for calculated parameters across independent molecular trajectories. Each simulation comprised of a total of 5,632 interacting potentials, and each run was conducted using a single core of an Intel Xeon 1.86 GHz CPU, taking approximately four hours to perform 10^6 molecular dynamics timesteps. Including the equilibration and production run for each pressure increment, a single compression sweep took approximately five days of CPU time.

As an initial overview to the results of the simulations performed, the mean values for the uniaxial order parameters Q^2_{00} with respect to the reduced pressure P^* are shown for several of these runs in Fig. 3.4.

Although the uniaxial order parameter alone is insufficient for analysing phase behaviour, two broad concepts can be drawn from this plot. Firstly, it can be seen that the transition from a isotropic phase at low pressure, to a non-isotropic system with a degree of alignment, occurs at increasingly higher pressures as the bend angle between the two arms is decreased. Secondly, systems of molecules in the range $140^\circ \leq \theta \leq 170^\circ$ have final uniaxial order parameter values of $Q^2_{00} > 0.75$, indicating a high level of alignment, whilst systems with bend angles of $\theta < 140^\circ$ exhibit low but non-zero levels of levels of uniaxial alignment, with $Q^2_{00} < 0.5$. In the context of these two observations, we will now examine the phase behaviour of the $\theta = 160^\circ$, 140° and 130° compression runs in more detail, in order to characterize the different types of phase behaviour observed.

3.3.1 $\theta = 160°$

Five separate trajectories were used to track the phase behaviour of $\theta = 160°$ molecules. Fig. 3.5 shows the equation of state for a system of $160°$ molecules as they were compressed from an initial isotropic phase at a pressure of $P^* = 0.17$, along with a theoretical liquid phase curve from Eqn. (2.31). The uniaxial and biaxial nematic order parameters are shown in Fig. 3.6. A sequence of snapshots from a single trajectory run are presented in Fig. 3.7.

The equation of state shows that the system is initially a good fit for the theoretical liquid density. As the system is compressed from its isotropic state (Fig. 3.7a), it undergoes its first phase transition in the interval $0.35 < P^* < 0.52$, transitioning to a

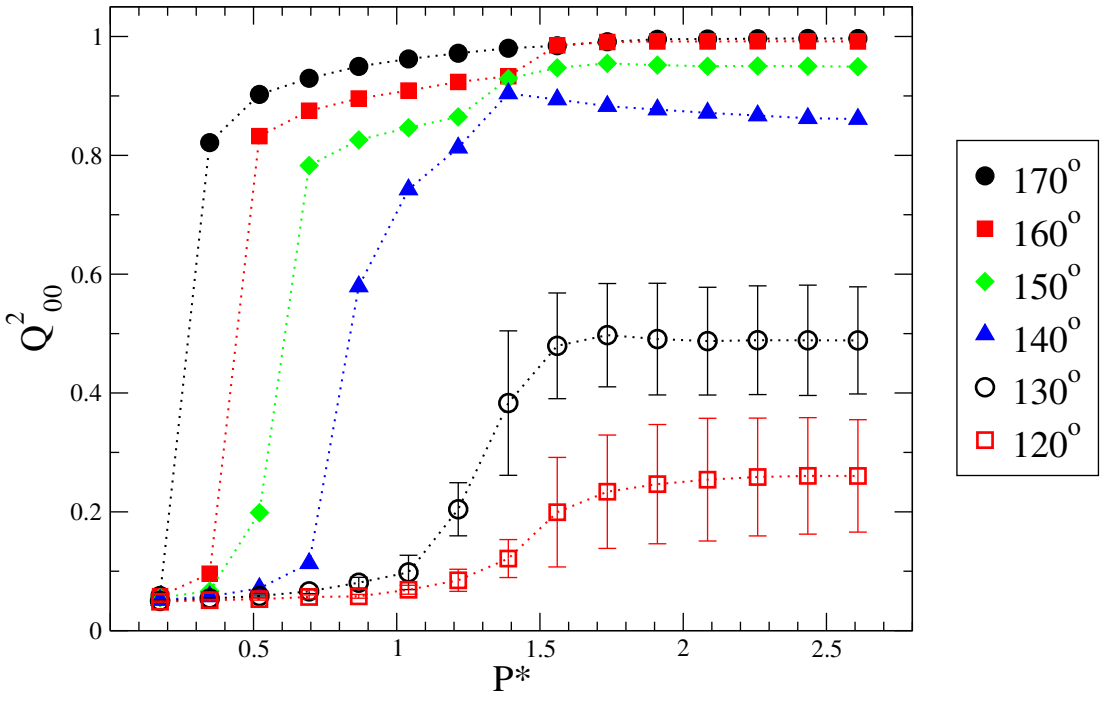

Figure 3.4: The change in the uniaxial order parameter Q^2_{00} with increasing pressure P^* for six different systems of $N = 512$ 11-bead molecules. Legend values correspond to the molecular bend angle θ. Small error bars for $\theta > 130°$ are omitted for clarity.

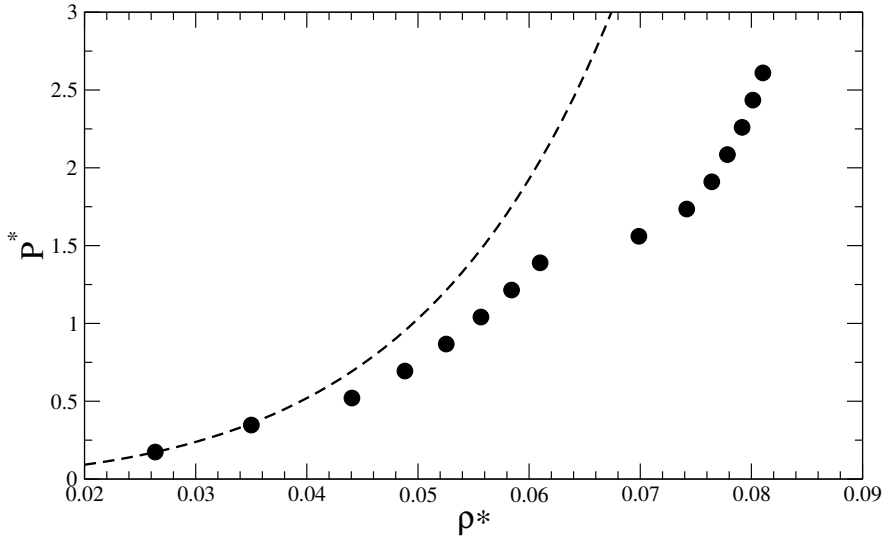

Figure 3.5: The equation of state for a system of $N = 512$ 11-bead, $\theta = 160^\circ$ molecules on compression. The dotted line indicates the theoretical liquid equation of state. Error bars are smaller than symbol size.

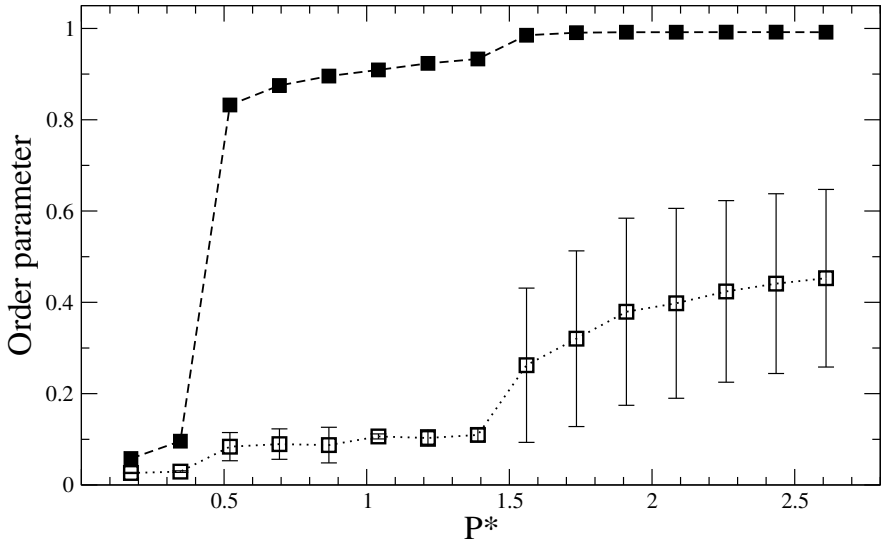

Figure 3.6: The uniaxial order parameter (filled symbols) and biaxial order parameter (hollow symbols) for a system of $N = 512$ 11-bead, $\theta = 160^\circ$ molecules on compression.

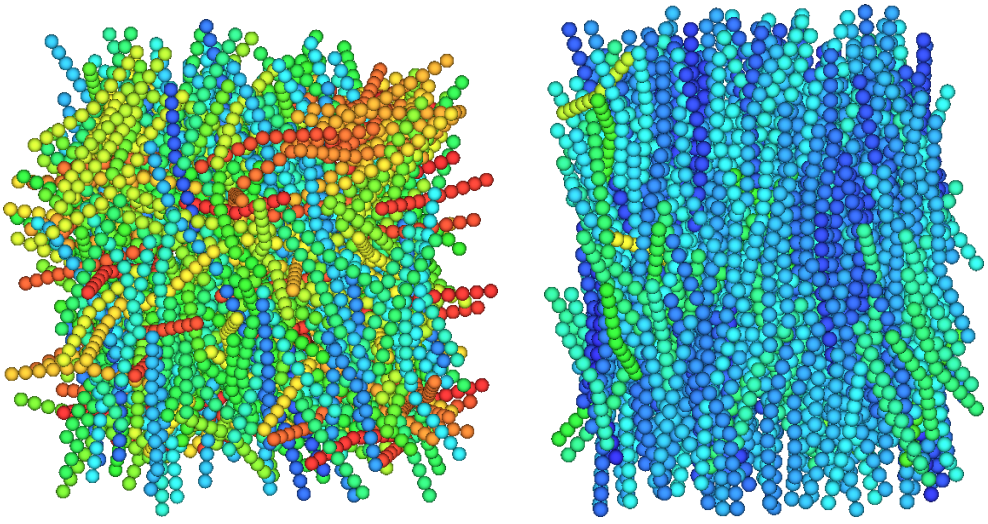

(a) $P^* = 0.35$ (b) $P^* = 0.52$

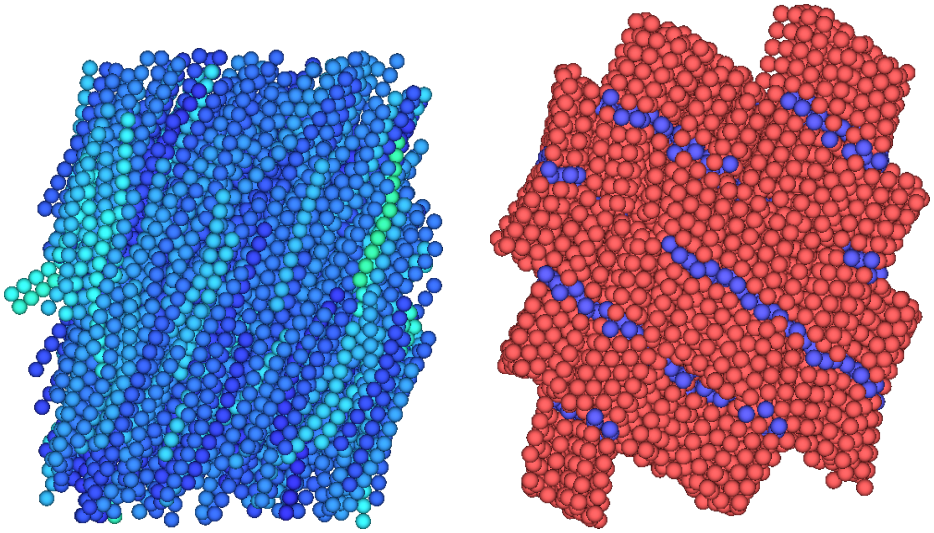

(c) $P^* = 1.39$ (d) $P^* = 1.56$

Figure 3.7: Snapshots from a compression run of $N = 512$ 11-bead molecules with a bend angle of $\theta = 160°$, showing isotropic (a), uniaxial nematic (b and c) and smectic-like layered phases (d). Molecules in (d) have their "apex" bead differentiated in order to visualise their layering.

uniaxial nematic (Fig. 3.7b). There is a sharp increase in the uniaxial order parameter Q_{00}^2 from less than 0.1 to over 0.8, while Q_{22}^2 remains under 0.1, confirming that one set of molecular axes have aligned strongly while the other two have not. As the barostat pressure is increased through the uniaxial nematic phase, the global alignment director rotates towards a longer free axis of the cubic periodic simulation cell, i.e. between two opposite corners, as shown in Fig. 3.7c.

A second more distinct transition occurs as the pressure is increased through the interval $1.39 < P^* < 1.56$. The resulting phase has a slightly higher level of uniaxial alignment than the nematic phase, but a large jump in reduced density as the degree of molecular packing increases sharply. The biaxial nematic order parameter averaged across the five trajectories also has a considerable increase, but its value remains below 0.5 and with very large variation between the runs. The pair correlation function between the central beads of the molecules at $P^* = 1.56$ (coloured blue in Fig. 3.7d) is shown in Fig. 3.8. The height of the first peak and significant subsequent peaks indicates that this is a phase with a degree of long-range ordering. Visual inspection of the phase shows that the system consists of a number of poorly organised smectic-like layers, with "clusters" of smectic-like alignment offset by a single arm length, approximately half the length of the long axis of the molecule. Visually, this presents itself as the the extremeties of the arms of two molecules meeting together within the "knuckle" of another molecule, rather than all the knuckles aligning together.

This clustering behaviour also explains the small climb and broad range of values for Q_{22}^2. As the biaxial order parameter is effectively a measure of the level of alignment of the short axes of the molecules, these clusters give rise to a number of polarized groups, all sharing a common short axis alignment director. However, this director differs between clusters, and so the resulting value of Q_{22}^2 can vary significantly depending on

the number and average short axis alignment of these clusters. It is possible that, if the system size were increased to incorporate more clusters, the net short axis alignment would average out and the biaxial order parameter would not deviate so far from zero in this phase.

The formation of these clusters can potentially be attributed to two things. The first is insufficient equilibration, and that smaller pressure steps may allow for better alignment of the formed layers. The second more likely explanation is the relatively small size of the simulation cell. From Fig. 3.7d it can be seen that three full smectic layers cannot fit in the cubic simulation box at this density. The rotation of the nematic phase to line up along the longest free axis of the box (Figs. 3.7b and 3.7c) also indicates that the box is not large enough for the lowest energy configuration to fit regardless of orientation within the simulation cell. It is likely that the dislocation of these smectic layers into offset clusters pays a relatively low free energy cost. Therefore there is a danger that the self-interaction of molecules across the periodic boundary conditions is distorting proper formation of whatever true smectic-like phase exists at this density. In other MC based works from initially aligned crystal states, a cuboidal box is used,

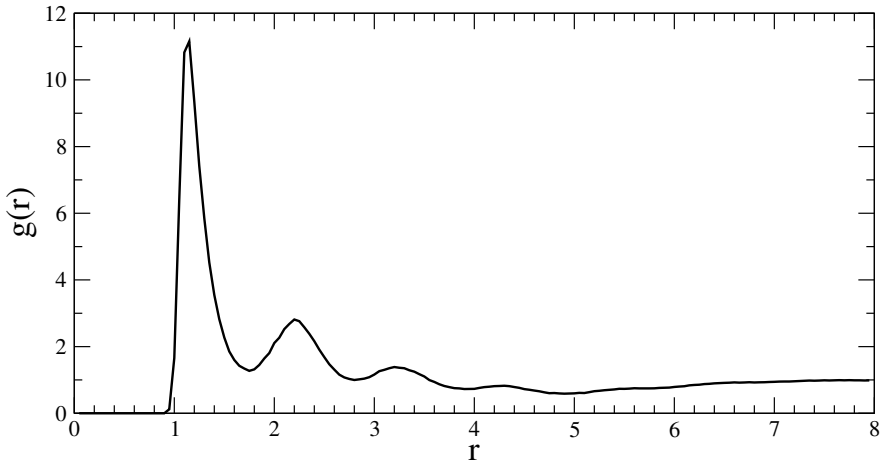

Figure 3.8: The pair correlation function between the molecules of a system of $N = 512$ 11-bead, $\theta = 160^\circ$ molecules at a pressure of $P^* = 1.56$.

sized exactly in order to fit the expected number of smectic layers with a predetermined uniaxial orientation vector. As our simulations are from isotropic initial conditions, the system cannot be forced to select a specific global director without the introduction of an external field or force, negating the purpose of using a cuboidal simulation cell. To increase the space for allowing smectic layers to form in a cubic cell requires a much larger number of molecules, and the simulation of far larger systems.

Overall, the presence of isotropic, a wide uniaxial nematic and a third phase with smectic-like traits indicates that the same phases are being seen here at a bend angle of 160° as in Fig. 3.2, and fits with the results reported in the work by Camp *et al.* [67]

3.3.2 $\theta = 140^\circ$

Phases for systems of $\theta = 140^\circ$ molecules under compression were obtained through simulation of eight independent trajectories. Fig. 3.9 shows the values for the equation of state from an initial pressure of $P^* = 0.17$, along with the theoretical liquid density curve. Calculated values of the Q^2_{00} and Q^2_{22} order parameters are presented in Fig. 3.10.

As compression begins, the first transition from an isotropic to a uniaxial nematic occurs between $0.69 < P^* < 0.87$, a higher pressure than for molecules with a bend angle of 160°. This is also shown by the values of the equation of state remaining close to the theoretical liquid curve for a larger range of pressures. This is expected, as the relative length of the short axis to the long axis has increased, and therefore so has the biaxiality of the molecules. The higher density of the isotropic–nematic transition for molecules with a higher biaxiality is shown in the phase diagrams in Refs. [22] and [69]. The value of the uniaxial order parameter is also noticeably lower,

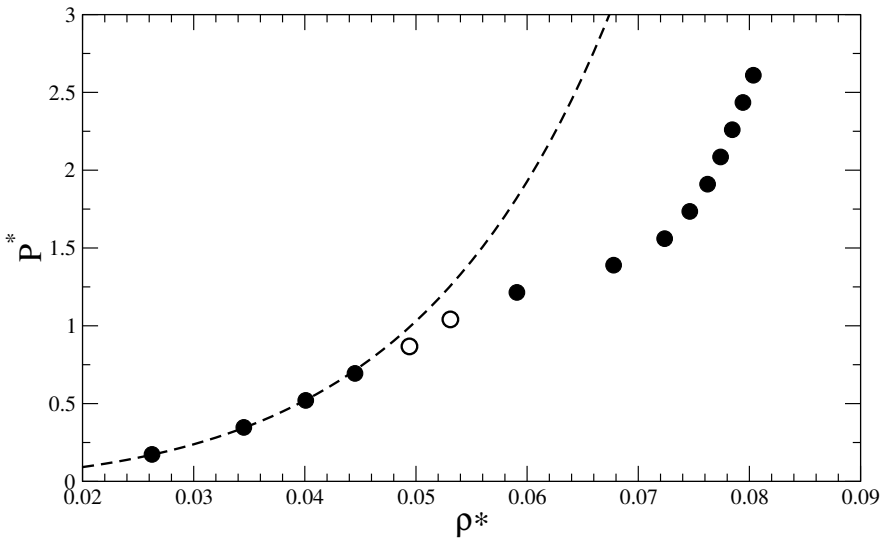

Figure 3.9: The equation of state for a system of $N = 512$ 11-bead, $\theta = 140^\circ$ molecules on compression. The dotted line indicates the theoretical liquid equation of state. Points in the fully equilibrated uniaxial nematic phase are hollow. Error bars are smaller than symbol size.

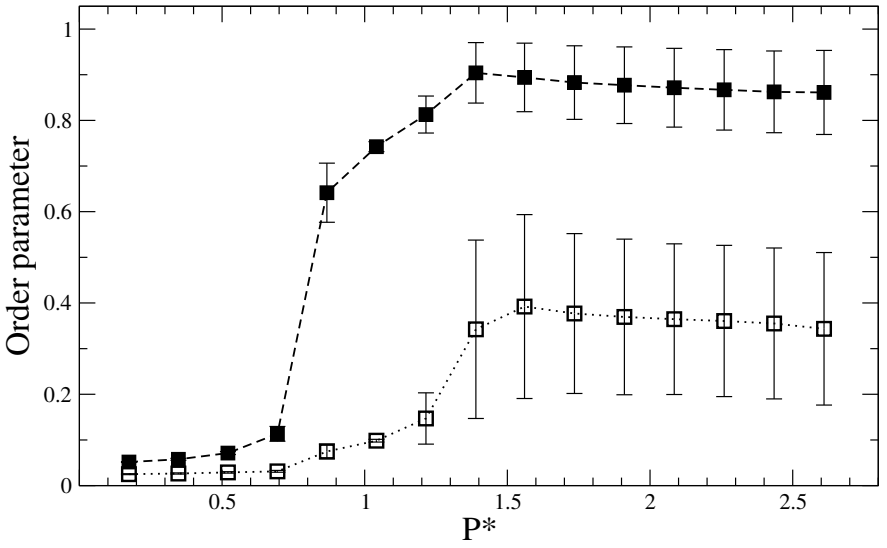

Figure 3.10: The uniaxial order parameter (filled symbols) and biaxial order parameter (hollow symbols) for a system of $N = 512$ 11-bead, $\theta = 140^\circ$ molecules on compression.

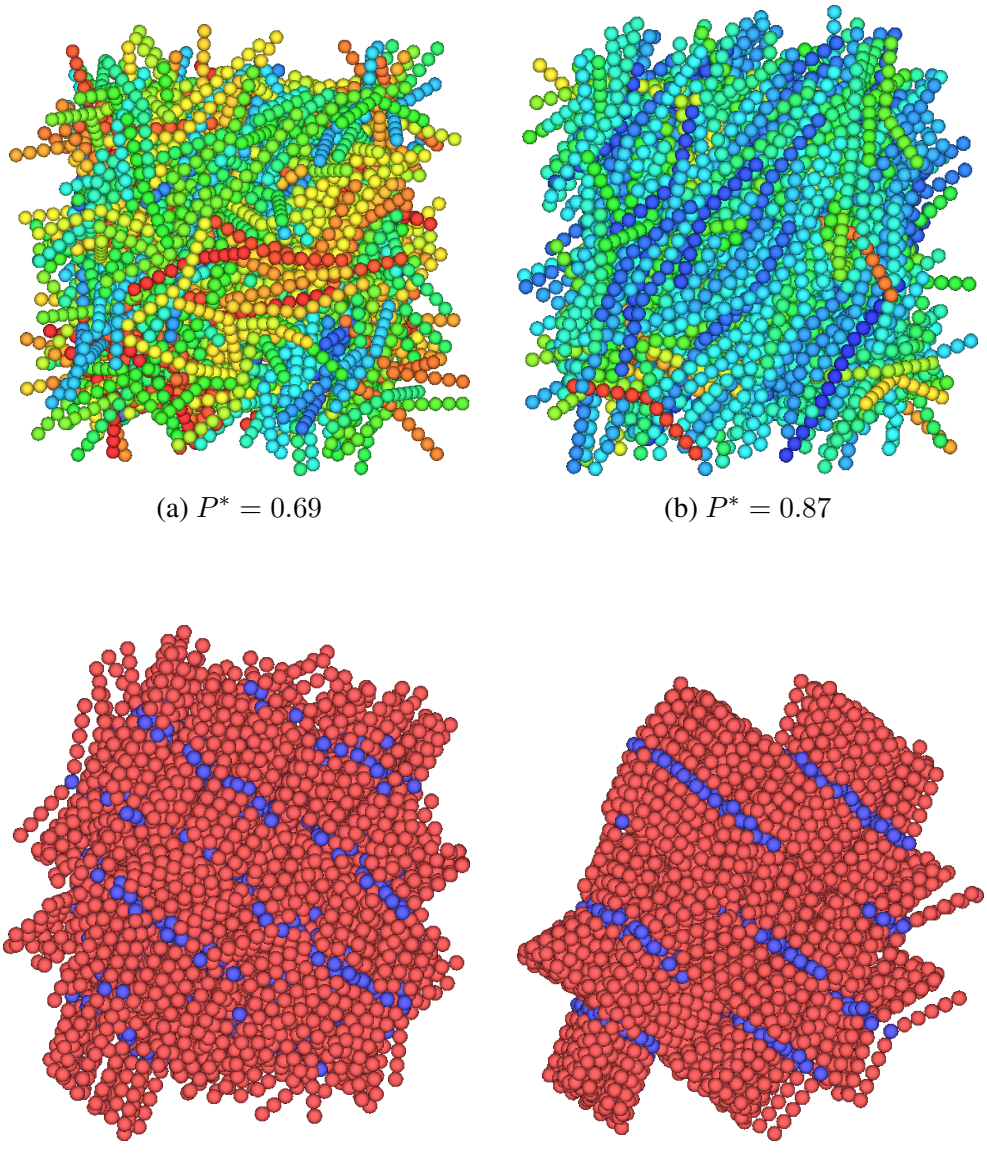

(a) $P^* = 0.69$ (b) $P^* = 0.87$

(c) $P^* = 1.21$ (d) $P^* = 1.39$

Figure 3.11: Snapshots from a compression run of $N = 512$ 11-bead molecules with a bend angle of $\theta = 140°$, showing isotropic (a), uniaxial nematic (b) and smectic-like layered phases (c and d). Molecules in (c) and (d) have their "apex" bead differentiated in order to visualise their layering.

reaching $Q_{00}^2 \approx 0.6$ just after the transition, compared to $Q_{00}^2 > 0.8$ for wider angled molecules. It continues to climb all the way to the second phase transition, indicating the possibility of a wide, more continuous phase.

On increasing the pressure further, the system undergoes a second transition from the uniaxial nematic to the offset smectic layering mentioned previously for the $160°$ molecules. A snapshot of such a phase is shown in Fig. 3.11c. Neither Q_{00}^2 or Q_{22}^2 can distinguish this phase change with any clarity. Aided by the theoretical liquid curve, it can be seen that there is a small phase where the values of the equation of state do not match the liquid density curve (hollow points) before having another discontinuity at the second phase transition (Fig. 3.9). The pair correlation function in Fig. 3.12 shows the distinction between the two phases most clearly, with a strongly enhanced first

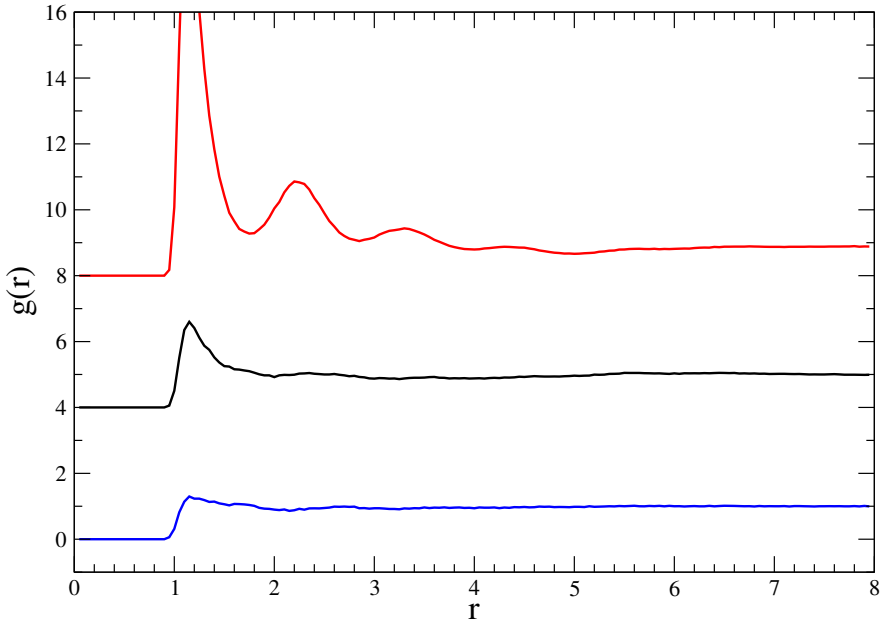

Figure 3.12: The pair correlation function between the molecules of a system of $N = 512$ 11-bead, $\theta = 140°$ molecules at a pressure of $P^* = 0.87$ (bottom, blue), $P^* = 1.21$ (middle, black) and $P^* = 1.39$ (top, red). The plots have been offset for clarity, and the peak of the $P^* = 1.39$ line at a value of 11.6 (19.6 on the offset axis) has been truncated.

peak showing a greater level of short-range ordering compared to the uniaxial nematic phase.

As the pressure is increased further, another jump in the equation of state occurs as the short axes of the molecules align. A snapshot at $P^* = 1.39$ in Fig. 3.11d shows the arrangement of the offset smectic-like clusters which the phase is comprised of. The pair correlation function indicates a significant degree of longer range ordering, and the low but broad range of values for Q^2_{22} arises once again from the polarization of the short axes in the clusters.

A significant difference from the order parameter behaviour of the 160° systems is that there is both a significant uncertainty on Q^2_{00}, and that it declines after the transition. This arises due to the offset nature of the layers. When the lower arm of a molecule is aligned with the upper arm of a molecule in the layer below, the bend angle of the molecule dictates how the half-offset molecule in the next layer aligns itself. The tighter angle in these molecules means that the alignment of each half-layer is forced to deviate further from the average global alignment director, before righting itself in the next layer in a "zig-zag" fashion. As the pressure continues to increase, the ability for molecules to relax back to the global director is reduced and the deviations are enhanced. Again, much of this behaviour is due to the nature of the offset smectic layers, which may be an artefact of simulation cell size as previously mentioned.

The increased pressure required to transition from the isotropic to the uniaxial nematic phase compared to 160°, as well as the reduced width of the nematic phase, are both consistent with the phase diagram in Fig. 3.2.

3.3.3 $\theta \leq 130^\circ$

The behaviour of molecules with a bend angle $\theta < 140^\circ$ is distinctly different from those where $\theta \geq 140^\circ$, as illustrated in Fig. 3.4. Here, simulation results averaged across nine different trajectories of systems of molecules with a 130° bend angle are presented. The equation of state and order parameters for these systems are shown in Figs. 3.14 and 3.14 respectively.

The equation of state shows that there is only one significant transition, occuring at a slightly lower pressure window between $1.04 < P^* < 1.21$, indicated by the small deviation from the theoretical isotropic liquid curve.

The values of Q^2_{00} and Q^2_{22} also demonstrate the existence of only one phase transition, with both values increasing simultaneously. The uniaxial order parameter eventually settles at $Q^2_{00} < 0.5$, indicating a very poor level of alignment.

Snapshots from a trajectory at $P^* = 1.04$ and $P^* = 1.39$ are shown in Fig. 3.15, which reveals the absence of a global orientation director. Instead, the molecules form small clusters with significant ordering of both their long and short axes, but only on a local scale. At narrower bend angles of $\theta = 120^\circ$ the size of these clusters decreases, as shown in the snapshots in Fig. 3.20.

While this phase may possibly the resolved through more intensive equilibration, it is more important to note the lack of a uniaxial nematic. The melting simulations by both Lansac *et al.* [71] and Dewar and Camp [77] indicate that, above a critical angle, their systems see no uniaxial nematic liquid crystal phases, and instead see direct transitions from the smectic phase to the isotropic phase. We propose that the phase observed here is driven by the same mechanism that transitions a nematic to a smectic. The

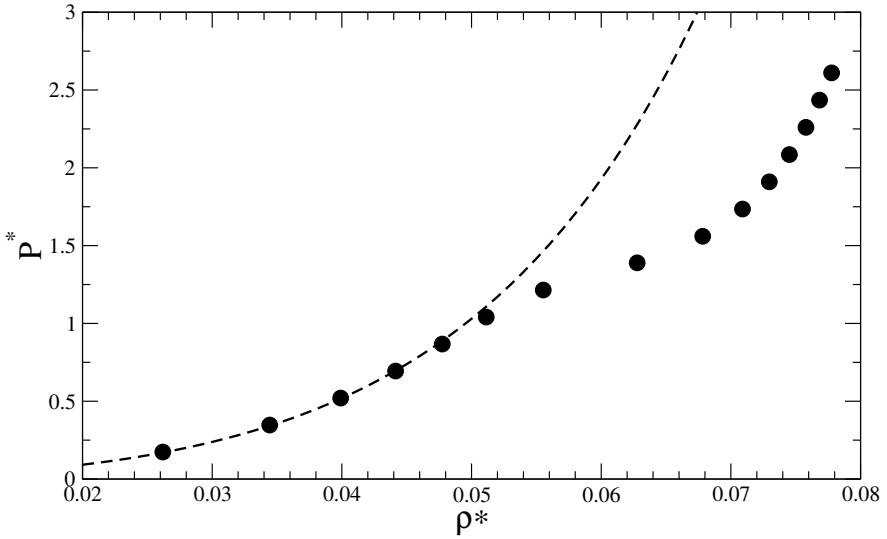

Figure 3.13: The equation of state for a system of $N = 512$ 11-bead, $\theta = 130^\circ$ molecules on compression. The dotted line indicates the theoretical liquid equation of state. Error bars are smaller than symbol size.

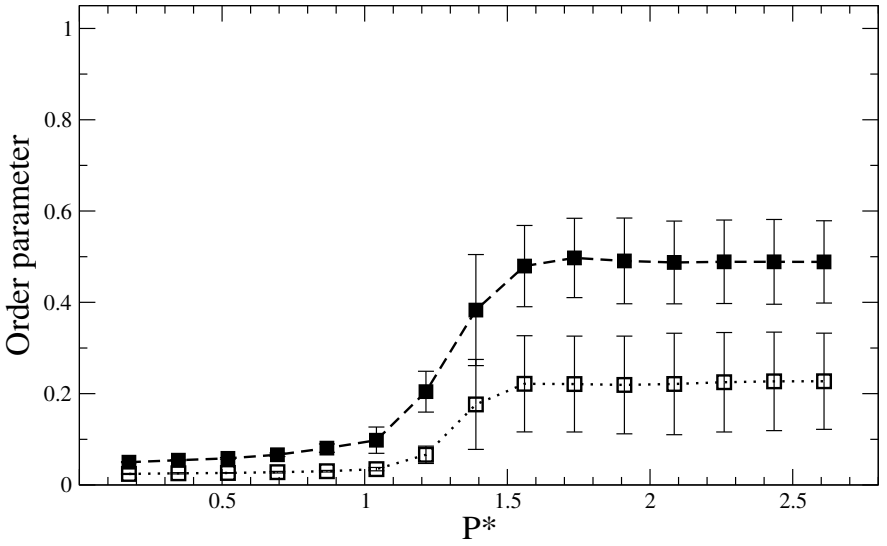

Figure 3.14: The uniaxial order parameter (filled symbols) and biaxial order parameter (hollow symbols) for a system of $N = 512$ 11-bead, $\theta = 130^\circ$ molecules on compression.

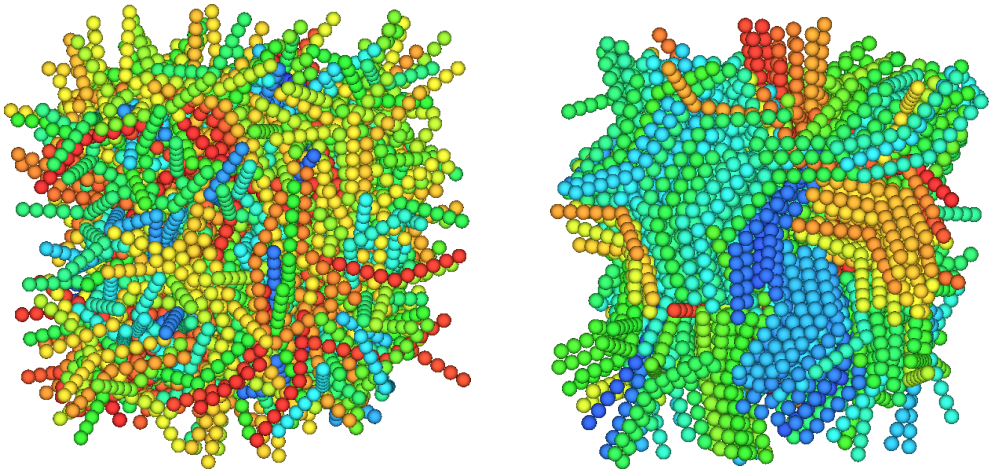

(a) $P^* = 1.04$ (b) $P^* = 1.39$

Figure 3.15: Snapshots from a compression run of $N = 512$ 11-bead molecules with a bend angle of $\theta = 130°$, showing (a) isotropic and (b) clustered behaviour.

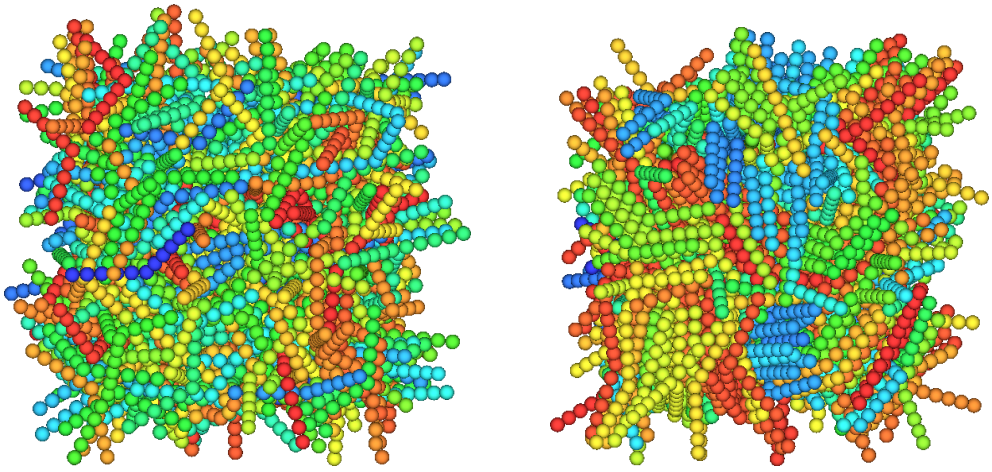

(a) $P^* = 1.04$ (b) $P^* = 1.39$

Figure 3.16: Snapshots from a compression run of $N = 512$ 11-bead molecules with a bend angle of $\theta = 120°$, showing (a) isotropic and (b) clustered behaviour.

inhibition of the alignment of the long axes, due to the increased molecular biaxiality, prevents a global direction vector from being formed. When the smectic-like behaviour is spontaneously induced, the resulting layers or clusters have no uniform direction, and the phase seen reflects this lack of global long-axis ordering.

The "jamming" of this system at molecular bend angles $\theta \leq 130^\circ$ corresponds with the lack of a uniaxial phase in Fig. 3.2 for bend angles $\theta \leq 135^\circ$. Therefore, while this model can be linked to the Lansac phase diagram, it also means that it is highly unlikely that the biaxial nematic phase would be obtainable with this model system.

3.3.4 Decompression simulations

In order to validate the location of these phase transitions with respect to pressure, the final molecular configurations obtained from the previous compresion runs were used as the initial input for a reversed series of decompression runs. The simulation methodology was the same as already discussed, but instead decreasing the barostat pressure by a fixed quantity at each step.

Comparsions between the average Q_{00}^2 order parameters during compression and decompression are shown in Fig. 3.18 for the $\theta = 160^\circ$, 140° and 130° systems described in the previous sections.

The fit between the two set of Q_{00}^2 values for the 160° systems is extremely good, with values calculated in all three of the smectic, uniaxial nematic and isotropic phases matching to within error. The only deviation of any significance is at the point of the smectic–nematic transition, where the difference in values shows that the long axes of the molecules remain well organised for slightly longer on decompression.

The $140°$ systems show similar behaviour, with the order parameter giving an excellent fit between the values in both the smectic and isotropic phases. The smectic phase extends downwards slightly further on these runs, with the transition to the nematic occuring within the $0.87 < P^* < 1.04$ range, which narrows the nematic phase slightly further.

In contrast, the decompression values for $130°$ molecules show distinctly different behaviour around the phase transition. As the system is decompressed, the value of Q^2_{00} climbs significantly from 0.49 at $P^* = 2.61$ to 0.61 at $P^* = 1.21$, before dropping away towards its isotropic value. A comparison for the equation of state on compression and decompression is shown in Fig. 3.18, where it can be seen that the systems retain a higher density as they are decompressed, with $\rho^* = 0.056$ at $P^* = 1.21$ on

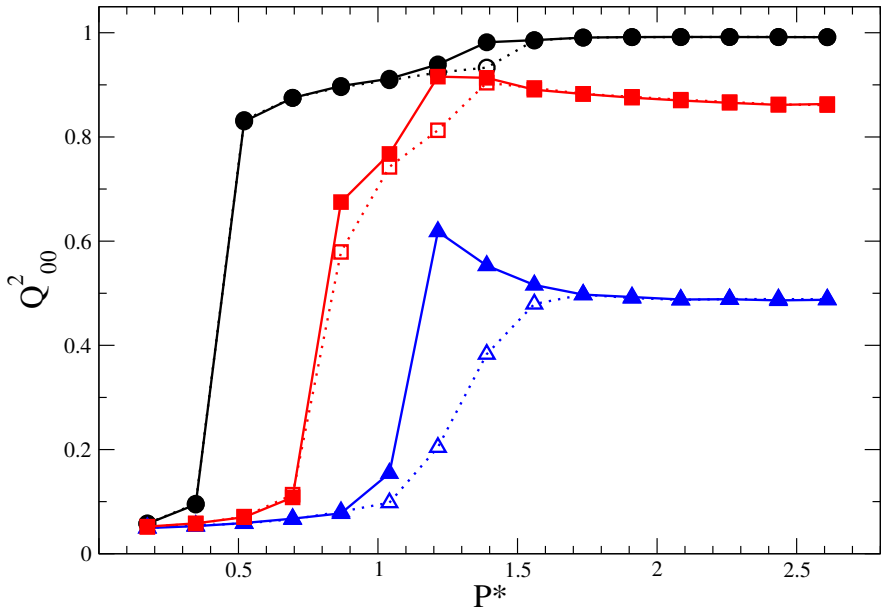

Figure 3.17: The uniaxial order parameter for systems of $N = 512$ 11-bead molecules on both compression (hollow symbols, dashed lines) and decompression (filled symbols, solid lines). Values are shown for molecules with internal bend angles of $\theta = 160°$ (black circles), $\theta = 140°$ (red squares) and $\theta = 130°$ (blue triangles). Errors have been omitted for clarity.

compression and $\rho^* = 0.062$ at the same pressure on decompression. Fig. 3.19 shows the difference in the pair correlation functions for these two systems. The enhanced height of the first peak, along with a significant second peak on decompression indicates that there is considerably more short range correlation on decompression.

Snapshots of the system at this pressure are presented in Fig. 3.20. The large blue cluster is developing a significant amount of smectic ordering, as nearby clusters rotate into place and begin to align to a mutual director. This indicates that the smectic phase described in other works is most likely the underlying phase here, and could potentially be achieved with extended cycles of compression and decompression.

3.4 Results for $N = 4096$ molecules

While the locations of the phase transitions identified from the simulations of $N = 512$ systems are compatible with previous literature, the actual phases themselves show a number of differences, particularly in the offset smectic-like layering beyond the uniaxial nematic phases for $\theta \geq 140^\circ$, and the clustered systems without a global director for $\theta \leq 130^\circ$. One strong possibility is that the relatively small size of the simulation cell is preventing more than two smectic layers from forming, and that molecules are self-interacting due to finite size problems with the periodic boundary conditions.

In order to examine whether the phases seen in the $N = 512$ simulations are representative of bulk system behaviour, a set of much larger $N = 4096$ runs were conducted for sets of molecules with bend angles in the range $170^\circ \leq \theta \leq 120^\circ$, and their phase behaviour compared to the smaller systems. Due to the much larger number of

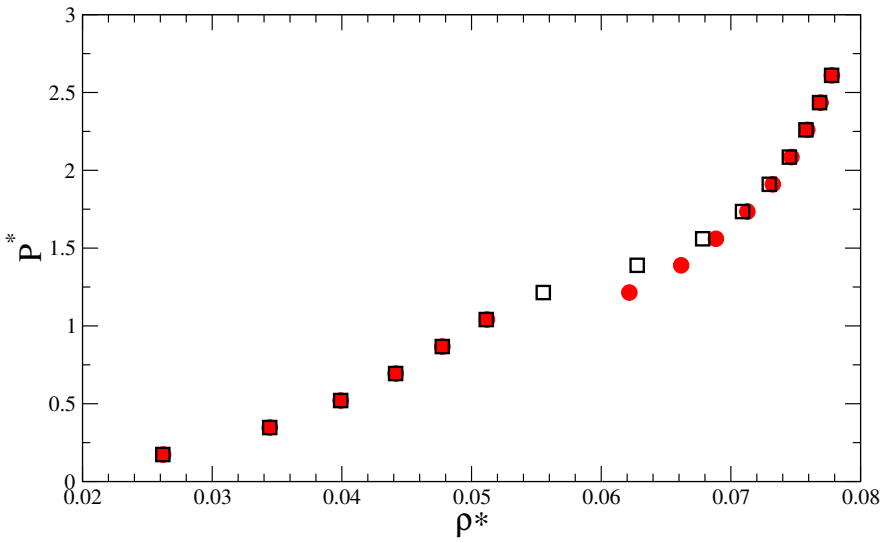

Figure 3.18: The equation of state for a system of $N = 512$ 11-bead, $\theta = 130^\circ$ molecules. Hollow black squares are from a compression run, while filled red circles are from a subsequent decompression run.

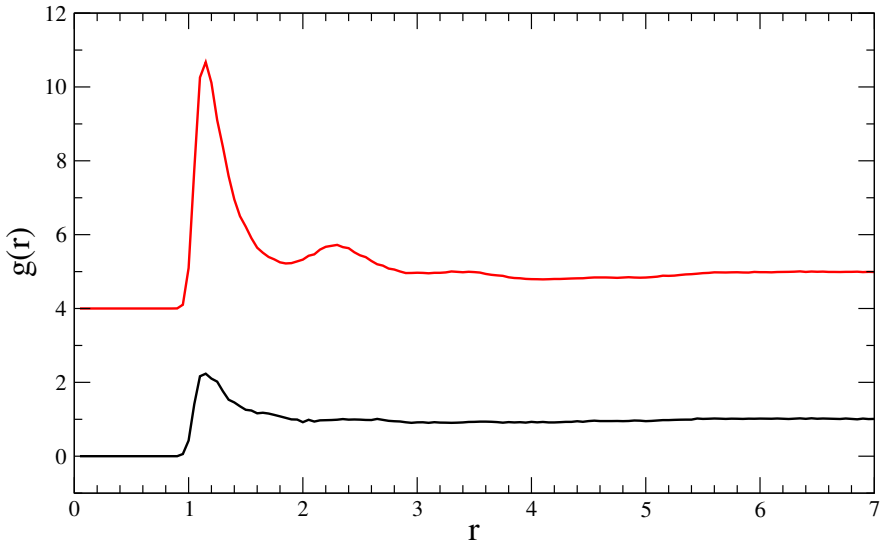

Figure 3.19: The pair correlation function $g(r)$ for a system of $N = 512$ 11-bead, $\theta = 130^\circ$ molecules at $P^* = 1.21$ on a compression run (bottom, black) and a decompression run (top, red). Lines are offset vertically for clarity.

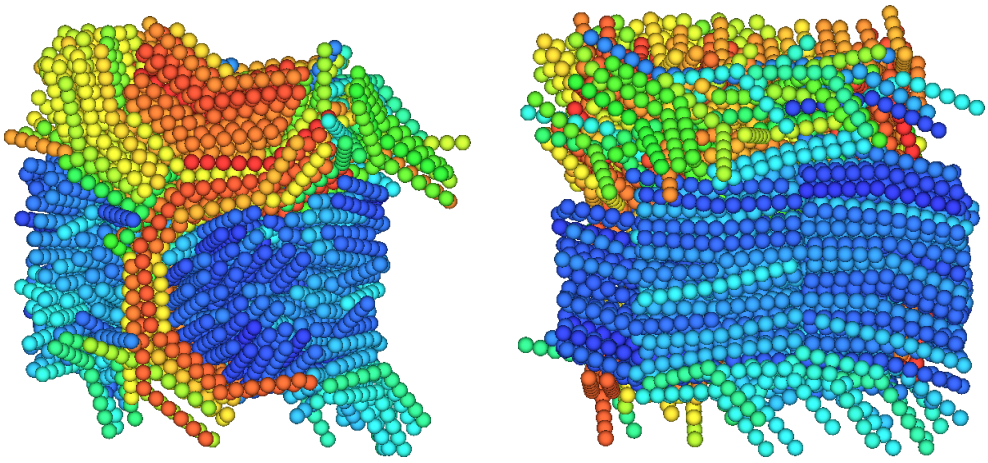

Figure 3.20: Front and side snapshot views at $P^* = 1.21$ during a decompression run of of $N = 512$ 11-bead molecules with a bend angle of $\theta = 130°$.

interacting potentials in these systems (45,056), the simulations are much more computationally expensive. A set of 10^6 timesteps of these systems, performed in parallel across four cores of an Intel Xeon 1.86 GHz CPU using `DL_POLY_2`, took between 18–36 hours. As such, only a single system trajectory was conducted for each bend angle. Therefore, proper error estimates across multiple runs for the order parameters and equation of state were not possible with this data, as the only errors are those associated with time-averaging the values across a single run.

In order to ensure better equilibration, the simulation procedure was also changed from that used in Sec. 3.3. The default size of the pressure step increment was halved to $P^* \approx 0.08$. After each production run, the Q_{00}^2 and equation of state were checked for evidence of a phase change between $P_A \leq P^* \leq P_B$. If one had occured, the system was rewound to the final configuration at the end of the run for P_A, the pressure step reduced to one-fifth of its size, and the next five pressure steps conducted at a higher resolution. After the transition had occured, the original pressure step size was re-established.

As in Sec. 3.3, the aggregated Q_{00}^2 values for a subset of these runs are shown in Fig. 3.21 in order to provide an overview of the phase behaviour exhibited. The gradual increase in pressure required to induce the isotropic-uniaxial nematic phase transition for molecules $\theta > 140^\circ$ is clearly visible, and the isotropic–nematic phase transition pressure windows for all the simulated $N = 4096$ systems on compression are given in Table 3.1. Discontinuities in the equation of state for these systems were used to obtain values for the nematic–smectic transition windows, also given in Table 3.1.

3.4.1 $\theta = 160^\circ$

Comparisons between the two nematic order parameters for 160° 11-bead molecule systems in the $N = 512$ and $N = 4096$ simulations are given in Fig. 3.22. The change in the size of the system has not notably affected the transition pressures, with both transitions occuring in the same windows. The increase of the Q_{22}^2 order parameter after the second transition indicates that the system still has a net polarization. The equation of state in Fig. 3.23 indicates that the densities of the system after the second phase transition are larger in the $N = 4096$ system, and the molecules are more efficiently packed, giving the greatest evidence for differing phase behaviour.

A snapshot of the system at $P^* = 1.47$ is given in Fig. 3.24, showing clear smectic layering, with some small smectic clusters offset by half a molecule length visible in the bottom left of the snapshot. Combined with the non-zero polarization given by Q_{22}^2, this configuration is determined to be a polar smectic phase. Examination of the pair correlation function shows no splitting of the second peak at this point, which is typically representatve of hexagonal packing, and so this is most likely a polar smectic A phase. Although there is a small degree of molecular tilt, it is not uniform

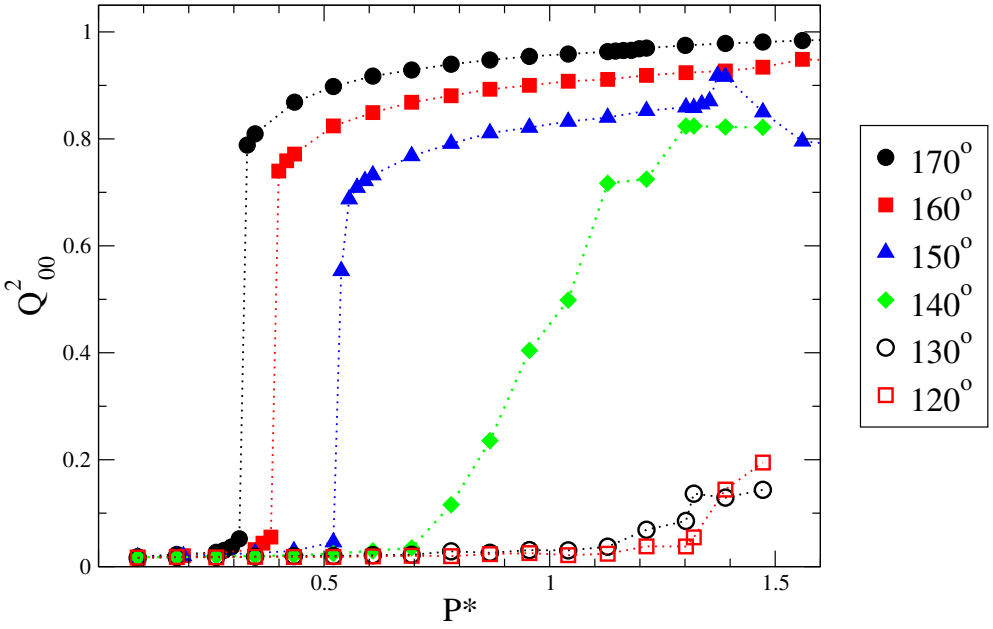

Figure 3.21: The change in the uniaxial order parameter $\langle Q^2_{00} \rangle$ with increasing pressure P^* for six different systems of $N = 4096$ 11-bead molecules. Legend values correspond to the molecular bend angle θ.

θ	$\rightarrow$ N	$\rightarrow$ Sm
170°	0.312 – 0.330	1.181 – 1.199
165°	0.347 – 0.365	1.372 – 1.399
160°	0.382 – 0.400	1.399 – 1.473
155°	0.433 – 0.452	1.399 – 1.473
150°	0.521 – 0.538	1.337 – 1.355
145°	0.608 – 0.694	1.215 – 1.302
140°		1.215 – 1.302

Table 3.1: The isotropic–nematic and nematic-smectic transition windows for systems of $N = 4096$ 11-bead molecules on compression.

across layers. A strongly tilted smectic phase as reported in other works [73, 77] is not observed, but this may exist further towards the crystallization point.

It is worth noting at this point that the assembly of larger smectic layers did not occur in all $N = 4096$ simulations. The peak and sharp fall in Q_{00}^2 for $\theta = 150^\circ$ (shown in Fig. 3.21) is due to the same reasons as given for the $\theta = 140^\circ$ systems in Sec. 3.3.2, whereby the formation many half-offset layers do not give a highly aligned global director overall. The equation of state of this system is given in Fig. 3.25, where the transition from nematic to smectic is actually seen to consist of two very close transitions. There is a metastable state between the points where the molecules have formed their offset layers but are not yet packed densely enough to strongly align the short axes of the molecules, which in turn would push the long axes of the clusters away from the global director. As the phase consisting of offset smectic clusters is likely an artefact of finite system size, further simulations of different trajectories at this system size would be required to find whether this pair of phase transitions is worth investigating.

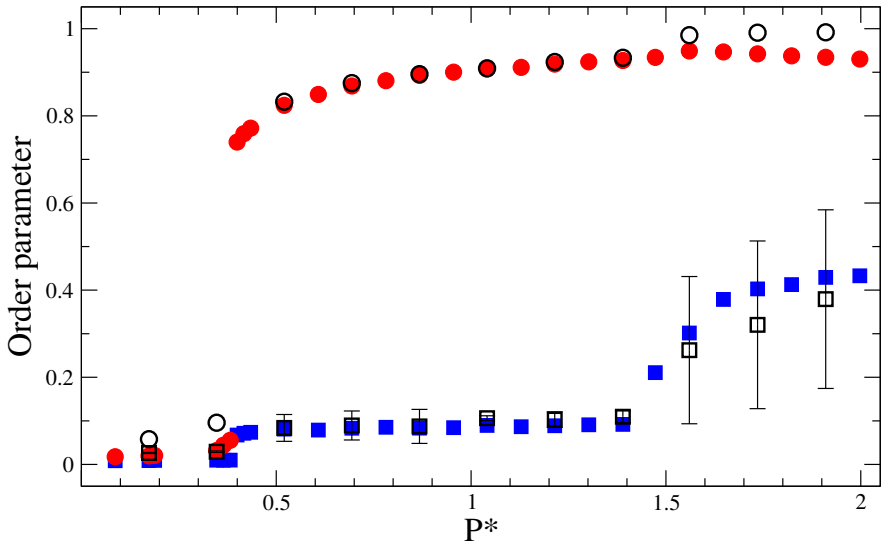

Figure 3.22: Order parameters for $\theta = 160°$ 11-bead systems on compression. Filled red circles and filled blue squares are the Q_{00}^2 and Q_{22}^2 order parameters for a system of $N = 4096$ molecules, while hollow circles and hollow squares are the order parameters for systems of $N = 512$ molecules.

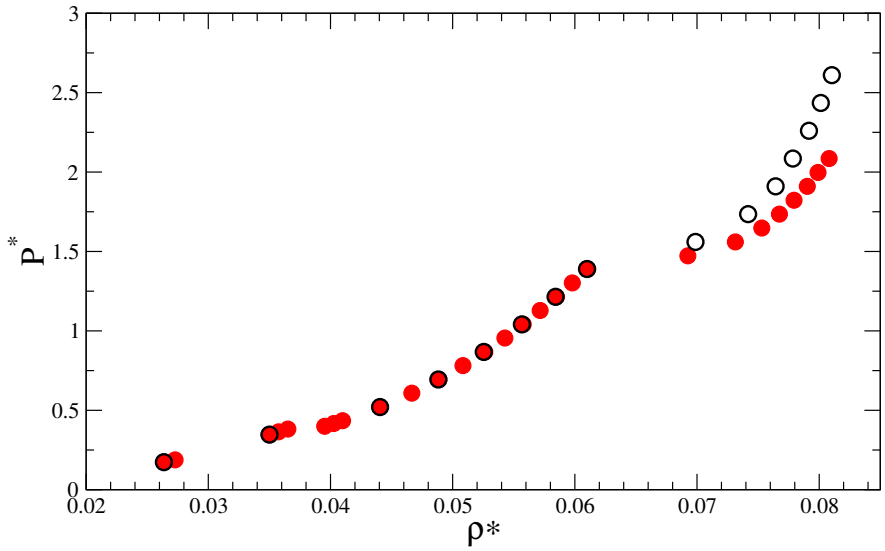

Figure 3.23: Equation of state for $\theta = 160°$ 11-bead molecules on compression, in systems of $N = 4096$ molecules (filled red) and $N = 512$ (hollow black).

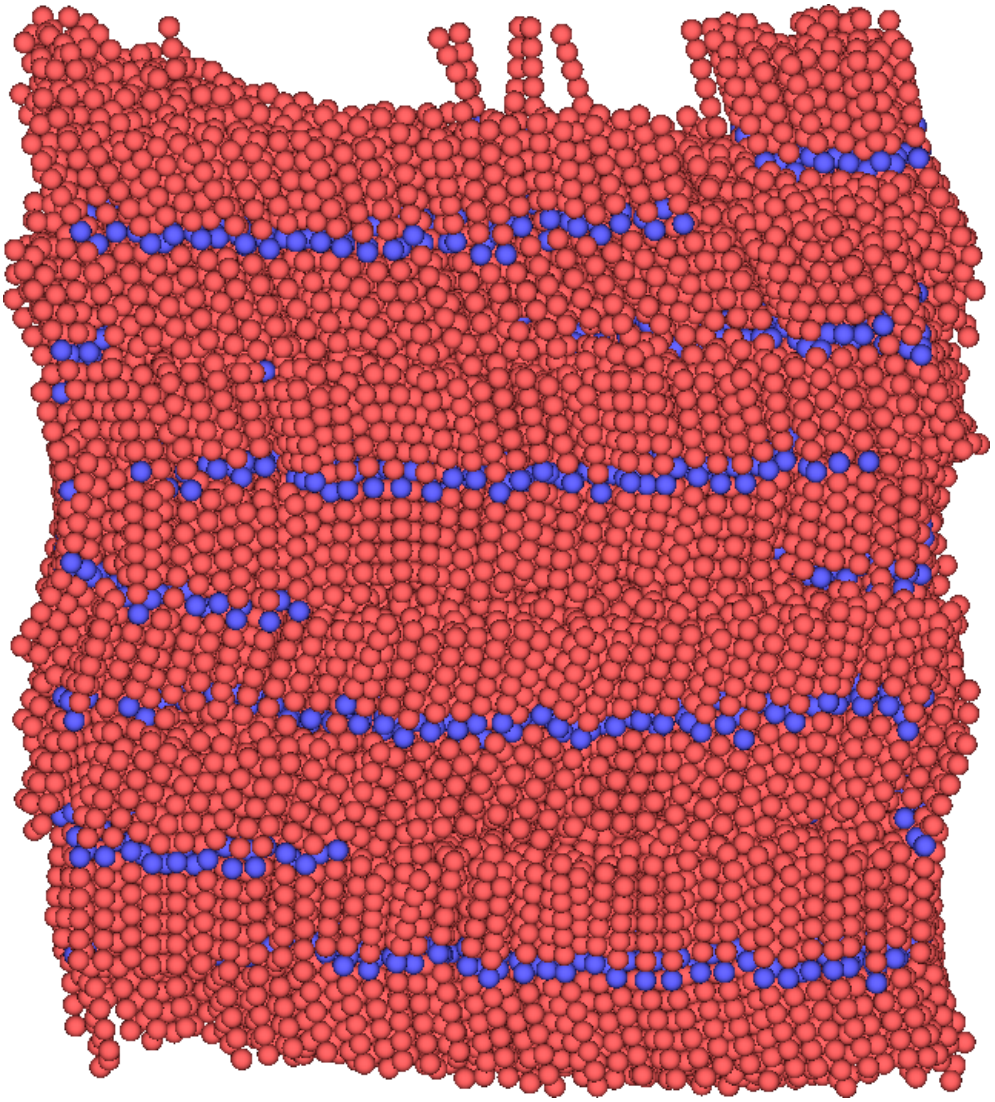

Figure 3.24: Snapshot from a compression run of $N = 4096$ 11-bead molecules with a bend angle of $\theta = 160^\circ$ at $P^* = 1.47$. Central beads are coloured blue to visualise smectic layering.

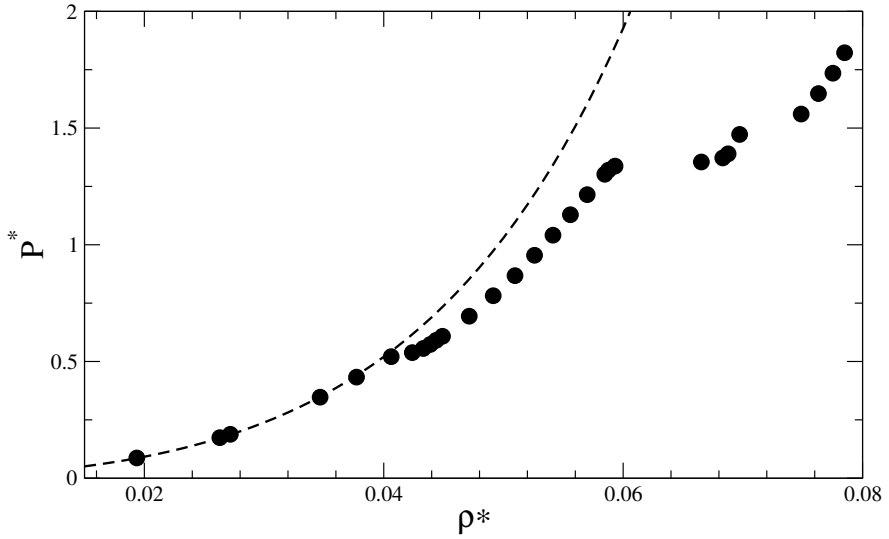

Figure 3.25: Equation of state for $N = 4096$, $\theta = 150^\circ$ 11-bead molecules on compression. The dotted line indicates the theoretical liquid equation of state. Four distinct phase branches are visible, with two close yet separate transitions in the high density region.

3.4.2 $\theta = 140^\circ$

Similar to how the smectic clusters for the 160° systems are resolved into full smectic layers with a larger system size, the clusters in the 140° systems demonstrate the same behaviour as the system size is increased to $N = 4096$ molecules. Fig. 3.26 shows the levelling-off of the Q^2_{00} order parameter and small increase in Q^2_{22} after the nematic-smectic transition, and visual inspection of the system shows the presence of smectic A layers.

The isotropic–nematic transition is actually hindered by the increased system size of the $N = 4096$ system, as shown by the depressed values of Q^2_{00} compared to those for the $N = 512$ system. As the pressure of the system is increased, the nematic phase begins with localized areas of mutual alignment. As the pressure of the system is increased, the growth of these regions results in the entire system eventually aligning

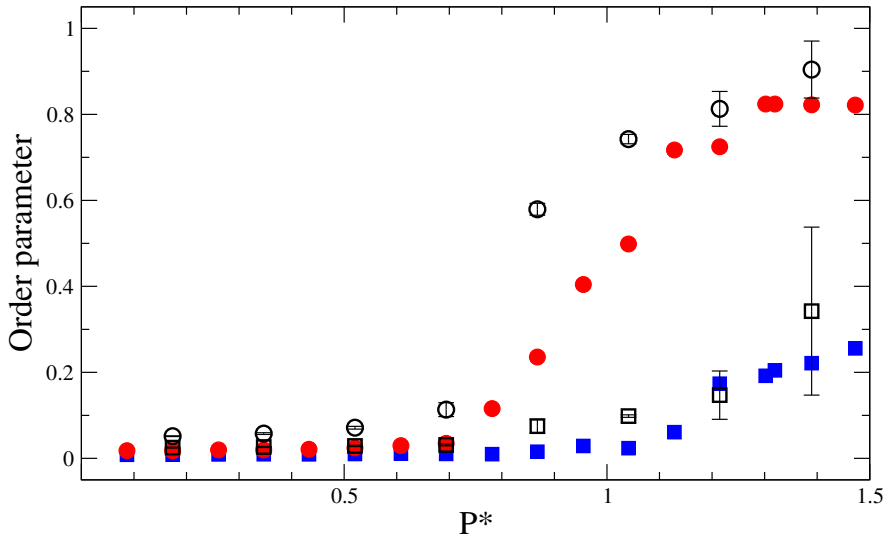

Figure 3.26: Order parameters for $\theta = 140^\circ$ 11-bead systems on compression. Filled red circles and filled blue squares are the Q^2_{00} and Q^2_{22} order parameters for a system of $N = 4096$ molecules, while hollow circles and hollow squares are the order parameters for systems of $N = 512$ molecules.

to a common director. In the smaller systems, there are fewer localized regions and so the mutual alignment is achieved more rapidly, while the competing nematic regions in the larger system continue to grow before one dominates the system.

The onset of this behaviour begins at $P^* \approx 0.78$, and the system is a fully aligned uniaxial nematic phase by $P^* \approx 1.13$. In this window, multiple regions are competing for the global nematic alignment – a snapshot during this period is shown in Fig. 3.27 at a pressure of $P^* = 0.96$. Different regions of nematic alignment are visible by common colours, with the dominant region being blue-green and the smaller competing region being red-yellow.

The difficulty with which the system achieves a common global director in the nematic phase for $\theta = 140^\circ$ strongly suggests that the loss of a nematic phase for narrower bend angles is linked to the decline of the relative length of the long axis to the short axis of the molecules. Without a single clear molecular director, no one choice of alignment dominates the system at lower pressures. Separate regions of the simulation cell have short-range nematic alignment, but the propagation of this alignment through the system is low. Global mutual alignment is not achieved regardless of how long the simulation is run for, indicating it is unlikely to be a simple equilibration issue.

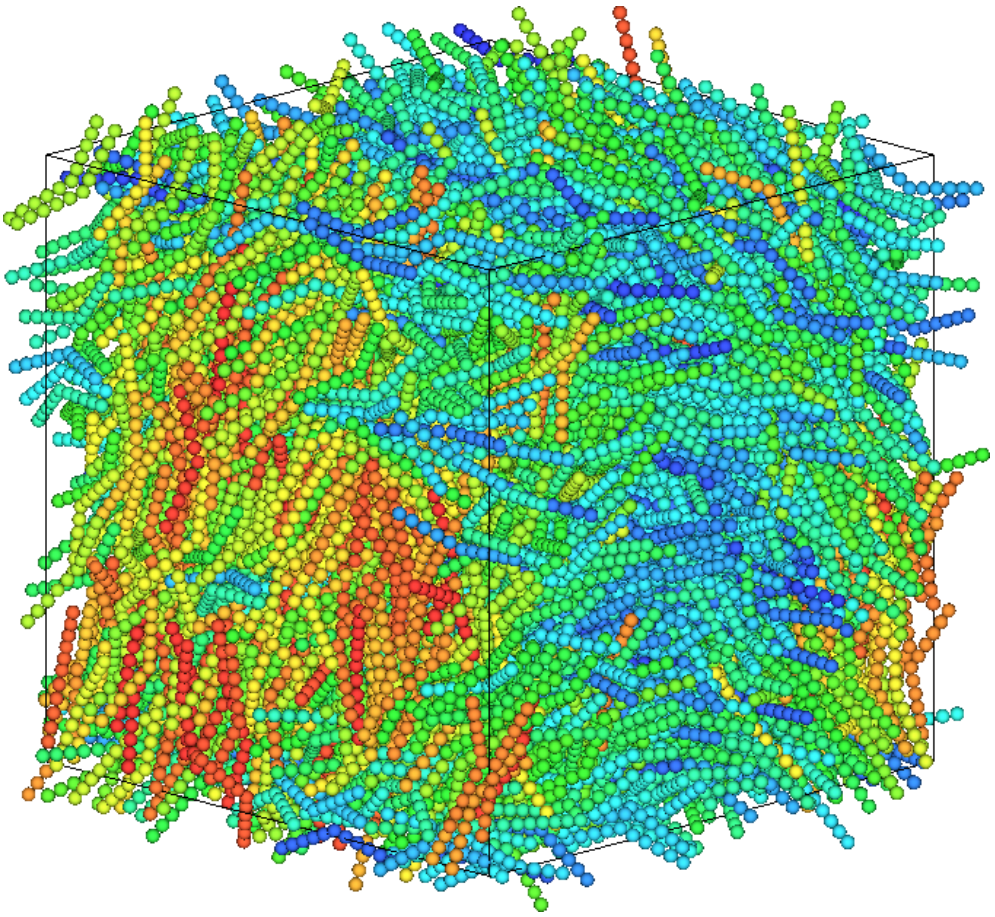

Figure 3.27: Snapshot from a compression run of $N = 4096$ 11-bead molecules with a bend angle of $\theta = 140^\circ$ at $P^* = 0.96$. Molecules are coloured based on the orientation of their long axis.

3.4.3 $\theta = 130^\circ$

The "jammed" structure of the $\theta = 130^\circ$ systems mentioned in Sec. 3.3.2 is not resolved through a bigger system size or narrower pressure steps. Both the Q_{00}^2 and Q_{22}^2 order parameters remain low, and are lower than the values obtained for $N = 512$ systems due to the averaging of more clusters. A snapshot of the system at $P^* = 1.31$ is shown in Fig. 3.29, showing the number and assorted orientations of the long axes of the molecules within these clusters.

The pair correlation functions given in Fig. 3.28 show the level of structural ordering within the clustered systems at the same pressure between the different system sizes. The higher first peak for the $N = 4096$ system indicates that the typical size of the formed clusters is larger, similar to the formation of larger smectic groups in systems with wider molecular bends.

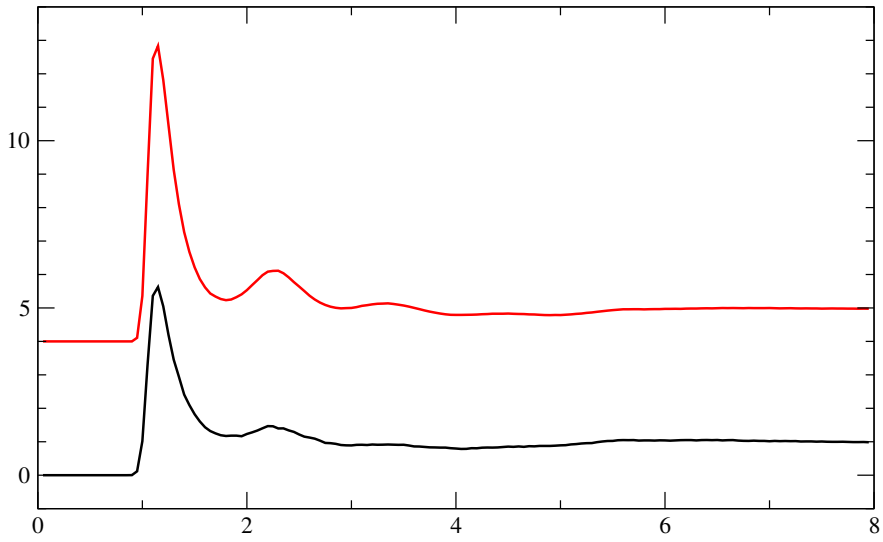

Figure 3.28: Pair correlation functions for $\theta = 130^\circ$ 11-bead molecules at $P^* = 1.39$, in system sizes of $N = 512$ (bottom, black) and $N = 4096$ (top, red). Lines have been vertically offset for clarity.

As shown with the decompression of smaller systems in Sec. 3.3.4, better equilibration may be achieved by repeated decompression and compression around the transition pressure. However, the presence of the clusters in the larger system, even with smaller pressure steps, suggests that the smectic phases are not achievable with compression alone.

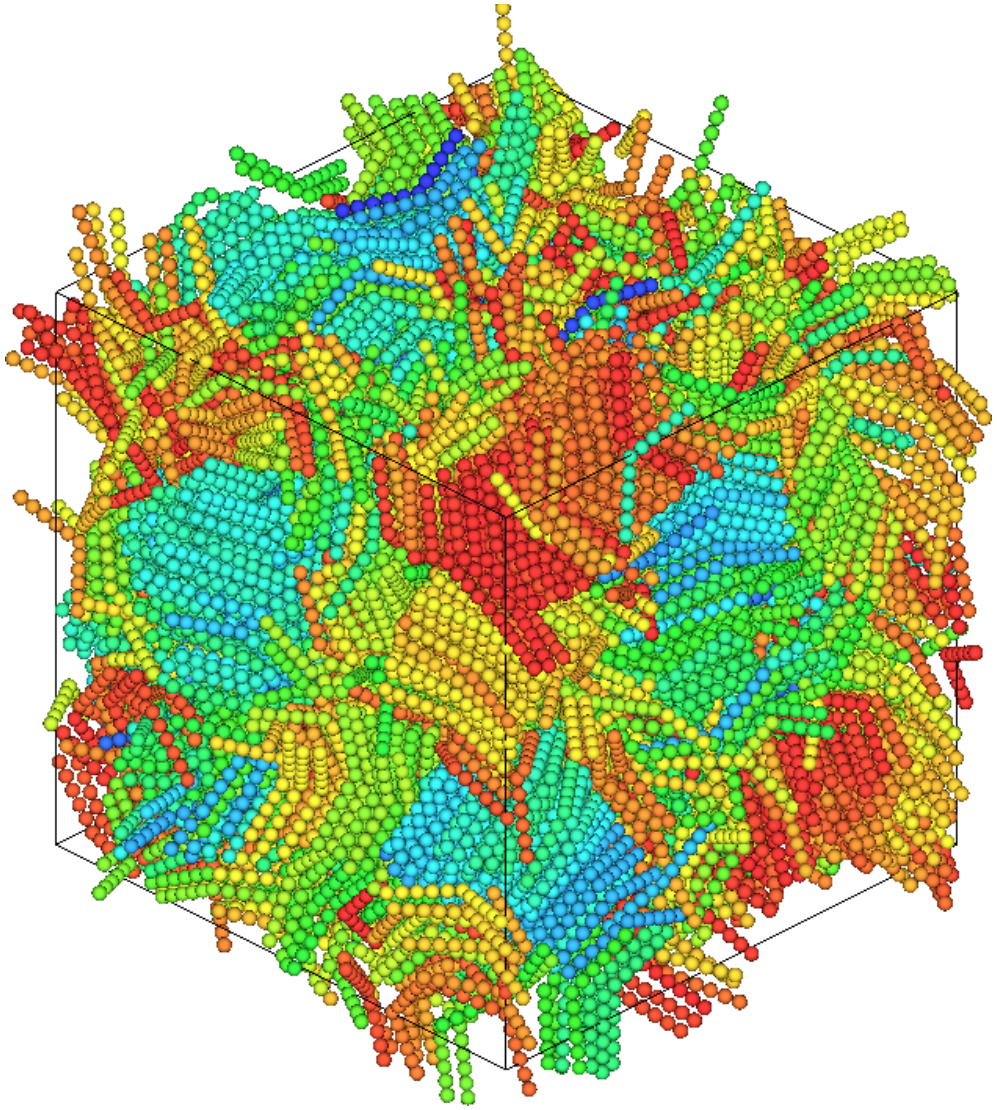

Figure 3.29: Snapshot from a compression run of $N = 4096$ 11-bead molecules with a bend angle of $\theta = 130^\circ$ at $P^* = 1.31$. Molecules are coloured based on the orientation of their long axis.

3.5 Conclusions

In this chapter we have used molecular dynamics simulations to study the phase behaviour of systems of 11-bead bent core molecules under compression, and compared the results to existing theory. A range of molecular bend angles have been used, and the effects of finite system size have been studied by performing a small number of simulations using a greatly increased number of molecules.

For molecules with a bend angle of $\theta \geq 140^\circ$, phase behaviour including isotropic, uniaxial nematic and smectic A phases have been observed. The pressure at which these phases spontaneously appear depends on the angle between the molecular arms, which governs the level of biaxiality of the molecule. As the level of biaxiality increases, the nematic phase becomes narrower and the pressure required to reach the isotropic–nematic phase transition increases. At $\theta = 140^\circ$, the molecules are close to the threshold where the uniaxial nematic phase is no longer exhibited, and considerably higher pressures are required for systems to undergo a transition to a single, well-aligned uniaxial nematic phase.

For those systems that have a uniaxial nematic phase on compression, a smectic A phase follows, with strong in-layer polarization seen for bend angles of $\theta = 160^\circ$ and $\theta = 140^\circ$. The formation of the smectic layers depends strongly on the size of the simulation cell, and too small a simulation cell can result in many smectic clusters offset by half a molecule length in order to optimize packing.

Below a critical angle of $\theta \approx 130^\circ$, the uniaxial nematic phase does not appear upon compression. Instead, the short axes of the molecules drive the formation of clusters, without a common global alignment vector between the clusters. Decompression simulations indicate that a smectic phase might be achieveable with repeated increases

and decreases in the system pressure, but it appears to be very difficult to reach using compression alone.

With the exception of the inability to reach a smectic phase directly from the isotropic phase below a critical angle, these results fit very well with the phase behaviour seen by Lansac *et al.* in their phase diagram for the melting of hard spherocylinder dimer crystals with arm length of $L/D = 5$ [71], despite using a soft, composite model and completely different simulation technique.

The disappearance of the nematic phase at $\theta \approx 130^\circ$ suggests that the existence of the biaxial nematic cannot be achieved using this exact model, as the theoretical phase diagram indicates that we need the uniaxial nematic to extend towards the region of $\theta \approx 110^\circ$. As the theoretical phase diagram for the biaxial nematic is in the Onsager limit of $L \gg D$, the ratio L/D likely plays a large importance in the width of the liquid crystal phases across both pressure and angle.

By varying the number of beads within our molecules, we can easily adjust the effective L/D ratio of the arms of our molecules in discrete units. Simulations that explore the effect of changing this number of beads will be explored in the following chapter.

Chapter 4

Effect of arm length on bent-core mesogen phase behaviour

In the previous chapter we used a fixed size of bent-core mesogen to determine how the bend angle θ between the two arms of the molecule affects the resulting phase behaviour. A strong relationship between the two was demonstrated, with a loss of a uniaxial nematic phase for angles of $\theta > 135°$. As mentioned at the start of Chapter 3, excluded volume theories for molecules with an arm length of $L \gg D$ suggest that the uniaxial nematic phase should be seen right the way up to the biaxial nematic phase bounary, close to $\theta = 110°$ [69]. It is therefore clear that the L/D ratio must play a large part in the phase behaviour of bent-core mesogens.

We can compare the effect of modifying L/D to our results from Chapter 3 by making alterations to our choice of mesogenic model as previously defined in Sec. 3.2.1. By adding or removing beads to the molecule, the L/D ratio of the arms can be changed. An example of a 7-bead molecule is shown in Fig. 4.1, shaded in grey.

Reducing the L/D ratio of the arms affects the overall biaxiality of the molecule. The dashed circles in Fig. 4.1 show the difference between an 11-bead molecule and a 7-bead molecule. The ratio of the long axis to the short axis of the molecule ($\mathbf{a} : \mathbf{b}$) is not affected by the reduction in the number of beads. However, the ratio of the short axis to the thickness of the molecule ($\mathbf{b} : \mathbf{c}$) is decreased, and therefore the deviation from cylindrical rotational symmetry is reduced.

In order to perform a systematic study of the combined effects of arm length and bend angle, in this chapter we will present the phase behaviour exhibited by systems of 9-, 7- and 5-bead bent-core mesogens.

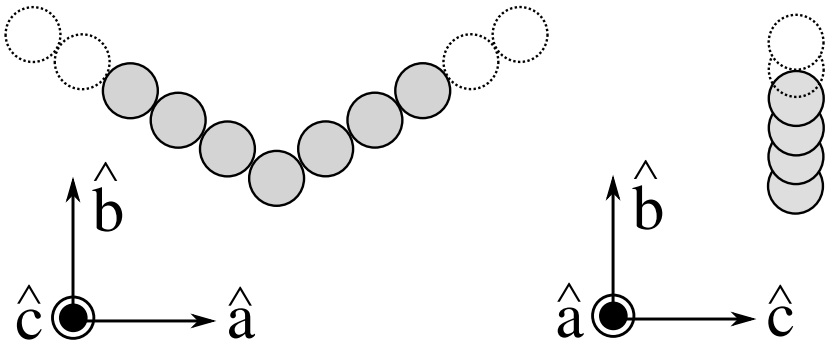

Figure 4.1: A front and side view of a 7-bead bent-core molecular model assembled out of spherical potentials, showin in grey. The dotted circles show the effect of changing the L/D ratio of the molecule by adding more potentials.

4.1 Background

The effect of the L/D ratio on the phase behaviour of linear mesogenic molecules has been well-studied. The earliest molecular dynamics works in the 1950s by Alder, Wainright, Wood and Jacobson [36, 37] were effectively a study of molecules with

$L/D = 0$, showing the presence of isotropic liquid and crystalline solid phases. Even earlier theoretical work in the 1940s by Lars Onsager showed that thin needle-like particles (where $L \gg D$) were capable of an isotropic to nematic phase transition at sufficiently high densities [83].

Monte Carlo simulations of linear molecules with more reasonable values of $L \sim D$ began with the work of Vieillard-Baron [84]. Simulations were performed on systems of hard spherocylinders with a ratio of $L/D = 2$, in order to test the validity of the predictions made by scaled-particle theory [85]. It was found that the isotropic–nematic transition densities predicted by the theory were too low, and their simulations remained in the isotropic state.

A range of L/D ratios for the hard spherocylinder mesogen were first simulated by Stroobants *et al*. They indicated that nematic, smectic and columnar mesophases all had some degree of metastability depending on the molecular ratio [86], albeit with the mesogens unable to rotate from a perfectly parallel alignment. Veerman and Frenkel examined a range of hard spherocylinder systems with ratios between 0 and 5 with the addition of free rotation, and found that the onset of nematic and smectic mesophases regions occurs in the $3 \leq L/D \leq 5$ range of ratios [87]. A more detailed study by McGrother *et al.* determined that, within the $3 \leq L/D \leq 5$ window, the I–SmA–solid triple point occured at a lower L/D ratio than the I–N–Sm triple point [62]. A finer detailed study by Bolhuis and Frenkel established that the onset of smectic and nematic phases occurs at $L/D = 3.1$ and $L/D = 3.7$ respectively [88]. A reproduction of their phase diagram is shown in Fig. 4.2

They also predicted that the stability of the nematic phase relative to the smectic phase increased with larger L/D, with the transition density between the isotropic and nematic phases dropping significantly with increased elongation. They also suggested

that two solid behaviours would be observed as $L/D \to \infty$ – at lower ratios, the tips of the molecules between crystal layers would interdigitate and the layers would be offset slightly. This behaviour changes in favour of the spherocylinders lying end-to-end at higher elongations.

Besides hard spherocylinders, other molecular models have also been studied. de Miguel and coworkers have studied the phase behaviour of Gay-Berne molecules with a $3 : 1$ aspect ratio in some depth, and have and accurately mapped out the phase diagram to include nematic and smectic B mesophases [89, 90, 91]. Brown *et al.* performed a more systematic study over a range of Gay-Berne aspect ratios, and showed that a small region of smectic A stability occurs for aspect ratios of $3.2 : 1$ and upwards [92]. They also note that there is no obvious transition between the smectic B

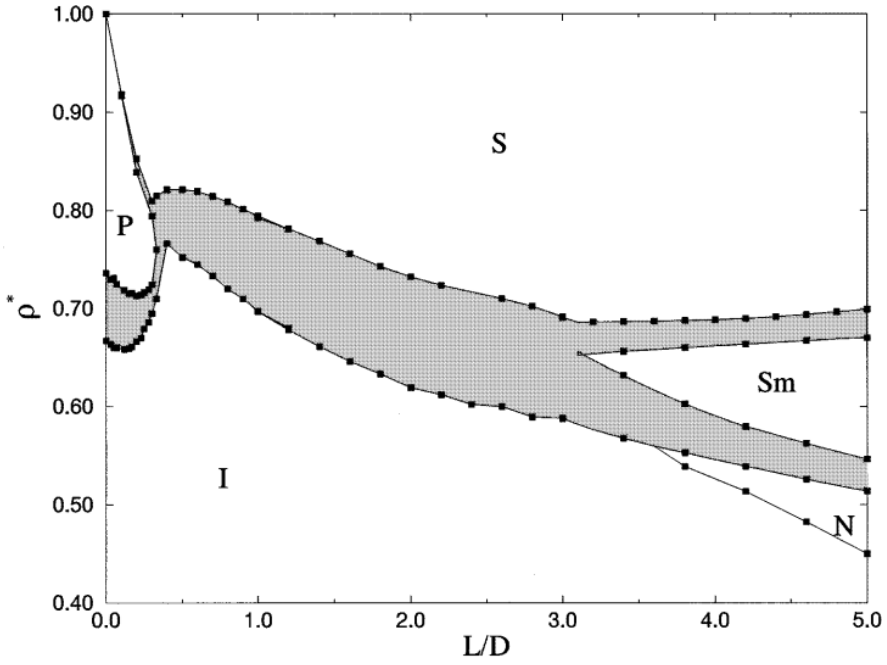

Figure 4.2: A reproduction of the phase diagram of number density against L/D ratio for hard spherocylinders by Bolhuis and Frenkel [88]. Labelled regions are isotropic (**I**), nematic (**N**), smectic (**Sm**), crystal solid (**S**) and plastic solid (**P**).

and crystal phases upon melting, indicating that they may be the same phase.

There have also been a number of studies on elongated molecules constructed from fused spherical components. Vega *et al.* studied systems of rigid linear molecules assembled from between 3 and 7 hard spheres [93]. For systems of less than 5 spheres, no liquid crystal mesophases were observed; for 5 to 6 bead molecules, a smectic A mesophase was observed; and both nematic and smectic phases were observed for systems of 7 bead molecules.

Equivalent models constructed out of hard spheres include the work of Perera and Sokolic [94] and Galindo *et al.* [95]. The work of Perera and Sokolic used molecules assembled from 2, 3 and 5 Lennard-Jones potentials fused at a separation of 0.5σ (such that the minimum of one potential was located at the center of its neighbour). These were equivalent to L/D ratios of 0.5, 1 and 2 respectively. No mesophases were seen, only isotropic and ordered solid phases [94]. Galindo *et al.* used Lennard-Jones potentials with a separation of σ, fused into rigid linear chains of 3 and 5 potentials (effective L/Ds of 2 and 4), and equally saw no liquid crystal mesophases [95]. Longer chains constructed from WCA potentials have been shown to give nematic and smectic mesophases as studied by Cinacchi *et al.* [96], using 9 potentials separated by 0.6σ, equivalent to an L/D ratio of ≈ 4.8. The early work by Paolini *et al.* showed the presence of nematic and smectic behaviours with linear repulsive molecules constructed from 11 beads with a separation of 1.2σ, giving a ratio closer to $L/D \approx 12$ [76].

There has been little work to systematically study the effects of arm lengths on a bent-core mesogen using a single type of interaction potential. Camp *et al.* [67] examined phase behaviour of a number of different bend angles using hard spherocylinder dimers with individual ratios of $L/D = 2$ per arm, while Lansac *et al.* [71] mapped out the entire phase diagram for dimers with $L/D = 5$ per arm. Dewar and Camp have also

studied the mesophases of composite molecules assembled from seven Lennard-Jones potentials at a selection of bend angles [77].

In this chapter, we extend the results from Chapter 3 for our model of a bent-core mesogen. Using molecular dynamics simulations, we study a parameter space increased to include the number of beads per mesogen arm. For each variant of molecule, we perform a sweep of both bend angle and pressure values.

4.2 Simulation method

Results in this chapter are obtained from a similar method to that outlined in Sec. 3.2.3. Molecules were constructed by assembling either 5, 7 or 9 WCA spherical potentials (see Eqn. (3.2)) along two intersecting arm vectors $\widehat{\mathbf{e}}_1$ and $\widehat{\mathbf{e}}_2$, as demonstrated in Fig. 4.3. Individial beads are placed such that they are a distance of σ apart. The arrangement of beads within the molecule remain fixed relative to the two arm vectors, resulting in a molecule that is entirely rigid in shape.

As the overall shape of the molecule does not change, the same set of orthogonal vectors were used as the molecular frame of reference regardless of size, where $\widehat{\mathbf{a}}$, $\widehat{\mathbf{b}}$ and $\widehat{\mathbf{c}}$ are defined by Eqns. (3.1). The direction of the long axis of the molecule is the straight vector between the centers of the two "tip" beads, and the short axis director is the vector perpendicular to the long axis that passes through the middle of the central bead.

Systems were initialized by placing 512 identical molecules of a common arm length and bend angle on the sites of an expanded primitive cubic lattice. Lattice spacings were set such that the initial molecular density was $\rho^* \sim 0.001$, large enough to allow

free initial rotation without collision or overlaps.

Simulations were conducted using the DL_POLY_2 [82] molecular dynamics package using cubic periodic boundary conditions, velocity Verlet integration and the Nosé-Hoover thermostat and barostat, at a fixed temperature of $T^* = 1$. The initial arrangement was run under NVE conditions with a timestep of $t^* \sim 0.01$, and sampled every 10^5 timesteps to provide pseudorandom isotropic gaseous starting configurations.

Each of these configurations were used to begin a compression simulation run, where they were switched to an NPT ensemble and compressed to an isotropic liquid state below the onset of any mesophases. Equilibration was performed for 10^6 timesteps. A compression sweep then consisted of increasing the barostat by a fixed pressure step; equilibrating for 10^6 timesteps; checking that values for order parameters and densities had settled; then either equilibrating further, or sampling the system configuration 100

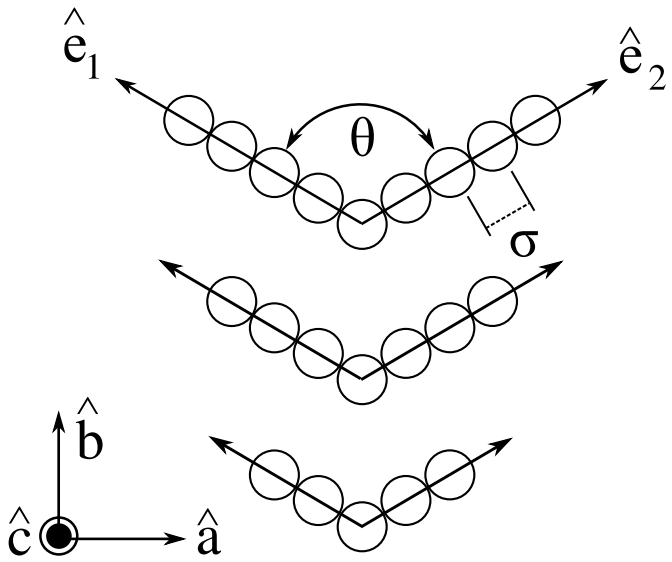

Figure 4.3: A representation of 9-bead (top), 7-bead (middle) and 5-bead (bottom) bent-core molecules, with a set of common orthogonal frame vectors. The centres of the spherical potentials along an arm vector are separated by a distance σ.

times over the next 10^6 timesteps. Each sequential pressure step was initialized using the final molecular configuration generated by the previous run.

4.3 9-bead molecules

Simulations using 9-bead molecules were conducted for a range of different bend angles in the interval $160^\circ \leq \theta \leq 130^\circ$. The thermostat temperature was fixed at $T^* = 1$ while the system was compressed from an initially isotropic state at a pressure of $P^* = 0.17$. In each instance, five distinct trajectories were used in order to obtain error estimates for calculated parameters, and to ensure any observed phase behaviour was not unique to a specific configuration.

To broadly summarize the results obtained from these simulations, a plot of the uniaxial order parameters Q^2_{00} is shown in Fig. 4.4. This illustrates the mean values for Q^2_{00} with respect to the reduced pressure P^* for the bend angles of $\theta = 160^\circ$, 150°, 140° and 130°.

This plot is similar in appearance to Fig. 3.4, in that it illustrates two main points. Firstly, the transitions from an isotropic phase to a non-isotropic mesophase with a degree of common alignment occur at increasingly higher pressures as the bend angle of the mesogen is reduced. In addition, the final values of the Q^2_{00} order parameters are split at high pressures. The $\theta = 130^\circ$ systems reach a maximum value of $Q^2_{00} < 0.5$, while the high pressure Q^2_{00} values for the $\theta > 130^\circ$ systems reach maximum values of $Q^2_{00} > 0.9$. This indicates that the final arrangements of the $\theta = 130^\circ$ simulations have a significantly decreased level of uniaxial alignment in their final configurations, compared to those for $\theta > 130^\circ$.

There are a number of significant differences between the 11-bead and 9-bead plots in Figs. 3.4 and 4.4 respectively. The first is that a noticeably higher pressure required to induce the first transition from an isotropic to a non-isotropic mesophase for the $\theta > 130°$ systems – for example, the $\theta = 160°$ system at $P^* = 0.5$ appears to be isotropic in the 9-bead systems, while the systems have already transitioned to a uniaxial nematic in the 11-bead simulations. Although unclear from the Q^2_{00} values alone, the second "bump" in the values corresponding to the nematic–smectic transition is also at a significantly higher pressure, increasing from $P^* < 1.5$ for 11-bead molecules while $P^* > 2$ for the 9-bead systems. Finally, the Q^2_{00} values are slightly lower in the region corresponding to the uniaxial nematic phases for the 11-bead systems. This indicates that there is a lower level of orientational alignment in the uniaxial nematic phase in the 9-bead systems.

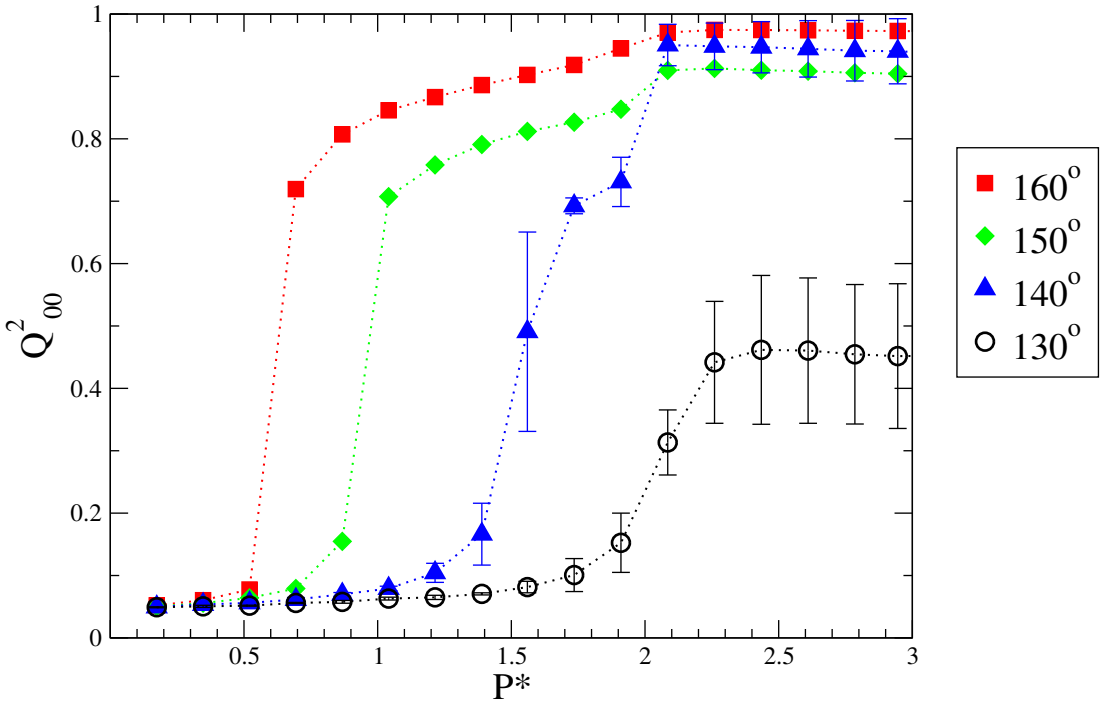

Figure 4.4: The change in the uniaxial order parameter Q^2_{00} with increasing pressure P^* for four different systems of $N = 512$ 9-bead molecules. Legend values correspond to the molecular bend angle θ.

We will now show direct comparisons between the results for our simulations of 11-bead and 9-bead molecules at identical bend angles for the $\theta = 160°$, $140°$ and $130°$ systems.

4.3.1 $\theta = 160°$

The values for the equations of state in both the 9-bead and 11-bead systems are shown in Fig. 4.5, while their uniaxial and biaxial nematic order parameters Q^2_{00} and Q^2_{22} are compared in Fig. 4.6. Due to the different molecular sizes, the isotropic liquid phases are fitted to two different curves determined from Eqn. (2.31). As predicted by theory, the smaller molecules reach higher numerical densities for the same pressure, and as such the isotropic liquid phases are not coincident.

As with the 11-bead molecules, the equation of state for the 9-bead molecules shows two phase branches beyond the initial isotropic phase. The first transition occurs in the pressure window $0.52 < P^* < 0.69$, where the points break from the isotropic liquid theory. This is accompanied by a sharp increase in the uniaxial order parameter from $Q^2_{00} < 0.1$ to $Q^2_{00} \approx 0.7$, while the biaxial order parameter Q^2_{22} remains low. This indicates the presence of a uniaxial nematic phase – a snapshot of a system at $P^* = 0.69$ is shown in Fig. 4.7a.

A second phase transition occurs as the pressure is increased through the range $1.74 < P^* < 1.91$. A snapshot of a system at a pressure of $P^* = 1.91$ is shown in Fig. 4.7b. There is a small bump in the upward trend of Q^2_{00} at this point, while the Q^2_{22} begins to increase from $Q^2_{22} < 0.1$ towards 0.7 at the highest pressures. This is the same transition to a smectic-like offset layered phase as seen for the simulations of 11-bead molecules. Comparisons of the 11-bead and 9-bead pair correlation functions

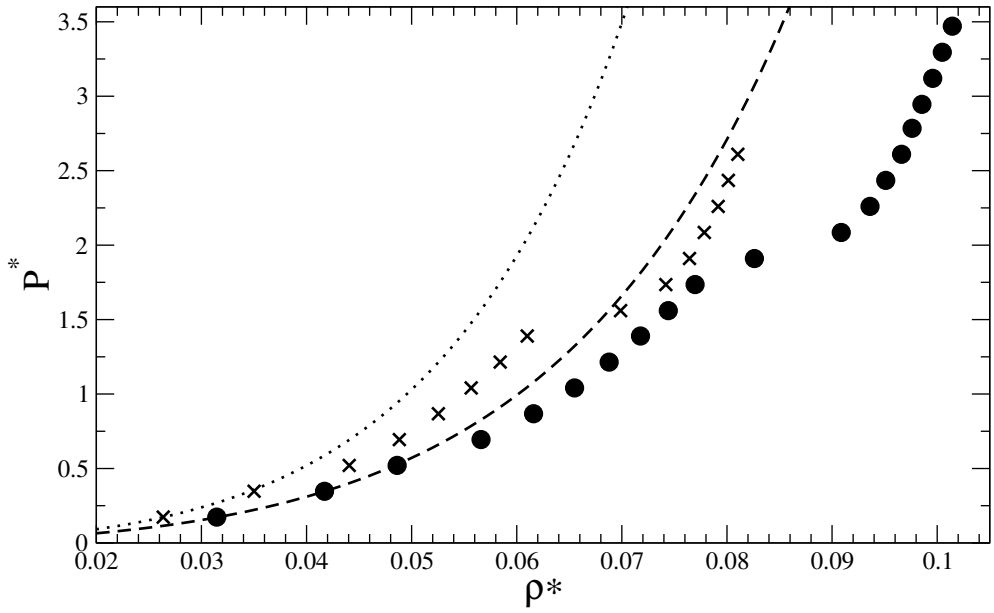

Figure 4.5: The equations of state for systems of 512 9-bead (circles) and 11-bead (crosses) $\theta = 160^\circ$ molecules on compression. The lines indicate the theoretical liquid equations of state for the 9-bead (dashed) and 11-bead (dotted) systems. Error bars are smaller than symbol size.

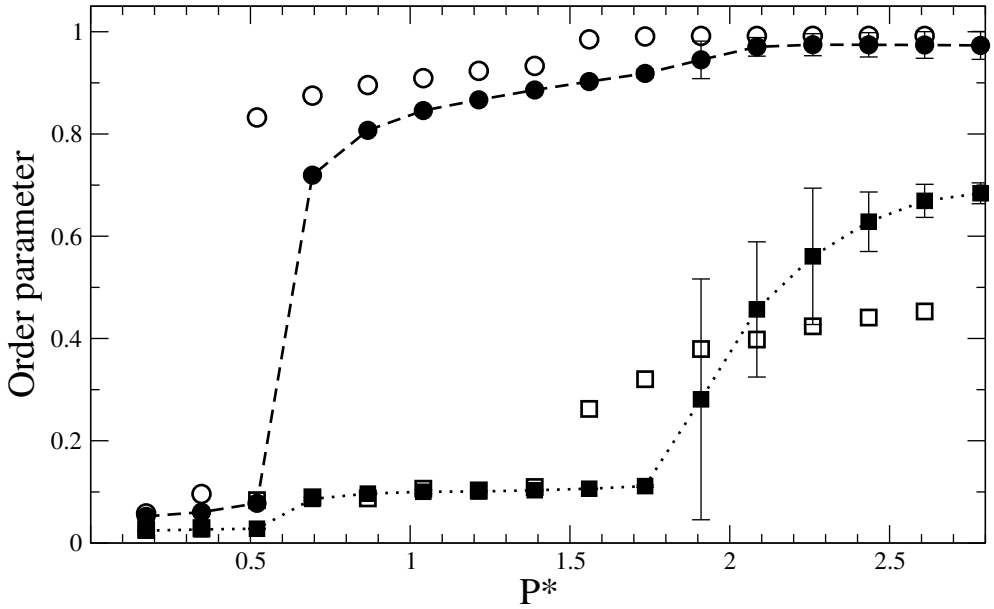

Figure 4.6: The uniaxial (circles) and biaxial (squares) order parameters for systems of 512 9-bead (filled) and 11-bead (hollow) $\theta = 160^\circ$ molecules on compression. Errors bars have been omitted from the 11-bead points for clarity.

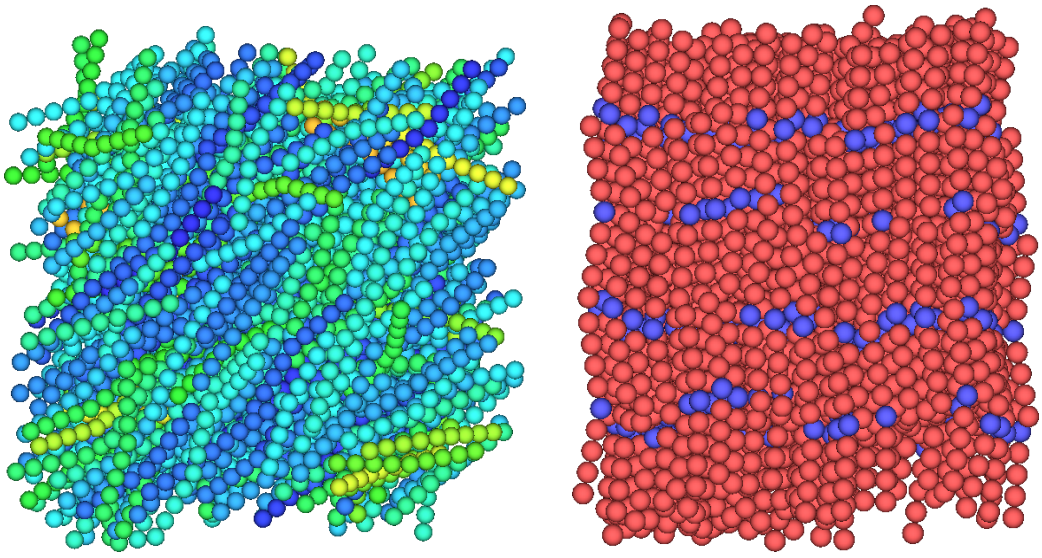

(a) $P^* = 0.69$ (b) $P^* = 1.91$

Figure 4.7: Snapshots from a compression run of 512 9-bead molecules with a bend angle of $\theta = 160°$, showing (a) nematic and (b) smectic-like mesophases.

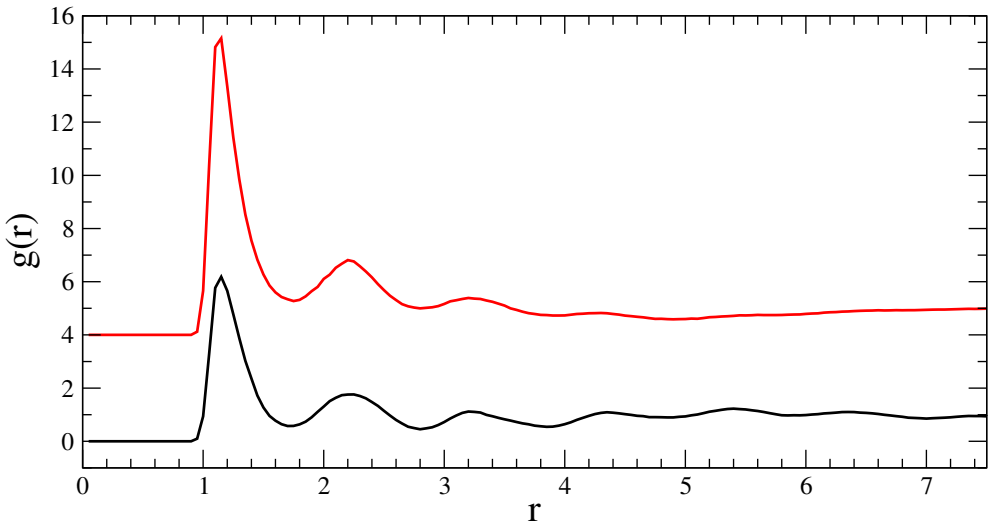

Figure 4.8: The pair correlation function between 512 $\theta = 160°$ molecules in a system of 9-bead molecules at $P^* = 1.91$ (bottom, black) and of 11-bead molecules at $P^* = 1.56$ (top, red). The plots have been vertically offset for clarity.

are shown in Fig. 4.8, which illustrates similar molecular structure for as far as $g(4)$, the distance from the central bead to the outer extent of a 9-bead molecule's arm. The slowly increasing Q_{22}^2 parameter is again related to the polarization of the clusters, which becomes more pronounced as the system is compressed and the "knuckles" fit inside one another. The larger value of the parameter indicates that the relative polarization is larger, due to the smaller number of clusters that occur when using a smaller molecule size but the same quantity of molecules in total.

Overall, we can see that the 11-bead and 9-bead 160° molecules share similar phase behaviour. However, the onset pressure for the emergence of a uniaxial nematic phase is increased, as is the transition pressure to a smectic-like phase. The main modification to the phase behaviour with shorter 160° molecules is that the uniaxial nematic phase has been broadened slightly.

4.3.2 $\theta = 140^\circ$

The equations of state for 9-bead and 11-bead molecules with an internal bend angle of 140° are shown in Fig. 4.9 along with their respective theoretical liquid density curves. Their Q_{00}^2 and Q_{22}^2 order parameters are simultaneously shown in Fig. 4.10.

There are again two phase transitions observed through the equation of state for the 9-bead molecules. The first is relatively small and occurs in the pressure window $1.39 < P^* < 1.56$. The change in density is quite small, and is only observable from the fact that the calculated values no longer fit to the theoretical isotropic liquid curve. There is then a much stronger phase transition as the system is compressed slightly further, occuring in the range $1.91 < P^* < 2.08$.

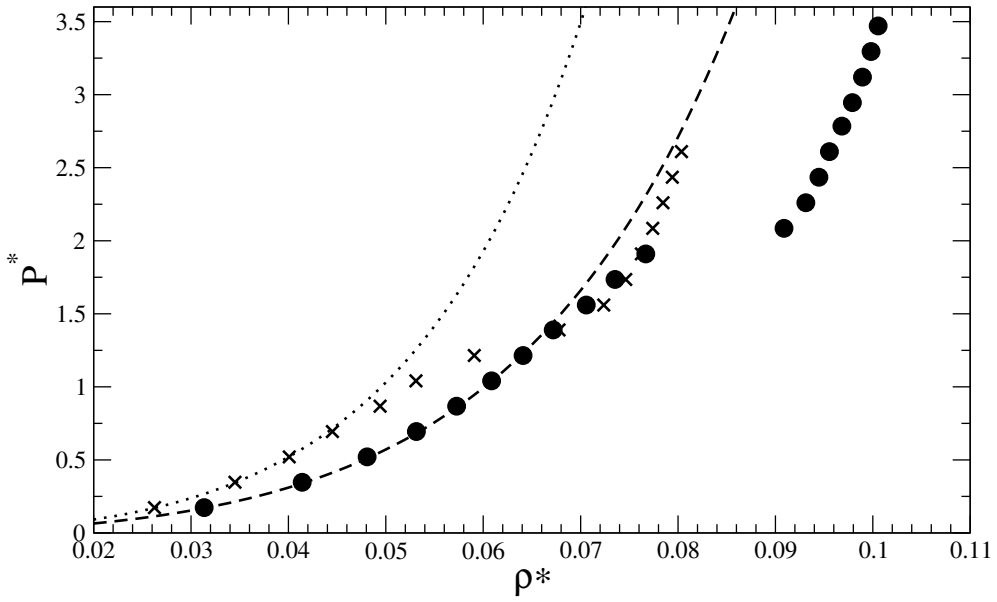

Figure 4.9: The equations of state for systems of 512 9-bead (circles) and 11-bead (crosses) $\theta = 140^\circ$ molecules on compression. The lines indicate the theoretical liquid equations of state for the 9-bead (dashed) and 11-bead (dotted) systems. Error bars are smaller than symbol size.

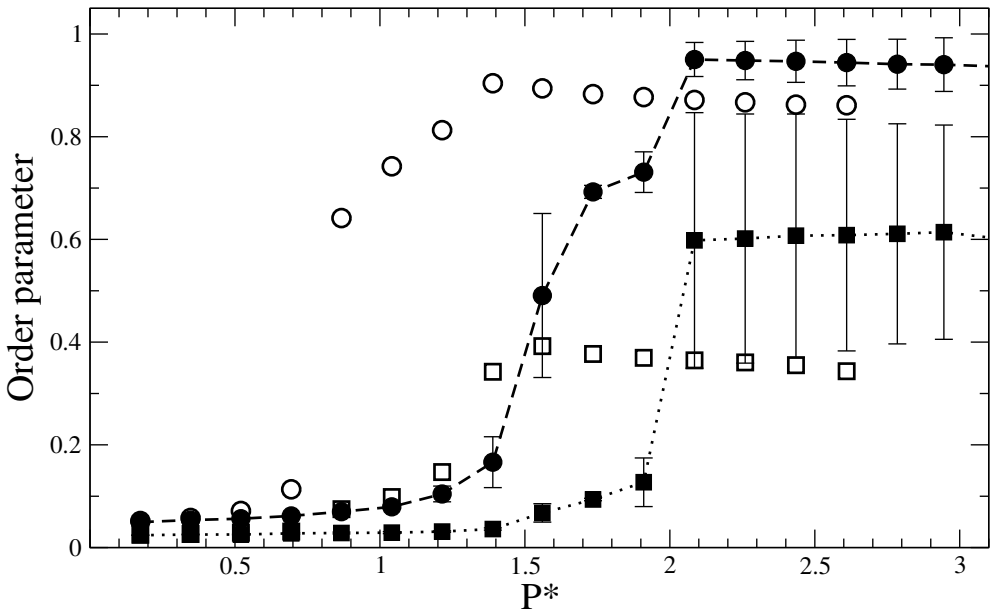

Figure 4.10: The uniaxial (circles) and biaxial (squares) order parameters for systems of 512 9-bead (filled) and 11-bead (hollow) $\theta = 140^\circ$ molecules on compression. Errors bars have been omitted from the 11-bead points for clarity.

The first of these transitons is from the isotropic to the uniaxial nematic, as shown by the increase in the Q_{00}^2 order parameter. The value of the parameter does not increase in one large jump, but is instead a slower increase, similar to the behaviour observed in large systems of 11-bead, $\theta = 140°$ mesogens as described in Sec. 3.4.2. A snapshot of a system in the nematic phase at $P^* = 1.56$ is shown in Fig. 4.11a, showing the system with a moderate level of nematic ordering.

The more distinct second transition to a offset smectic is indicated by a sudden jump in the uniaxial order parameter to $Q_{00}^2 > 0.9$, as well as a sharp increase in the biaxial nematic order parameter due to the polarization of the small number of clusters. This phase is shown in Fig. 4.11b. The large spread in values is due to the variation in cluster sizes and orientations across different trajectory runs.

Both the Q_{00}^2 and Q_{22}^2 values show higher degrees of alignment in the 9-bead system

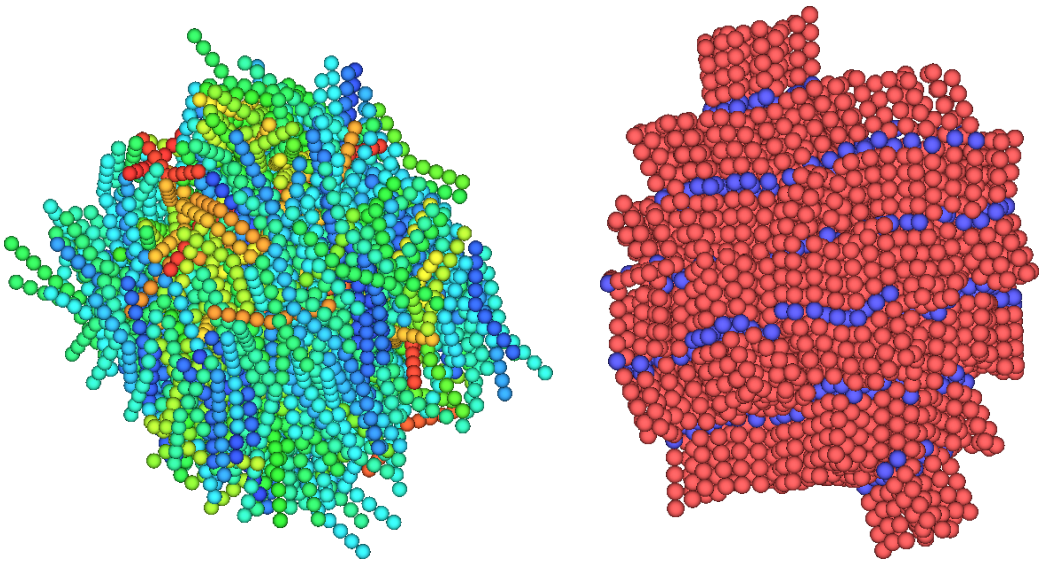

(a) $P^* = 1.56$ (b) $P^* = 2.08$

Figure 4.11: Snapshots from a compression run of 512 9-bead molecules with a bend angle of $\theta = 160°$, showing (a) nematic and (b) smectic-like mesophases.

compared to the 11-bead system. In Sec. 3.3.2 the decreasing value of Q_{00}^2 at high pressure was attributed to the "zig-zag" fashion in which neighbouring clusters aligned, dictated by the angle at which the upper arm of a molecule is aligning with the lower arm of the next layer. As the 9-bead molecules are shorter, neighbouring arms are not pushed so far from the global alignment director in order to align, and so the overall uniaxial alignment of the system is improved.

As with the 9-bead, $\theta = 160^\circ$ molecules, the phase behaviour is not notably different from the 11-bead phase behaviour. The slower increase of the Q_{00}^2 order parameter is observed in the larger simulations of 4096 11-bead molecules, and is indicative that the long axis of the molecule is close to the shortest limit in which it can induce a nematic phase by itself. Both transitions occur at much higher pressures for 9-bead molecules than for 11-bead molecules.

4.3.3 $\theta = 130^\circ$

Figures 4.13 and 4.14 show the equations of state and order parameters respectively for systems of 512 11-bead and 9-bead, $\theta = 130^\circ$ molecules upon compression. The 9-bead systems show the presence of only a single phase transition, occuring in the pressure window $1.74 < P^* < 1.91$. The values of Q_{00}^2 and Q_{22}^2 remain low after the transition, indicating a very similar level of alignment compared to the 11-bead molecules at the same bend angle.

Visual inspection of the phase at $P^* = 2.08$ (Fig. 4.12) indicates that the molecules are beginning to align into clusters through their short axes, in the absence of a global long axis director. This is the same as the "jammed" smectic phase behaviour observed in Sections 3.3.3 and 3.4.3 for 11-bead systems of 512 and 4096 $\theta = 130^\circ$ molecules,

corresponding to the isotropic–smectic transitions determined in melting simulations by Lansac *et al.* [71]. Once again, the phase behaviour is nearly identical to that of 11-bead molecules, with the exception that the transition pressure has been significantly elevated.

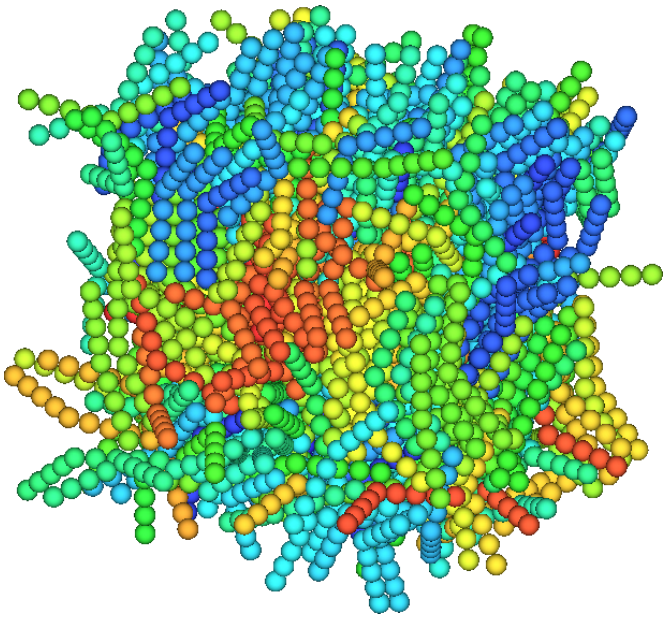

Figure 4.12: Snapshot of a compression run of 512 9-bead molecules with a bend angle of $\theta = 130^\circ$ at a pressure of $P^* = 2.08$.

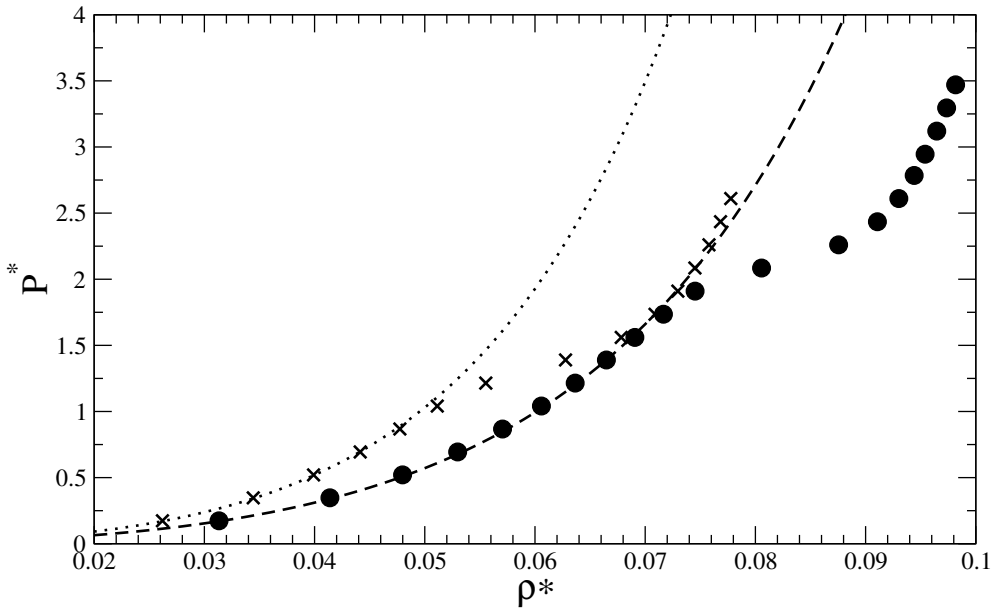

Figure 4.13: The equations of state for systems of 512 9-bead (circles) and 11-bead (crosses) $\theta = 130^\circ$ molecules on compression. The lines indicate the theoretical liquid equations of state for the 9-bead (dashed) and 11-bead (dotted) systems. Error bars are smaller than symbol size.

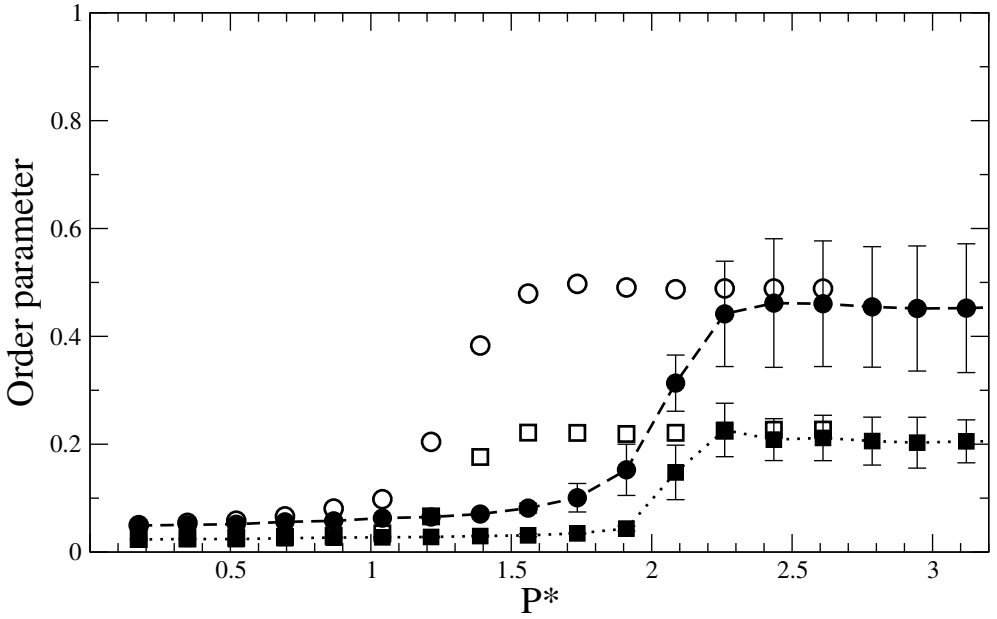

Figure 4.14: The uniaxial (circles) and biaxial (squares) order parameters for systems of 512 9-bead (filled) and 11-bead (hollow) $\theta = 130^\circ$ molecules on compression. Errors bars have been omitted from the 11-bead points for clarity.

4.3.4 Summary

Table 4.1 summarizes the transition pressure windows for the phase behaviour seen in simulations of 9-bead molecules in the range $160^\circ \leq \theta \leq 140^\circ$, of which the 160° and 140° systems have been more fully explained. Intermediate bend angles were analysed in similar ways and their phases determined to be the same, showing isotropic, nematic and offset smectic layers.

Overall, there is little effect on the relationship between bend angle and phase behaviour when reducing the mesogen size from 11 beads to 9 beads. Bend angles of $\theta \geq 140^\circ$ still exhibit isotropic, uniaxial nematic and offset smectic layer phases on compression of systems of 512 molecules. Similarly, the absence of a uniaxial nematic phase for bend angles of $\theta \leq 130^\circ$ persists, resulting in the formation of clusters with short range alignment, but without a common global alignment vector. On the other hand, the relationship between phase behaviour and pressure is greatly changed, with much higher system pressures being required to induce spontaneous alignment between molecules. The overall width of the nematic phase is also altered. Towards more linear molecules the nematic phase is seen to broaden, while the width of the phase remains relatively constant for bend angles of $\theta \approx 140^\circ$.

θ	$\rightarrow$ N	$\rightarrow$ Sm
160°	0.52 – 0.69	1.74 – 1.91
155°	0.69 – 0.87	1.74 – 1.91
150°	0.69 – 0.87	1.91 – 2.08
145°	1.04 – 1.21	1.91 – 2.08
140°	1.39 – 1.56	1.91 – 2.08

Table 4.1: The transition windows to nematic and smectic-like phases for systems of $N = 512$ 9-bead molecules on compression.

4.4 7-bead molecules

Simulations of systems of 7-bead molecules were conducted using a range of different bend angles in the interval $160^\circ \leq \theta \leq 130^\circ$ using a fixed thermostat temperature of $T^* = 1$. Due to the elevated transition pressures that occured as a consequence of shortening the molecule in the previous section, we increased the starting pressure of the simulations to $P^* \approx 0.27$ and increased the size of the pressure step likewise. All simulations still began from an initially disordered isotropic liquid state. Error estimates on calculated values were determined by averaging across the results obtained from five distinct trajectories.

The mean values for the uniaxial order parameters Q_{00}^2 against reduced pressure P^* for each set of bend angle runs are shown in Fig. 4.15. As with both the 11-bead and 9-bead molecules, the high-pressure behaviours are split into two regions, one of high uniaxial alignment in the region $Q_{00}^2 > 0.9$, and a second of reduced alignment where $Q_{00}^2 < 0.5$. The pressures required to induce the initial alignment changes are elevated once again – the first significant uniaxial ordering of the $\theta = 160^\circ$ systems does not occur until pressures in excess of $P^* = 1.5$.

The most significant change is that the $\theta = 140^\circ$ systems no longer show a good level of uniaxial alignment, and the value of Q_{00}^2 remains below 0.5 at pressures as high as $P^* = 4$. There is also significant error on the results, indicating an inconsistent level of alignment between systems.

The equation of state for the systems of 7-bead $\theta = 140^\circ$ molecules is shown in Fig. 4.16, fitted against the theoretical liquid equation of state for 7-bead polymers from Eqn. (2.31). It should be noted that the equation is no longer such a good fit for the data at low pressures – it appears to slightly overestimate the number density for

the range $1 < P^* < 3$. However, it still provides a clear indication of the branching of the equation of state as the system undergoes a phase transition in the pressure window $3.28 < P^* < 3.54$.

The presence of a single branch at high pressure indicates that there is a loss of a liquid crystal phase compared to the 9-bead and 11-bead, $140°$ systems. This branch occurs at the upper end of our pressure sweep, which could suggest that further phases could exist beyond the pressures explored. However, a comparsion between the pair correlation functions for the 9-bead and 7-bead systems is shown in Fig. 4.17, just after the first phase transition in each system. Small differences in the pair correlation functions indicate the presence of different phase behaviour – the 7-bead system has a much more strongly enhanced first peak at $r \approx \sigma$ in comparison to that of the nematic

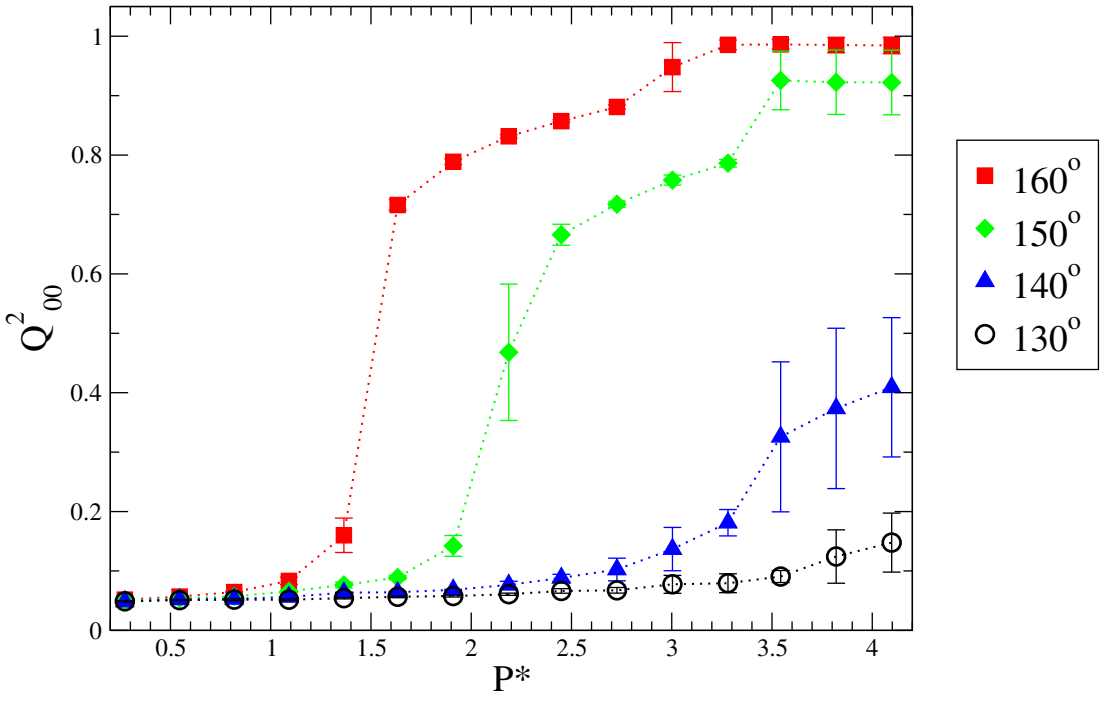

Figure 4.15: The change in the uniaxial order parameter Q^2_{00} with increasing pressure P^* for four different systems of $N = 512$ 7-bead molecules. Legend values correspond to the molecular bend angle θ.

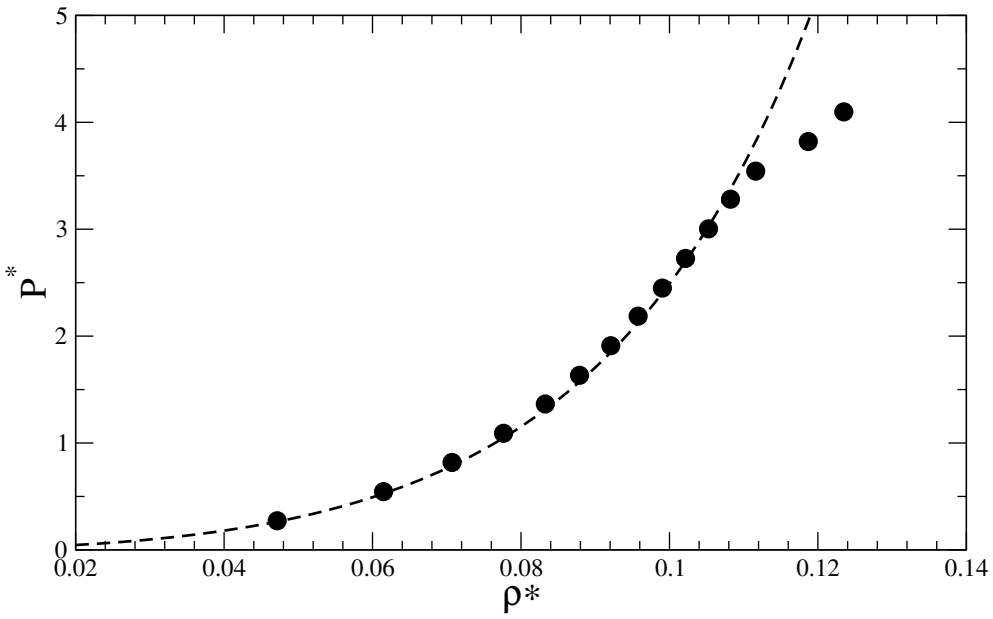

Figure 4.16: The equations of state for a systems of 512 7-bead $\theta = 140°$ molecules on compression. The dotted line indicate the theoretical liquid equation of state. Error bars are smaller than symbol size.

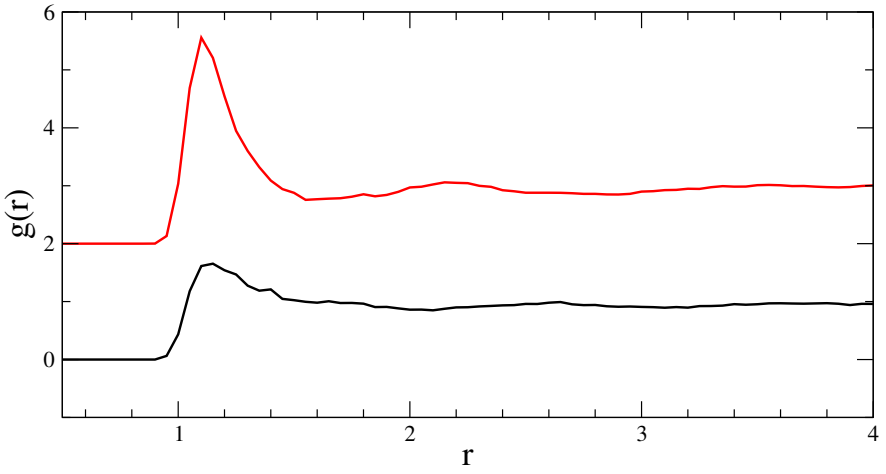

Figure 4.17: The pair correlation function between 512 $\theta = 140°$ molecules in a system of 7-bead molecules at $P^* = 3.54$ (top, red) and of 9-bead molecules at $P^* = 1.56$ (bottom, black). The plots have been vertically offset for clarity.

phase for the 9-bead system, while the presence of a small peak at $r \approx 2\sigma$ indicates the presence of a small degree of repeating structure.

Snapshots from a system at $P^* = 3.54$ are shown in Fig. 4.18, coloured two separate ways in order to highlight the long axis orientation and positions of the central beads of the molecules. It it not immediately obvious that this is not just a uniaxial nematic phase with lower alignment from simply observing the system configuration. However, the colouring on the right of Fig. 4.18 indicates that the central beads of the molecules are beginning to arrange into smectic-like clusters, as seen with narrower bend angles at larger molecule sizes.

For the simulations of 150° and 160° 7-bead molecules, the presence of two mesophases perseveres. The equation of state for the 160° molecules on compression is shown in Fig. 4.19, and indicates the presence of a first phase transition in the region $1.36 < P^* < 1.63$, followed by a second phase transition in the pressure window $2.73 <$

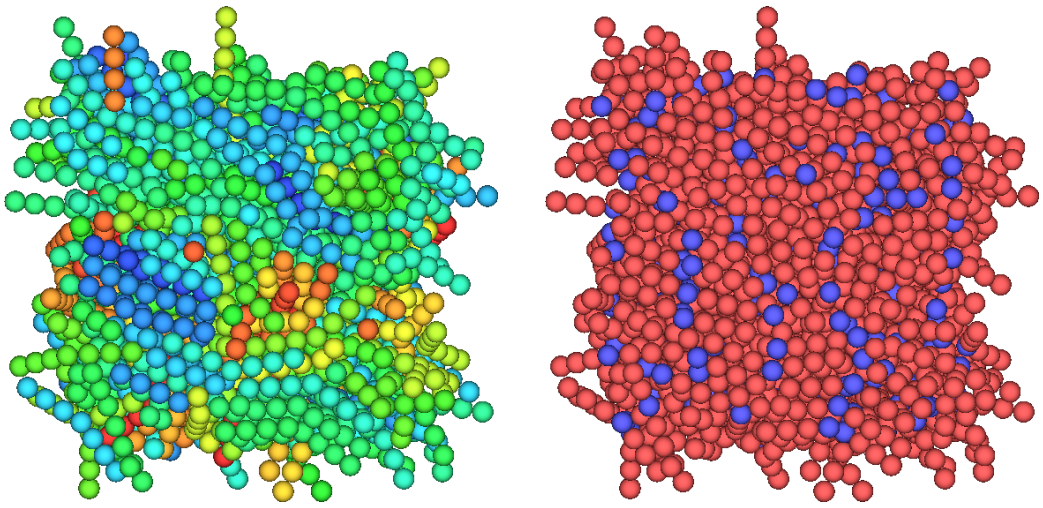

Figure 4.18: Snapshots of a system of 512 7-bead molecules with a bend angle of $\theta = 140^\circ$ and a pressure of $P^* = 3.54$. Two different colourings are used of the same system, either coloured based on long axis orientation (left) or to highlight the location of the central bead (right).

$P^* < 3.00$, corresponding to uniaxial nematic and smectic phases respectively. Similar analysis on the equation of state for the 150° simulations reveals transitions between $1.91 < P^* < 2.19$ and $3.28 < P^* < 3.54$. Snapshots of both systems just after their nematic–smectic transitions are shown in Fig. 4.20.

Interestingly, the quality of the smectic ordering across the two systems is quite different. For the 150° molecules the offset smectic layers remain, and the size of the individual clusters is smaller than for 9-bead and 11-bead systems. However, the 160° systems show completely distinct smectic layers without any arm length offsets whatsoever. A comparison of the pair correlation functions for these two snapshots is shown in Fig. 4.21. The split second peak for the 160° simulations indicates that the system is in the hexagonally packed smectic B phase immediately after transition, which is not

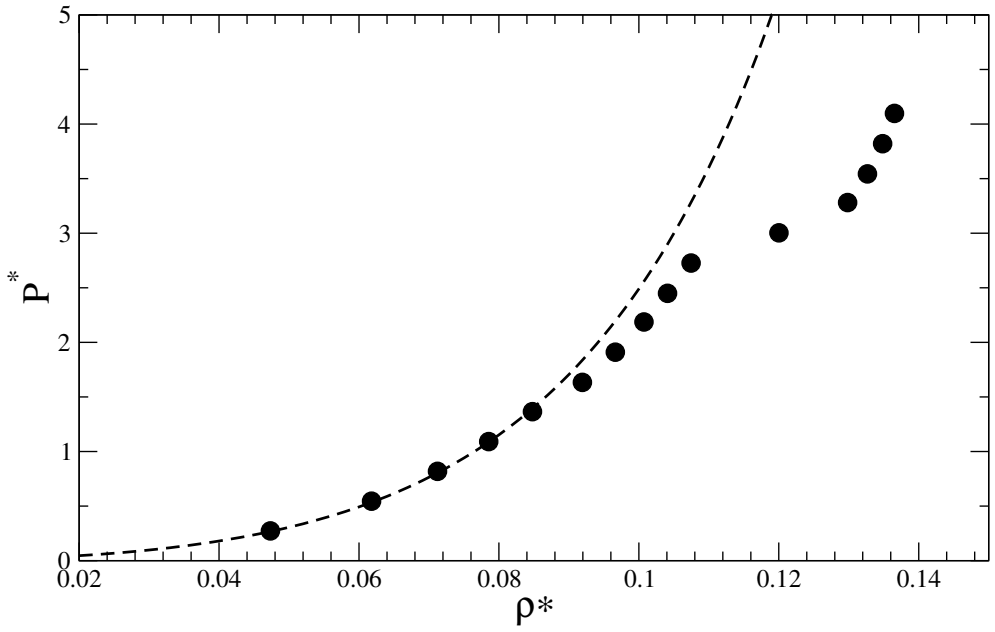

Figure 4.19: The equations of state for a systems of 512 7-bead $\theta = 160^\circ$ molecules on compression. The dotted line indicate the theoretical liquid equation of state. Error bars are smaller than symbol size.

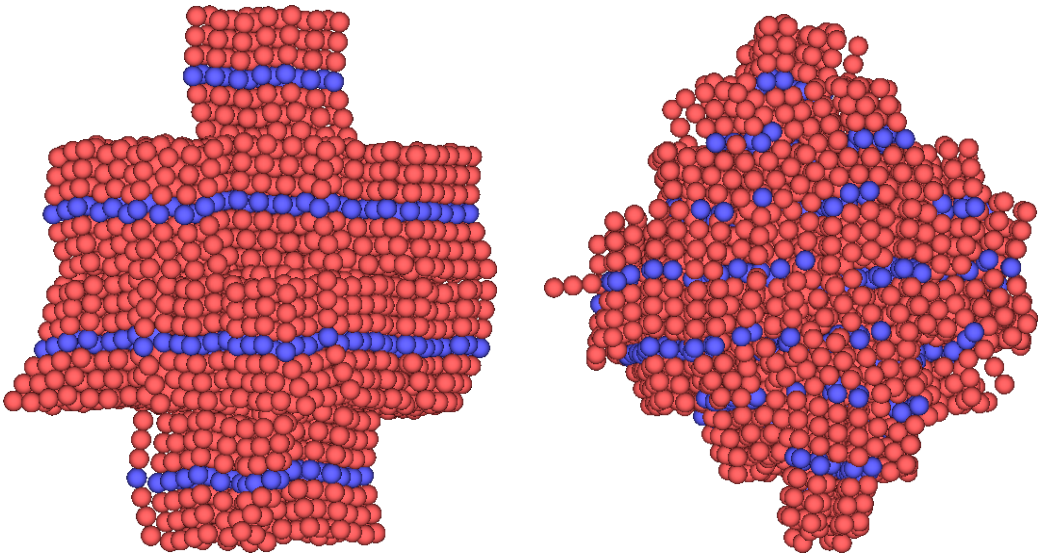

(a) $\theta = 160°, P^* = 3.00$ (b) $\theta = 150°, P^* = 3.54$

Figure 4.20: Snapshots from compression runs of 512 7-bead molecules with a bend angles of (a) $\theta = 160°$ and (b) $150°$, at pressures just after the nematic–smectic transition.

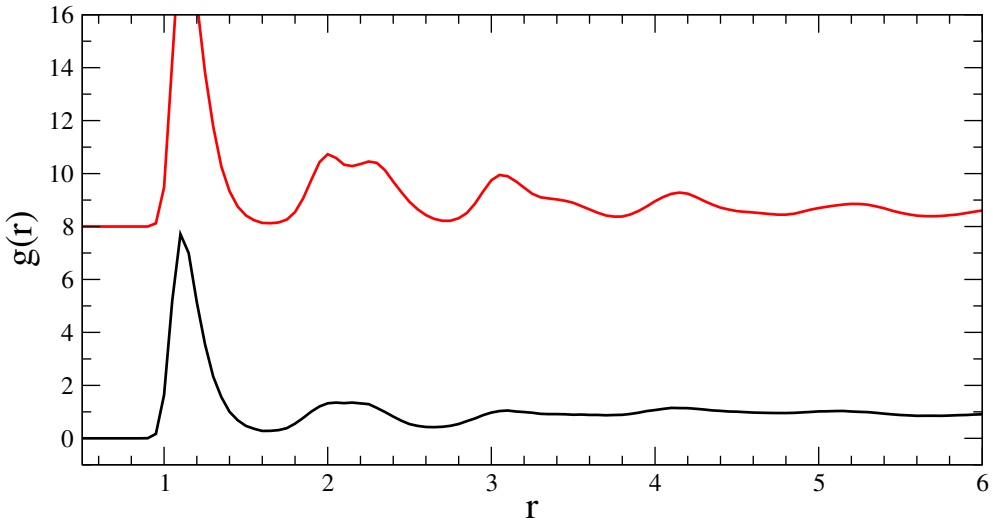

Figure 4.21: The pair correlation function between the molecules of systems of $N = 512$ 7-bead molecules of $\theta = 150°$ and $160°$ just beyond their respective nematic–smectic transitions. The $150°$ system (bottom, black) is at a pressure of $P^* = 3.54$, while the $160°$ system is at a pressure of $P^* = 3.00$. The plots have been vertically offset for clarity, and the peak of the $160°$ line at a value of 18.9 (26.9 on the offset axis) has been truncated.

true for the 150° systems. It is likely that at this size of molecule, the bend angle is sufficiently small that the mesogen now acts more like a linear molecule. The thickness to short axis ratio (see Fig. 4.1) is approximately $1 : 1.52$ for the $\theta = 160^\circ$ molecules, while the ratio is approximately $1 : 1.78$ for the $\theta = 150^\circ$ molecules. For the 9-bead molecules, these ratios are $1 : 1.7$ and $1 : 21$ respectively.

4.4.1 Summary

The change in the relationship between bend angle and phase behaviour is more notable when moving from a 9- to a 7-bead molecule, than the difference between the phase behaviours of the 11- and a 9-bead systems. Once again, the pressures required to induce the phase changes are increased, and the width of the nematic phase is broadened for the systems that demonstrate a uniaxial nematic phase. The uniaxial nematic phase disappears for $\theta = 140^\circ$, resulting in only isotropic and the clustered phase, with no global long axis alignment as seen for $\theta \leq 130^\circ$ systems in with longer molecules.

The loss of a uniaxial nematic phase for the systems of 140° 7-bead molecules is not unexpected. Previous work by Dewar and Camp [77] on the Monte Carlo melting of 7-bead bent-core molecules constructed from Lennard-Jones potentials has also noted the absence of a uniaxial nematic phase at a bend angle of 140°, while the phase was present for their systems of molecules with bend angles of 160°. At this point the ratio of the thickness of the molecule compared to the length of the short axis has become comparable, and the biaxiality of the molecule is reduced. This lessened biaxiality means that the molecules act more like linear mesogens and do not experience their arms becoming “trapped” within the knucles of neighbouring molecules.

4.5 5-bead molecules

Simulations of systems of 5-bead molecules were conducted using molecules with bend angles of $\theta = 160°$, $150°$ and $140°$, and a fixed thermostat temperature of $T^* = 1$. Again, due to the increasing pressures required to induce nematic phase behaviour in the 7-bead molecules compared to the 9-bead, we raised the starting pressure and size of the barostat pressure step to $P^* = 0.38$. Systems remained in a disordered isotropic liquid phase at this pressure. Simulations were then conducted using pressure sweeps up to $P^* = 5.78$.

Values obtained for the uniaxial order parameter Q_{00}^2 for these three systems are shown in Fig 4.22, while the equations of state for the three systems are shown relative to the isotropic liquid curve in Fig. 4.23. At no point during the course of any of these simulations did we see anything other than a disordered isotropic state, indicating the loss of all liquid crystalline phases. It is not obvious that there are any particular phase changes from the equations of state alone. Visual inspection of the systems revealed a very low level of diffusion and molecular movement at the highest pressures. Snapshots of a $160°$ system at low and high pressures are shown in Fig. 4.24, demonstrating no difference in alignment at the two ends of the simulation sweep.

The absence of any mesophases at this extent fits with the work of Galindo *et al.* [95], whose studies of rigid chains of five Lennard-Jones potentials indicated the presence of only solid and liquid phases. We therefore assume that, for a chain of five beads, the relative elongation of the molecule is insufficient for common alignment to be achieved between molecules. It is also worth noting that for a linear chain of five atoms, the effective L/D ratio of the entire molecule is 4 – a larger value than for the loss of nematic behaviour at $L/D = 3.1$ for hard spherocylinders as derived by Bolhuis

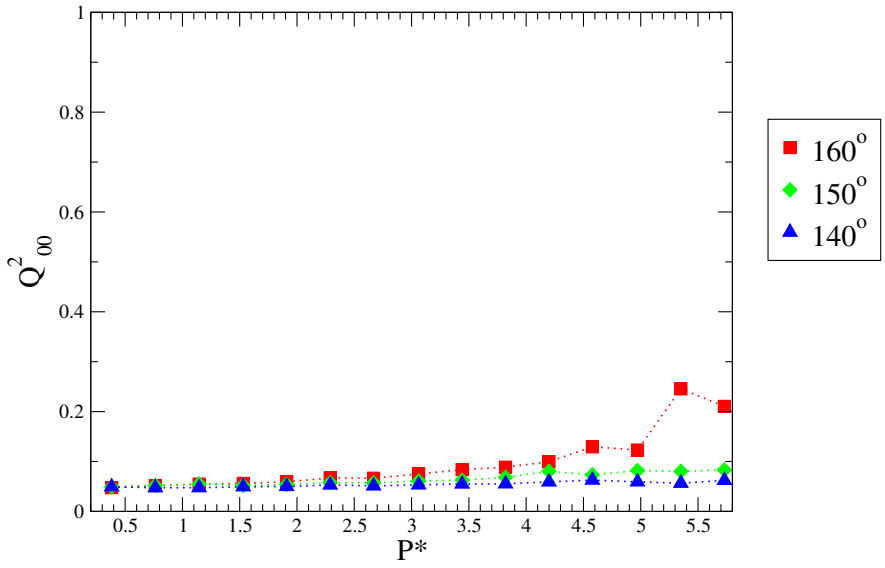

Figure 4.22: The change in the uniaxial order parameter Q^2_{00} with increasing pressure P^* for three different systems of $N = 512$ 5-bead molecules. Legend values correspond to the molecular bend angle θ.

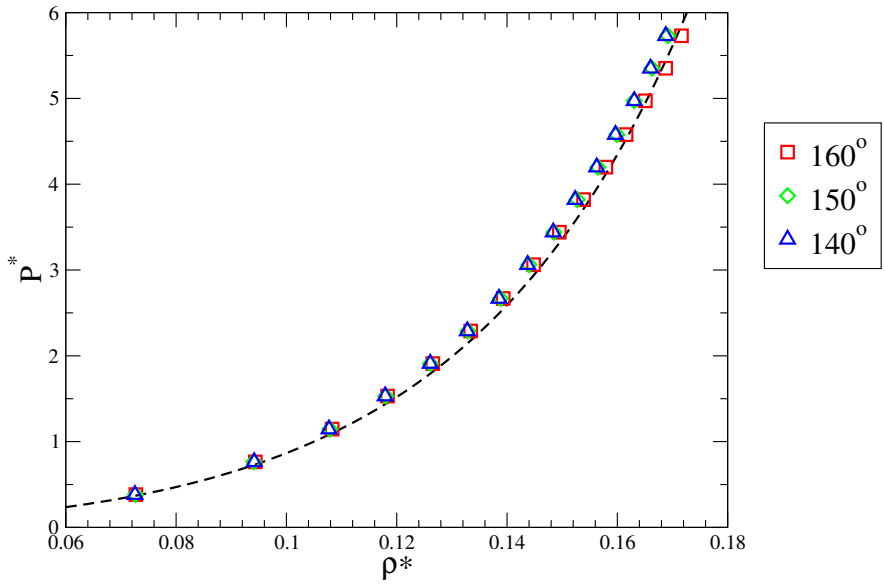

Figure 4.23: The equations of state for three systems of 512 5-bead molecules on compression. Legend values correspond to the molecular bend angle θ, while the dashed line corresponds to the theoretical liquid equation of state.

and Frenkel [88]. The relative softness of our mesogens therefore plays a much more significant part in the phase behaviour of our systems for small mesogen sizes than for our large ones, as the phase behaviour of our 11-bead molecules was a good match for the hard spherocylinder bent-core phase diagram, as described at the end of Chapter 3.

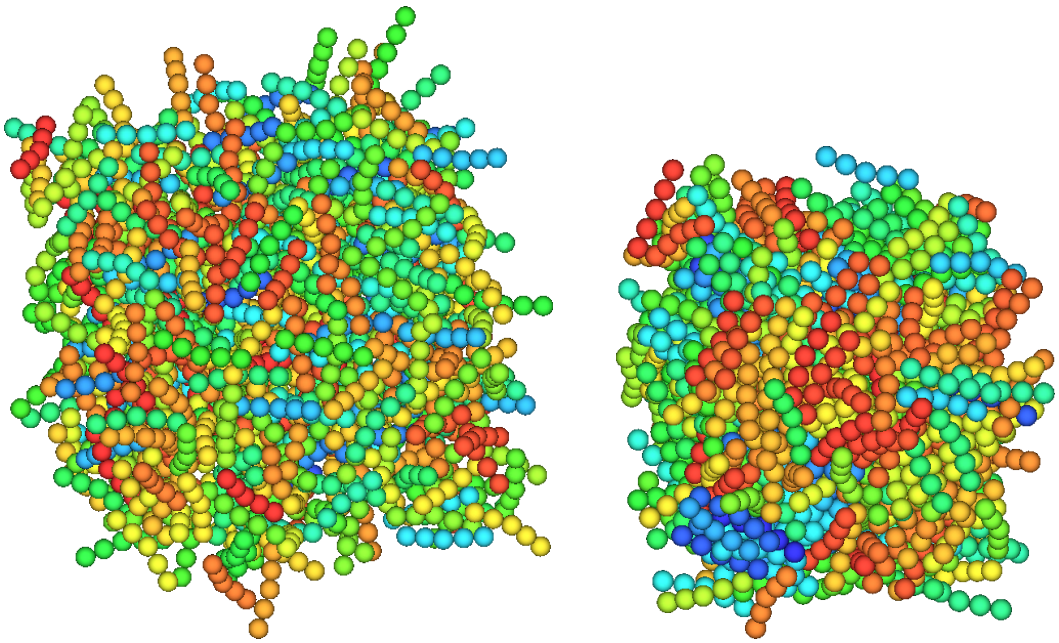

(a) $P^* = 0.38$ (b) $P^* = 5.73$

Figure 4.24: Snapshots from two ends of compression run of 512 5-bead molecules with a bend angle of $\theta = 160°$, showing isotropic behaviour throughout.

4.6 Conclusions

In this chapter we have studied the effects of modifying the number of beads from which our bent-core mesogenic models are constructed, and how this alters the phase behaviour of our simulated systems. By changing the number of beads, we are altering the L/D ratio of the arms of our molecules, with fewer beads resulting in "thicker" molecular arms.

There is little effect on the phase behaviour when moving from an 11-bead to a 9-bead molecule, with the loss of the uniaxial nematic phase still occuring in the range $130^\circ < \theta < 140^\circ$. Above this critical angle, uniaxial nematic and smectic A-like phases are seen. For smaller angles we do not see the presence of a global alignment director, and the same short-range clusters form as for the 11-bead molecules. The pressures at which the transitions occur are not the same, with significantly higher pressures required to induce phase transitions. In addition, the overall width of the uniaxial nematic phase is increased for the more linear molecules, while the width of the nematic phase changes little for angles closer to 140°.

On moving from a 9-bead to a 7-bead molecule, the increase in pressure required to induce a liquid crystal phase change is much more pronounced, with both the isotropic and uniaxial nematic phases persisting to much higher pressures. The width of the uniaxial phase is also significantly broadened throughout. We do see a small change in the overall phase diagram, with the loss of the global director occuring in the $150^\circ < \theta < 140^\circ$ window and the 140° systems no longer able to achieve a uniaxial nematic phase. The degree of smectic layer ordering becomes significantly improved for the 160° systems, as their biaxiality becomes less pronounced at smaller molecule sizes and they behave more like linear chains.

For molecule sizes of 5 linked beads, we see a total loss of any orientationally aligned phases, with the molecular systems remaining in the isotropic phase throughout the entire compression run. This is in agreement with the results by Galindo *et al.* [95], who saw no liquid crystal phases for linear molecules constructed from five Lennard-Jones potentials. At this point, the molecules are no longer sufficiently elongated to form mutually aligned mesophases, and so no orientational ordering is found.

In terms of our goal of simulating a thermotropic biaxial nematic phase, we recall from Fig. 3.1 that a bend angle of approximately 110° is required in the Onsager limit. From the results of these simulations, we see that the angle at which we lose the uniaxial nematic phase does not change much for the size modifications we have made in this chapter, with the angle slowly getting wider as the molecule size is reduced. It is likely that if the biaxial nematic was to be seen with a similar mesogenic model to ours, if it all, it would require far longer molecular arms in order to approach anything close to the $L \gg D$ values required.

There are significant problems with simulating highly elongated molecules. Firstly, the number of potentials required in our multi-bead models would be far larger than our current models, and impossible to simulate for a reasonable time without vast amounts of computational resources. Even if we used a model such as a spherocylinder or Gay-Berne dimer, the fact that the mesophases live between the liquid and solid phases means that any simulated system would need to be of sufficiently high density, and the number of simulated molecules would have to be of the order $10 \times (L/D)^2$. This is a very large number for highly elongated molecules.

Therefore, we must consider an alternative method of achieving a biaxial nematic through simulation. One way we can do this is by disrupting the polar smectic packing by somehow making molecules incompatible with one another so that they cannot

pack so neatly within one another. By introducing more free space into the system with non-tessellating shapes, we may be able to push back the onset of smectic behaviour such that a biaxial nematic can form instead. In the next chapter, we look to achieving this through the use of binary mixtures of bent-core mesogens.

Chapter 5

Binary mixtures of bent-core molecules

In Chapter 3 we explored the effect of bend angle on the liquid crystal phase behaviour of bent-core mesogens. In Chapter 4, we extended this to include the effects of the arm lengths of the molecules by varying the number of potentials that they are constructed from. Between them we have obtained a good understanding of the phase behaviour of monocomponent systems of our purely repulsive bent-core mesogens. However, we have not seen the presence of a biaxial nematic phase, and we believe that to do so with a monocomponent system would require molecules with arm lengths far larger than can be reasonably simulated today.

By mixing together different variants of bent-core molecules we propose that we may be able to manipulate where the phase transitions occur. We may even introduce new liquid crystal phases not seen in monocomponent systems – potentially including a biaxial nematic phase. In this chapter we explore the properties of a number of binary mixtures of bent-core mesogens, in order to understand how the phase behaviour differs to that of monocomponent systems.

5.1 Background

A binary mixture of two different mesogenic shapes was one of the earliest suggested systems for forming a biaxial nematic phase. In terms of intrinsically biaxial molecules, the biaxial nematic phase theoretically lies between the rod-like and plate-like nematic phases (see Fig. 3.1). Early lattice-based simulations by Alben in 1973 suggested that a mixture of rod-like and plate-like mesogens would be capable of exhibiting a biaxial nematic phase [97]. The plate-like mesogens were suggested to have one nematic alignment director, and the rod-like mesogens would have their own distinct nematic director. The two components would then pack in such a way that the two directors would be orthogonal.

Several other theoretical works followed, suggesting that biaxial nematic phases formed by a mixture of plate-like and rod-like mesogens were possible [98, 99]. However, further invesigation showed that a system comprised of mesogens that interacted purely through repulsive potentials would separate into two phases, each rich in either plates or rods [100]. Further lattice-based simulations where the mesogens were allowed to translate as well as rotate also showed that phase separation was thermodynamically preferable [101]. In order to encourage the two components to stay mixed, some models have employed an attractive rod-disk potential, but repulsive disk-disk and rod-rod potentials [102, 103]. It has been suggested that this may be possible to synthesize using molecules with rod-like and disk-like mesogenic components, attached by a flexible bond [104]. However, no spontaneous biaxial nematic has been seen using these techniques, although it has been suggested external stresses such as electric fields or shearing may be able to induce the phase [12].

Binary mixtures of similar but non-identical mesogens can also exhibit liquid crystal

phases that are not present in monocomponent systems of either mesogen individually. Stroobants demonstrated this by extending the earlier Monte Carlo simulation work on hard parallel spherocylinders [86] to binary mixtures of two spherocylinders with differing lengths, one fixed at $L_1/D = 1$ and the other at values between $1.3 \leq L_2/D \leq 2.1$ [105, 106]. It was found that as the ratio L_2/D increased the nematic–smectic transition was delayed until higher system densities, with a columnar phase appearing at $L_2/D > 1.6$, and the smectic phase disappearing entirely for $L_2/D > 1.9$. No phase separation of the two components was seen.

Further theoretical analysis by van Roij and Mulder [107] indicated that the phase separation of the two components in these systems does not occur until the ratio of the L/D values across the two molecules was greater than $5:1$. At this point, the two nematic phases of each component preferentially demix. Cinacchi *et al.* calculated theoretical phase diagrams for a number of binary hard spherocylinder systems [108] and found that the isotropic, nematic, and smectic phases remained mostly well-mixed for systems where $L_1/L_2 \approx 1.4$, but when $L_1/L_2 \approx 2$ the two phases separate. No smectic phase mixing was seen at all for mixtures where the mole fraction of the longer component was any greater than 0.2. In all systems, as the mole fraction of the longer molecule increased, the two smectic phases separated at progressively lower pressures.

Reducing the differences between the mesogens even further, it has been shown that a degree of polydispersity in molecular size can also help stabilize and broaden biaxial nematic phases in systems of board-like mesogens. By having a range of molecular ratios, the onset of the smectic phase can be disrupted and allow more space for the biaxial nematic phase to form [109]. van den Pol *et al.* undertook experimental work on colloidal suspensions of board-like molecules with $a:b \approx b:c$ and each dimension having a variation of $\sim 25\%$ [110]. By aligning the molecules in a magnetic field

to induce orientational ordering, they showed that a biaxial nematic phase was not only possible, but the width of the phase was quite broad. Recently, theoretical work by Belli *et al.* has shown that polydispersity in suspensions of board-like molecules creates a large region of stability for the biaxial nematic liquid crystal phase [111].

In this chapter, we aim to study the phase behaviour of binary mixtures of bent-core molecules. We suggest that, by mixing together variants of the same basic mesogenic shape, we may be able to observe new phase behaviour and potentially disrupt the smectic and smectic-like ordering that occurs. We will investigate two different types of mixtures, as illustrated in Fig. 5.1. The first consists of two molecules with the same bend angle but with different arm lengths. As the work of van Roij *et al.* showed that hard spherocylinders remain mixed so long as the L_2/L_1 ratio remains less than 2 [107], we expect the two components to remain mixed in the uniaxial nematic phase. If they remain mixed into the smectic phases, they may disrupt the ability of the smectic layers to pack neatly and introduce gaps, as shown in Fig. 5.1a.

The second kind of mixture consists of molecules of the same arm lengths, but of different internal bend angles, as shown in Fig. 5.1b. As the sizes of the molecules are identical, we expect the miscibility of the two components to be improved relative

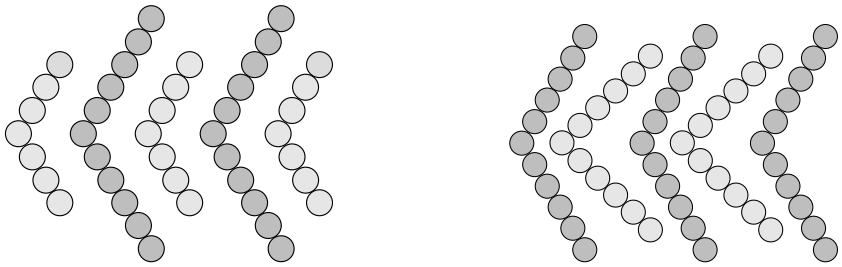

Figure 5.1: The different binary mixtures examined in this chapter, consisting of (a) molecules with the same bend angle but different arm length, and (b) molecules with the same arm length but different bend angles.

to that of mixtures of differing molecule sizes. The close packing of molecules in the smectic phase may leave extra free space, as the molecules will be unable to tessellate optimally. This extra free space may give the mesogens extra room to rotate around their long axes, and prevent such strong alignment of their short axes.

5.2 Simulation method

Molecules used in this chapter are constructed in the same fashion as described in Section 4.2. Systems were initialized by placing molecules of type A and type B on the sites of an expanded primitive cubic lattice. As the number of molecules used was not a cubic number, a larger lattice than necessary was used and the molecules placed sequentially, with the A molecules filling up the layers first. Any free lattice points were left unoccupied.

Simulations were conducted using the `DL_POLY_2` [82] molecular dynamics package with cubic periodic boundary conditions, velocity Verlet integration and the Nosé-Hoover thermostat and barostats, using a fixed temperature of $T^* = 1$ and a timestep of $t^* \sim 0.01$. In order to ensure that not only the positions and rotations of the molecules were randomized, but that the two components were well-mixed, the initial NVE runs were performed for an order of magnitude longer than with monocomponent systems. Initial isotropic gaseous starting configurations were generated by sampling this initial NVE run every 10^6 timesteps.

Each configuration obtained in this way was used as the beginning of a compression simulation run, whereby the system was switched to an NPT ensemble and compressed

to an isotropic liquid state. Equilibration was performed for 10^6 timesteps. A compression sweep then consisted of increasing the barostat by a fixed pressure step; equilibrating for 5×10^6 timesteps (longer than monocomponent systems due to the possibility of phase separation); checking that the order parameters of each of the individual components had settled; then either equilibrating further, or simulating for another 10^6 timesteps, during which the system would be sampled 100 times. The final molecular configuration after this last set of timesteps was then used as the starting configuration for the next sequential pressure step.

5.3 Mixtures of different molecule sizes

In this section we present results for binary mixtures comprised from two molecular types of different sizes – that is, assembled from a different number of WCA potentials, n_A and n_B. The internal bend angle of the two molecules is kept the same, such that $\theta = \theta_A = \theta_B$. As we are looking for thermotropic phase behaviour, the number of each type of molecule is fixed at $N_A = N_B$ for all simulations conducted.

5.3.1 Mixtures of $n_A = 11$, $n_B = 7$

We begin by looking at the phase behaviour resulting from mixtures of $n_A = 11$ and $n_B = 7$ molecules, with $N_A = N_B = 512$, for a total of 1024 molecules. The selection of these two molecule sizes was made as the phase behaviour of each was characterized in Chapters 3 and 4 respectively. Both were seen to have uniaxial nematic and smectic-like behaviour, with a loss of the nematic behaviour at different bend angles for each size of molecule ($\theta = 130^\circ$ for the 11-bead molecules, $\theta = 140^\circ$ for the 7-bead molecules). They are also sufficiently different in size that a transition to a smectic-like phase would contain a large amount of free space if the two components are mixed.

Simulations for the $n_A = 11$ and $n_B = 7$ mixtures were conducted for a range of different bend angles in the interval $160^\circ \leq \theta \leq 120^\circ$. Systems were compressed from an initially disordered, fully mixed isotropic state at a pressure of $P^* = 0.053$, with a pressure step size of between $0.053 \leq P^* \leq 0.21$.

5.3.1.1 $\theta = 160°$

In monocomponent systems, both 11-bead, $\theta = 160°$ and 7-bead, $\theta = 160°$ bent-core mesogens undergo phase transitions from isotropic to uniaxial nematic and then to smectic phases on compression. The pressure windows are significantly different, with the 7-bead molecules requiring much higher pressures.

Compressions runs were performed on binary systems comprised of equal parts of each type of $\theta = 160°$ molecule. The values for the order parameters Q^2_{00} and Q^2_{22} for the individual components are shown in Fig. 5.2. There are several features from this graph that indicate the presence of multiple phase transitions. The first occurs in the pressure window $0.42 < P^* < 0.64$, where the value of Q^2_{00} for both systems increases simulataneously, indicating both phases transitioning to a uniaxial nematic. A snapshot

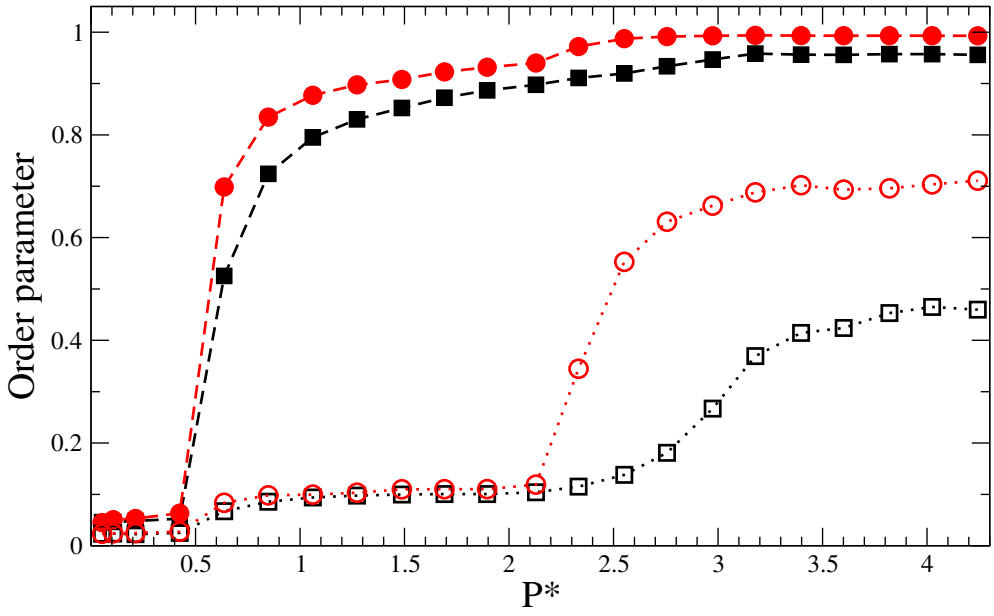

Figure 5.2: The uniaxial order parameter Q^2_{00} (solid symbols) and biaxial order parameter Q^2_{22} (hollow symbols) on compression, for a mixture of 512 11-bead molecules (red circles) and 512 7-bead molecules (black squares) with a common bend angle of $\theta = 160°$.

of this phase is shown in Fig. 5.3, with the 11-bead molecules in red-yellow and the 7-bead molecules in blue-cyan. This is slightly above the transition window for the 11-bead mesogens in a monocomponent system, but given the width of the windows, it is probable that this transition has not moved significantly. The 7-bead molecules have transitioned simultaneously, well below their monocomponent transition window of $P^* \sim 1.5$, and have been induced into a premature uniaxial nematic phase through being mixed with the longer 11-bead molecules. The pair correlation functions for the two types of molecules in isolation are shown in Fig. 5.4, with no long-range peaks indicating the presence of a uniaxial nematic phase in both components.

As the pressure is increased further, a second phase transition in the range $2.13 < P^* < 2.33$ is then observed by the sharp rise in the Q^2_{22} order parameter and small bump in the Q^2_{00} order parameter for the 11-bead molecules. There is no significant change in the order parameters for the 7-bead molecules at this point. A snapshot of a system at $P^* = 2.33$ is shown in Fig. 5.5, and the pair correlation functions for the individual components are shown in Fig. 5.6.

At this pressure, the 11-bead molecules have undergone a transition to their smectic-like behaviour, as shown by the alignment of their central atoms (yellow) in the snapshot, and by the presence of a secondary peak in the pair correlation function. The shorter 7-bead molecules have not followed suit, and instead remain in the uniaxial nematic phase, as seen by the absence of any long-range ordering in the pair correlation function.

The elevated height of the first peaks for both components of the pair correlation functions indicates that the distribution of molecules within the system has changed. These peaks indicate that the system is beginning to demix, as the distribution of molecules has changed such that the probability of finding two identical molecules next to one

another ($\mathbf{r}_{ij} \sim 1\sigma$) is much higher than for the well-mixed nematic shown in Fig. 5.4.

The pressure at which this transition is induced is also much higher than that for the smectic transition of the 11-bead, $\theta = 160^\circ$ molecules in isolation, which occurs at $P^* \sim 1.4$. The mixing of the two molecules has a significant effect on the width of the nematic phase for the longer molecules, extending it from $0.382 < P^* < 1.473$ in the monocomponent system, to $0.42 < P^* < 2.33$ in the binary mixture.

The final transition of the 7-bead molecules to a smectic-like phase is less distinct, as the aligned 11-bead molecules restrict space and common alignment cannot propagate easily through the system. By $P^* = 3.18$ the 7-bead molecules have themselves transitioned to a smectic-like phase, as shown by the alignment of the central beads (cyan) in Fig. 5.7. This is similar to the monocomponent 7-bead transition window which occurs around $2.73 < P^* < 3.00$. The pair correlation function in Fig. 5.8 shows the presence of a second peak at this pressure, indicating a repeating smectic-like structure. A snapshot of the system along the main system director (shown in Fig. 5.7b) shows that the two components are almost fully demixed at this point.

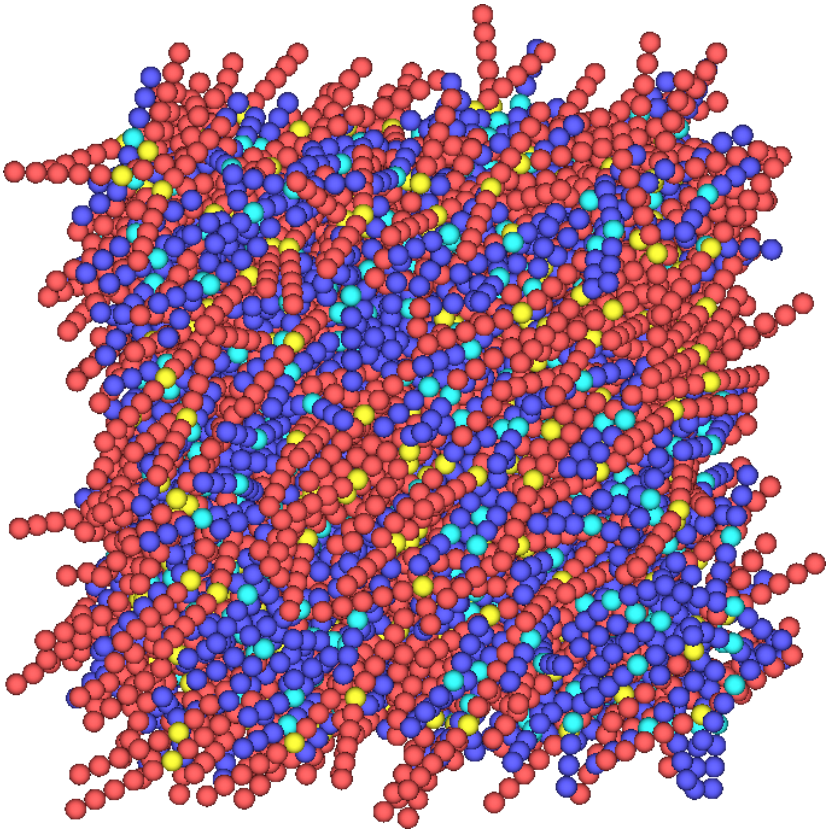

Figure 5.3: Snapshot at $P^* = 0.64$ from a compression run of 512 11-bead (red-yellow) and 512 7-bead (blue-cyan) molecules with a bend angle of $\theta = 160°$, showing a well-mixed uniaxial nematic phase.

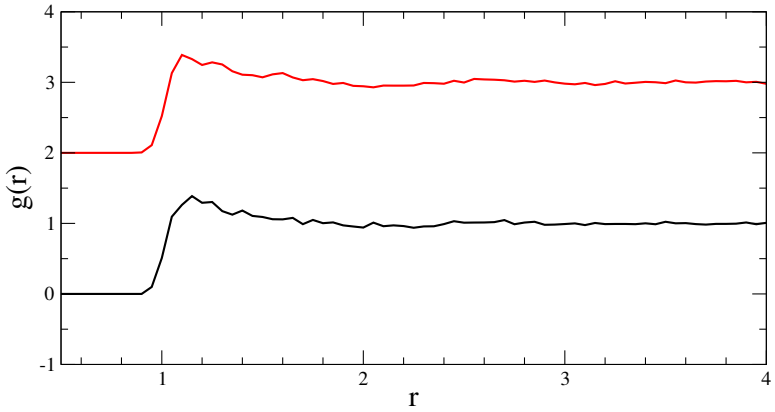

Figure 5.4: The pair correlation for the individual components in Fig. 5.3, showing 11-bead (top, red) and 7-bead components (bottom, black). The plots have been vertically offset for clarity.

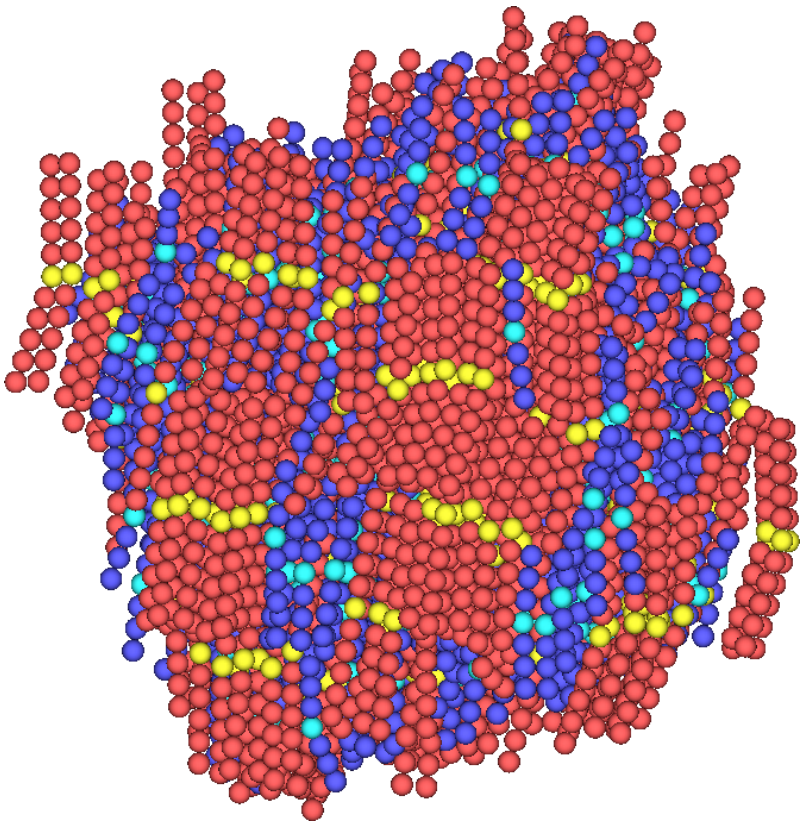

Figure 5.5: Snapshot at $P^* = 2.33$ from a compression run of 512 11-bead molecules (red-yellow) and 512 7-bead molecules (blue-cyan) with a bend angle of $\theta = 160°$. The alignment of the yellow beads (the central atom of the 11-bead molecules) indicates the presence of a smectic-like phase for the longer molecules.

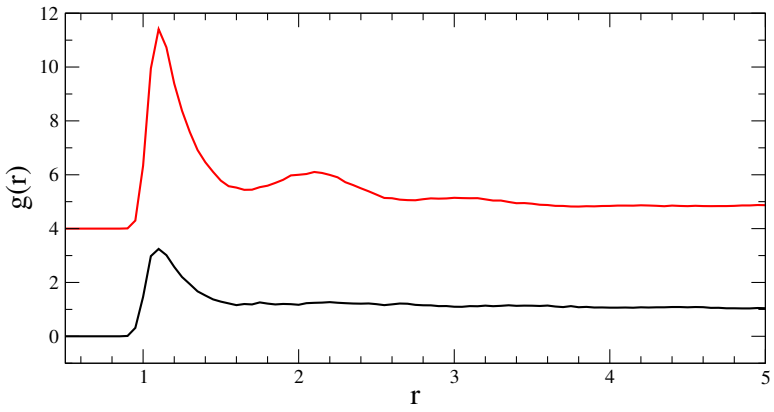

Figure 5.6: The pair correlation for the individual components in Fig. 5.3, showing 11-bead (top, red) and 7-bead components (bottom, black). The plots have been vertically offset for clarity.

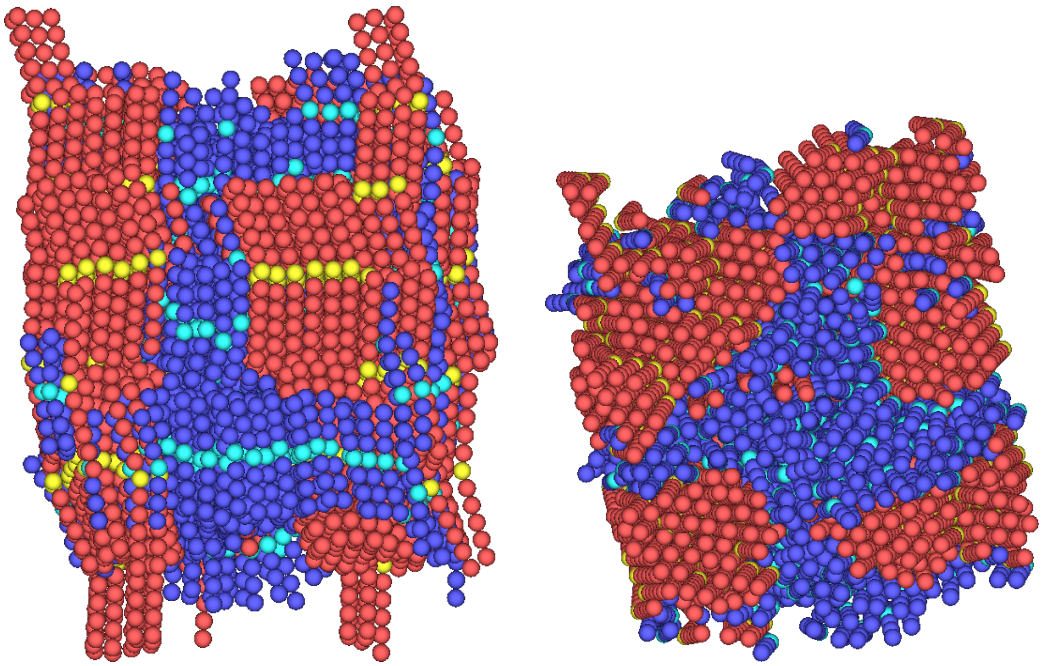

(a) (b)

Figure 5.7: Snapshots at $P^* = 3.18$ from a compression run of 512 11-bead (red-yellow) and 512 7-bead molecules (blue-cyan), with a mutual bend angle of $\theta = 160°$. Snapshots are (a) perpendicular and (b) parallel to the system director, clearly showing the demixing of the two components.

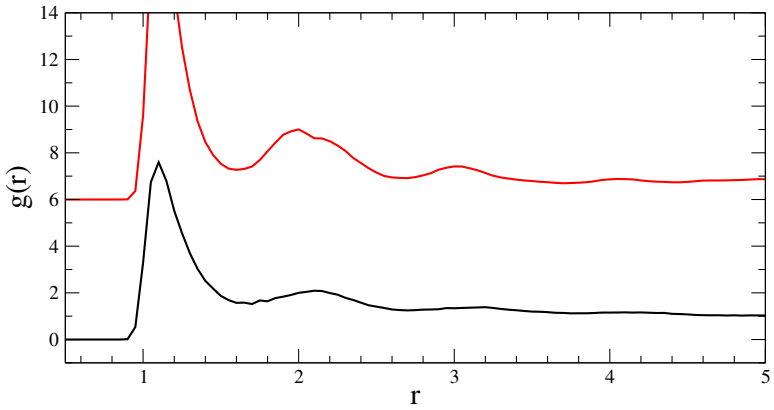

Figure 5.8: The pair correlation for the individual components in Fig. 5.7, showing 11-bead (top, red) and 7-bead components (bottom, black). The plots have been vertically offset for clarity, and the peak of the 11-bead line at a value of 13.6 (19.6 on the offset axis) has been truncated.

5.3.1.2 $\theta = 140°$

When simulated individually, the 11-bead, $\theta = 140°$ and 7-bead, $\theta = 140°$ bent-core mesogens have differing phase behaviours. The shorter molecules exhibit no uniaxial nematic phase at this bend angle. In larger systems of 4096 11-bead molecules, the formation of the uniaxial nematic phase was found to be slow, and unable to easily select a global alignment director.

Compressions runs were performed on binary systems comprised of equal parts of each type of $\theta = 140°$ molecule, 7-bead and 11-bead. The obtained values for the order parameters Q^2_{00} and Q^2_{22} for each of the two components are shown in Fig. 5.9. Unlike the $\theta = 160°$ binary mixture, the onset of the nematic behaviour in the 11-bead molecules is considerably delayed, from $P^* \sim 0.6$ to $1.27 < P^* < 1.49$. A snapshot

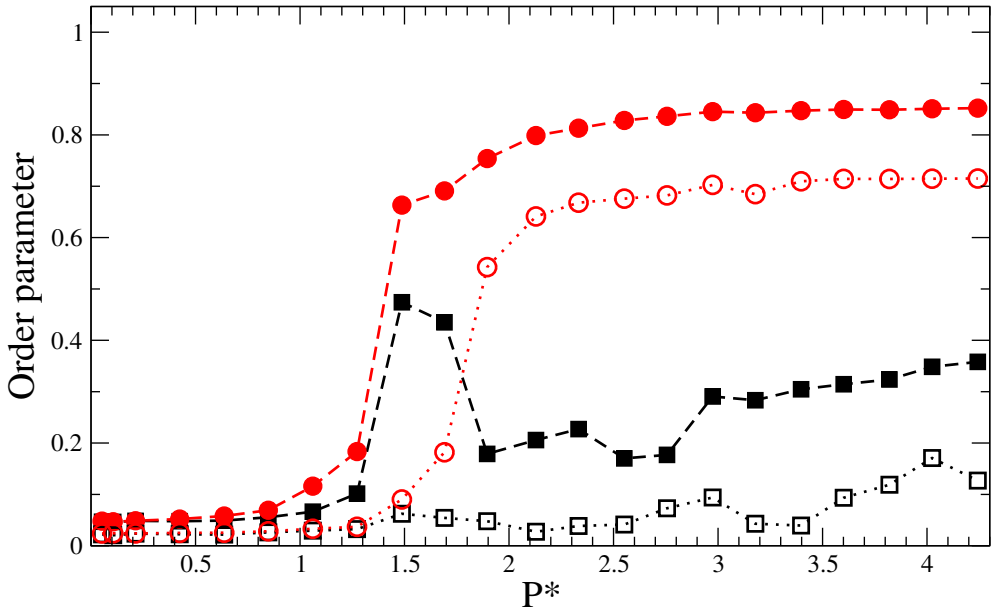

Figure 5.9: The uniaxial order parameter Q^2_{00} (solid symbols) and biaxial order parameter Q^2_{22} (hollow symbols) on compression, for a mixture of 512 11-bead molecules (red circles) and 512 7-bead molecules (black squares) with a common bend angle of $\theta = 140°$.

of the system at $P^* = 1.49$ is shown in Fig. 5.10.

As a result of the two components being well mixed, a more interesting property arises. The order parameters for the 7-bead molecules indicate that they too are in the uniaxial nematic phase, despite not having such a phase in a monocomponent system. The pair correlation functions in Fig. 5.13 confirm that both components are simultaneously in the uniaxial nematic phase.

The width of the phase for the 11-bead mesogens is short-lived, and in the pressure window $1.67 < P^* < 1.90$ the molecules undergo another transition to a smectic-like phase, shown by the snapshots in Fig. 5.12 and the pair correlation function in Fig. 5.13. Again, this transition is at a significantly higher pressure than the monocomponent smectic transition at $P^* \sim 1.3$ for the 11-bead, $\theta = 140^\circ$ molecules.

The demixing of the two phases is more rapid than for the $\theta = 160^\circ$ mixtures, and the value of Q^2_{00} for the 7-bead molecules *declines*, indicating a loss of orientational alignment. Visual inspection shows that the 7-bead mesogens have reverted to a near-isotropic state, with a small degree of alignment ($Q^2_{00} < 0.2$) due to confinement by the smectic phase of the 11-bead mesogens.

The extra "fluidity" provided by the isotropic 7-bead molecules allows the 11-bead molecules to move more freely, and the offset smectic clusters seen in monocomponent systems rearrange into full smectic layers. As the pressure is increased further, both Q^2_{00} and Q^2_{22} increase to over 0.6 for the longer mesogens. The high value of Q^2_{22} is indicative of a strong level of polarization within the system, and is due to the majority of the 11-bead molecules adopting a common short axis alignment. The 7-bead mesogens never transition to their "jammed" state with short-range alignment as seen in monocomponent systems, due to confinement between the organized 11-bead layers.

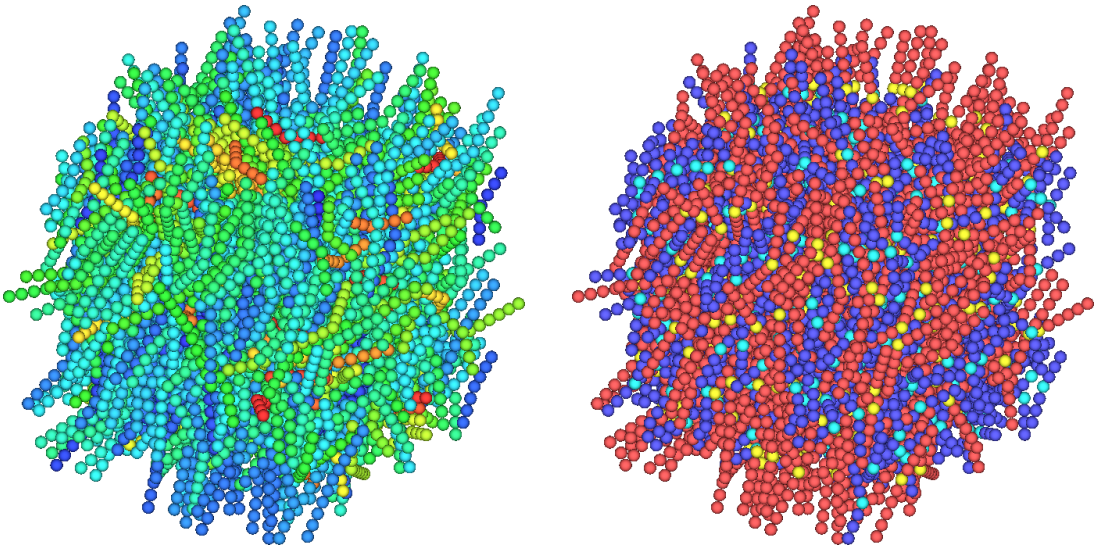

(a) (b)

Figure 5.10: Snapshots at $P^* = 1.49$ from a compression run of 512 11-bead (red-yellow) and 512 7-bead (blue-cyan) molecules with a mutual bend angle of $\theta = 140°$. Snapshots are coloured according to (a) orientation and (b) kind.

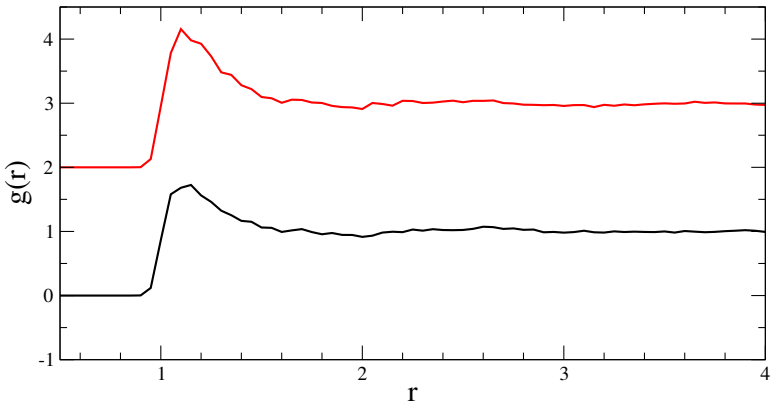

Figure 5.11: The pair correlation for the individual components in Fig. 5.10, showing 11-bead (top, red) and 7-bead components (bottom, black). The plots have been vertically offset for clarity.

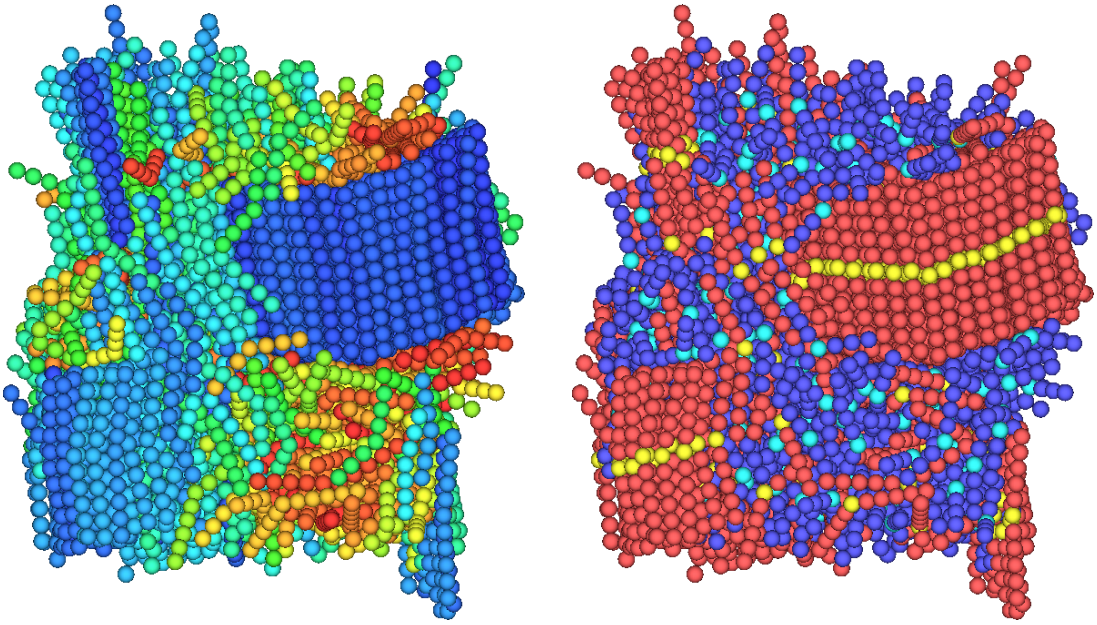

(a) (b)

Figure 5.12: Snapshots at $P^* = 1.90$ from a compression run of 512 11-bead (red-yellow) and 512 7-bead (blue-cyan) molecules with a mutual bend angle of $\theta = 140°$. Snapshots are coloured according to (a) orientation and (b) kind.

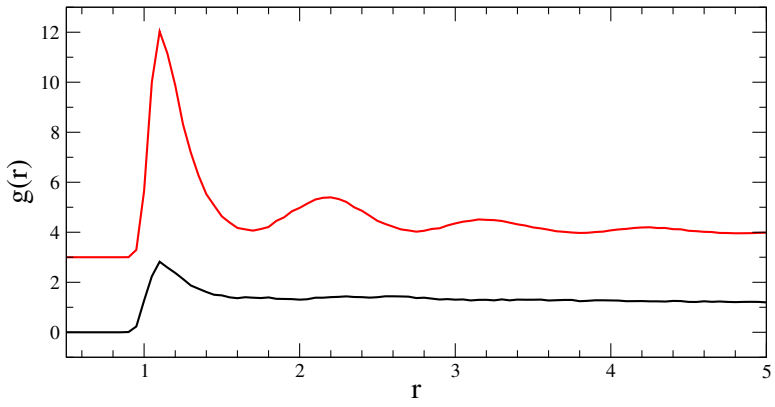

Figure 5.13: The pair correlation function for the individual components in Fig. 5.12, showing 11-bead (top, red) and 7-bead components (bottom, black). The plots have been vertically offset for clarity.

5.3.1.3 $\theta = 130°$

In individual monocomponent simulations, neither the 11-bead nor the 7-bead $\theta = 130°$ mesogens exhibited a uniaxial nematic phase. Instead both formed short-range aligned clusters along both their long and short axes, but with no overall global system director. Compression runs were performed on binary systems comprised of equal parts of each of these mesogens, and the obtained values for the order parameters Q^2_{00} and Q^2_{22} for each independent component are shown in Fig. 5.14. Neither component shows a significant degree of uniaxial alignment at any pressure, with $Q^2_{00} < 0.45$ for the 11-bead molecules and $Q^2_{00} < 0.25$ for the 7-bead molecules.

Given the relatively small system size, the rise in Q^2_{00} for $P^* \geq 1.49$ for the 11-bead molecules indicates that there is a transition of some kind. Fig. 5.15 shows the

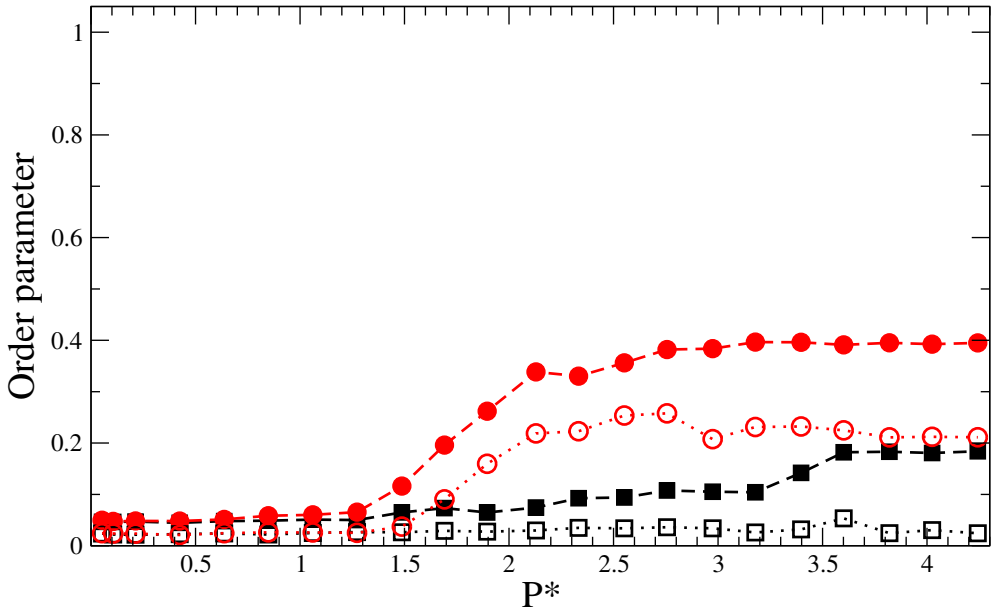

Figure 5.14: The uniaxial order parameter Q^2_{00} (solid symbols) and biaxial order parameter Q^2_{22} (hollow symbols) on compression, for a mixture of 512 11-bead molecules (red circles) and 512 7-bead molecules (black squares) with a common bend angle of $\theta = 130°$.

pair correlation function for the 11-bead components for a range of pressures in the interval $1.49 \leq P^* \leq 2.13$. The increasing height of the first peak and emergence of a second peak at $r \sim 2\sigma$ indicates the slow formation of an organised structure. Snapshots of the system at either end of this pressure window are shown in Fig. 5.16. At $P^* = 1.49$ a small aligned cluster is visible due to the alignment of the central atoms for a small number of the 11-bead molecules. As the pressure is increased to $P^* = 2.13$, more of these clusters form and the mixing of the 11-bead and the 7-bead molecules is significantly reduced.

Surprisingly, the extra mobility afforded to the 11-bead clusters by the still-fluid 7-bead component does not help in achieving a global uniaxial director, and the clusters observed in monocomponent simulations remain. Further work using repeated decompression and recompression (as described in Sec. 3.3.4) would be interesting, in order to see whether a single smectic-like phase could be formed by the 11-bead molecules.

As with the $\theta = 140^\circ$ binary mixtures, the 7-bead molecules do not achieve any aligned state, and do not form similar clusters to the 11-bead molecules as they would in a monocomponent system. Again, it is likely that the confinement between the 11-bead clusters is reducing the amount of free space required for the molecules to align, and prevents their transition to a clustered state.

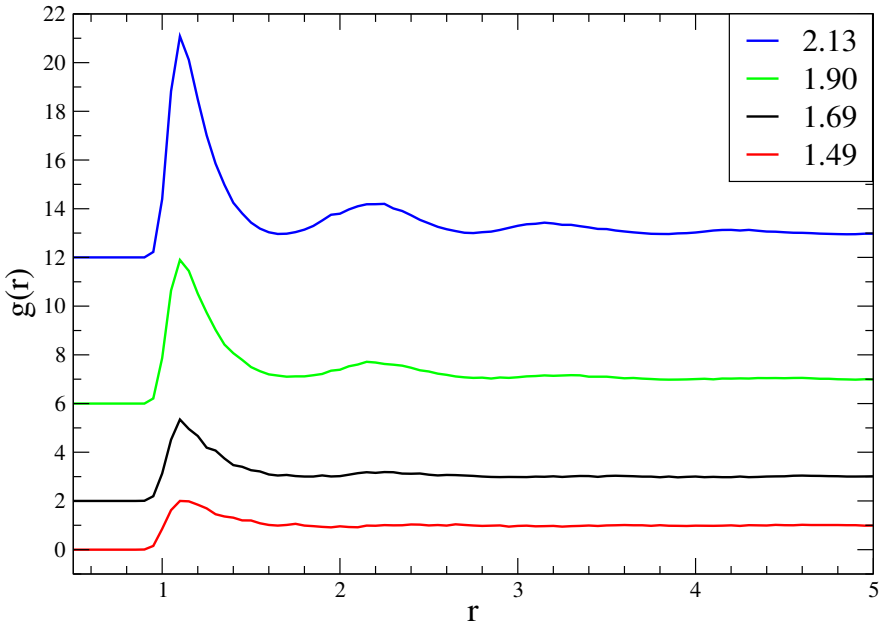

Figure 5.15: The pair correlation function for 512 11-bead $\theta = 130°$ molecules in a binary mixture with 7-bead $\theta = 130°$ molecules, at a selection of pressures. Legend values correspond to the reduced pressure P^*, and the plots have been vertically offset for clarity.

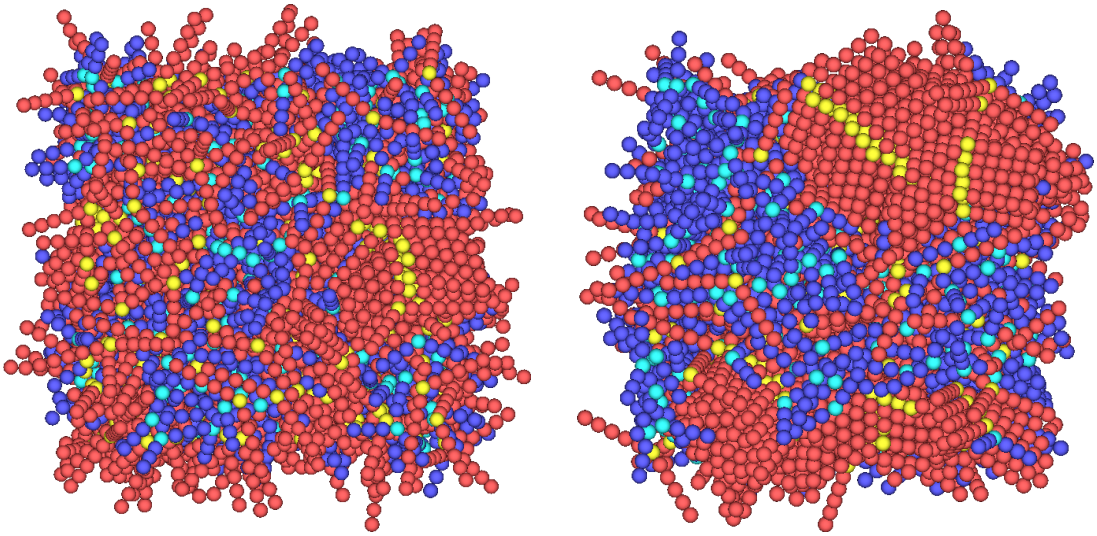

(a) $P^* = 1.49$ (b) $P^* = 2.13$

Figure 5.16: Snapshots from a compression run of 512 11-bead (red-yellow) and 512 7-bead (blue-cyan) molecules with a bend angle of $\theta = 130°$.

5.3.2 Mixtures of $n_A = 11$, $n_B = 5$

We now turn to the phase behaviour occuring in mixtures of $n_A = 11$ and $n_B = 5$ molecules, with equal parts $N_A = N_B = 512$ for a total of 1024 molecules. From Chapter 4 we have seen that systems of 5-bead molecules do not exhibit any mesophases in monocomponent systems. In addition, the size difference between the two molecules is $n_A > 2n_B$, so we expect the 5-bead molecules to demix and act as an isotropic liquid throughout.

Simulations for the $n_A = 11$ and $n_B = 5$ mixtures were conducted for a range of different bend angles in the interval $160^\circ \leq \theta \leq 120^\circ$. Systems were compressed from an initially disordered, fully mixed isotropic state at a pressure of $P^* = 0.06$, with a pressure step size of between $0.06 \leq P^* \leq 0.23$, increasing as the simulation progressed.

5.3.2.1 $\theta = 160^\circ$

The values for the order parameters Q^2_{00} and Q^2_{22} obtained from compression runs of 11-bead and 5-bead $\theta = 160^\circ$ molecules are shown in Fig. 5.17. From this plot, it can be seen that the 11-bead molecules undergo two clear phase transitions. The first is indicated by a sharp rise in the value of Q^2_{00} in the pressure window $0.48 < P^* < 0.72$, signifying the onset of orientationally ordered behaviour. The second transition occurs in the range $1.68 < P^* < 1.91$, with a small jump in Q^2_{00} and a large change in Q^2_{00}. These correspond to the isotropic–nematic and nematic–smectic phase transitions respectively, which occur at $P^* \sim 0.4$ and $P^* \sim 1.4$ in monocomponent systems. The value of $Q^2_{22} > 0.75$ indicates that there is a high level of mutual alignment of the short axes of the 11-bead molecules, much higher than for the $n_A = 11$, $n_B = 7$, $\theta = 160^\circ$ mixtures.

The most interesting property of the behaviour of the Q^2_{00} order parameters is the high level of uniaxial alignment for the 5-bead molecules in the pressure range $0.72 \leq P^* \leq 1.68$, coinciding with the uniaxial nematic phase of the 11-bead molecules. Snapshots of the system at $P^* = 1.68$ are shown in Fig. 5.18. At this pressure the two components remain well mixed, and the uniaxial nematic phase of the 11-bead molecules has induced a similar nematic phase in the 5-bead molecules – a phase that does not exist *at all* for monocomponent systems, regardless of bend angle.

As the system passes through the $1.68 < P^* < 1.91$ pressure window and the 11-bead molecules transition to a smectic phase, the two components completely demix, as shown in Fig. 5.19. The 5-bead molecules suddenly revert to an isotropic liquid phase, and the uniaxial order parameter falls from $Q^2_{00} > 0.6$ to $Q^2_{00} < 0.2$. The extra fluidity in the system provided by the isotropic 5-bead molecules allows the 11-bead

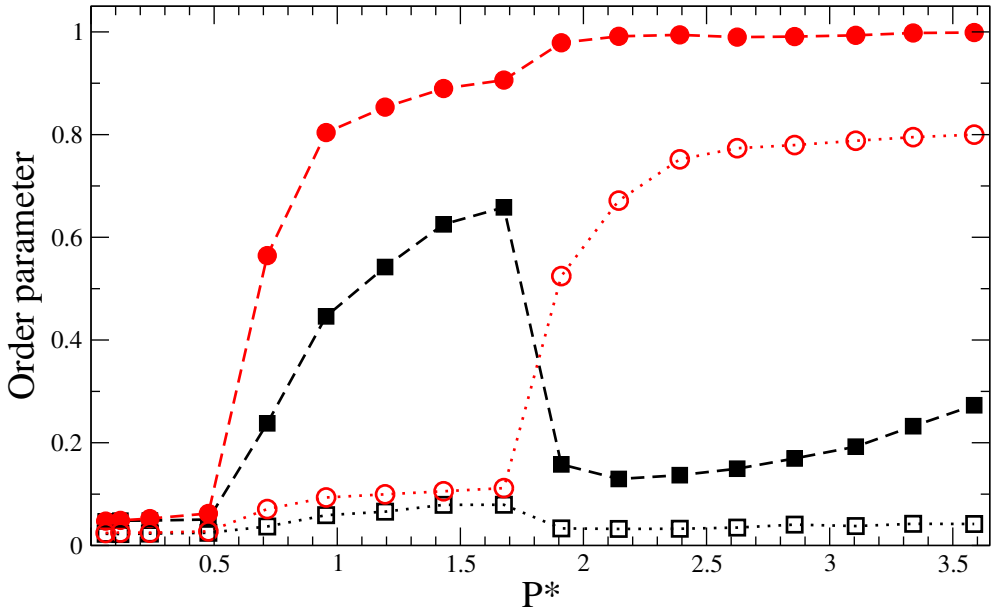

Figure 5.17: The uniaxial order parameter Q^2_{00} (solid symbols) and biaxial order parameter Q^2_{22} (hollow symbols) on compression, for a mixture of 512 11-bead molecules (red circles) and 512 5-bead molecules (black squares) with a common bend angle of $\theta = 160°$.

molecules to form full, well-organized smectic layers, similar to the phase behaviour of the $n_A = 11, n_B = 7, \theta = 140^\circ$ systems in Sec. 5.3.1.2. As the pressure is increased further, the 5-bead molecules remain in their isotropic state and undergo no further transitions.

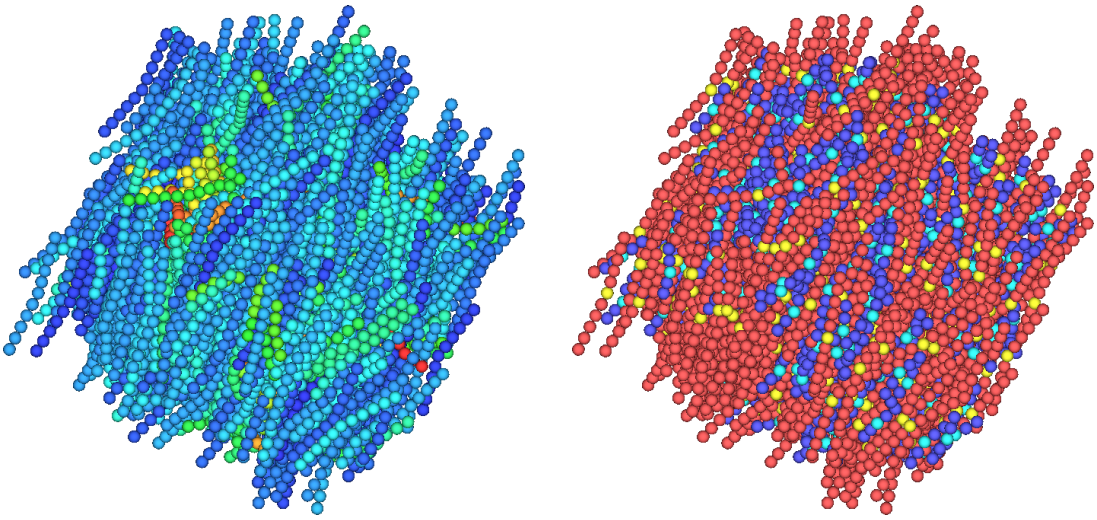

(a) (b)

Figure 5.18: Snapshots at $P^* = 1.68$ from a compression run of 512 11-bead (red-yellow) and 512 5-bead (blue-cyan) molecules with a mutual bend angle of $\theta = 160°$. Snapshots are coloured according to (a) orientation and (b) kind.

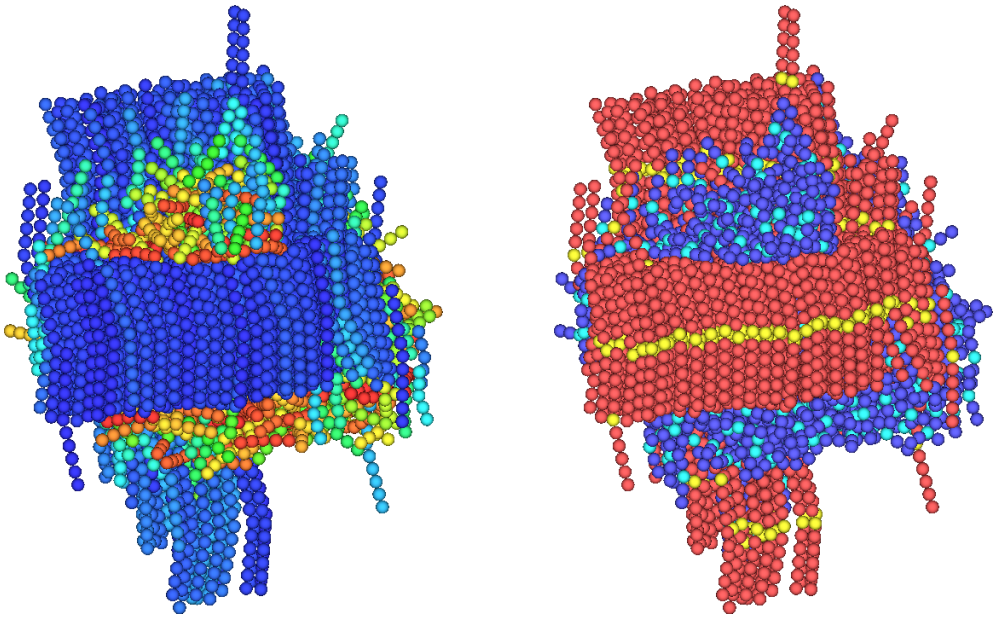

(a) (b)

Figure 5.19: Snapshots at $P^* = 1.91$ from a compression run of 512 11-bead (red-yellow) and 512 5-bead (blue-cyan) molecules with a mutual bend angle of $\theta = 160°$. Snapshots are coloured according to (a) orientation and (b) kind.

5.3.2.2 $\theta = 140^\circ$

The order parameters Q_{00}^2 and Q_{22}^2 for the components of a binary system of 11-bead and 5-bead molecules with a mutual bend angle of $\theta = 140^\circ$ are presented in Fig. 5.20. In contrast to the results for $n_A = 11, n_B = 5, \theta = 140^\circ$, there is only one notable phase change for the 11-bead molecules, beginning at $1.43 < P^* < 1.68$ where the value of Q_{00}^2 climbs from ~ 0.2 to ~ 0.8, in tandem with an increase in the Q_{22}^2 to a value of ~ 0.4. There is also no sign of any ordering in the 5-bead molecules, with both order parameters remaining below 0.1 throughout the course of the compression run.

A snapshot of the system at $P^* = 1.91$ is shown in Fig. 5.21. From this it can be seen that the 11-bead molecules have lost the uniaxial nematic phase and have transitioned straight to the clustered phase, as seen with narrower bend angles such as $\theta = 130^\circ$ in monocomponent systems.

In monocomponent systems of 11-bead, $\theta = 140^\circ$ molecules the uniaxial nematic phase is narrow, and in the simulations of systems of 4096 molecules it was seen that the system has difficulty in achieving a global system director amongst all molecules simultaneously (see Sec. 3.4.2). It appears that the presence of 5-bead molecules is preventing the formation of a uniaxial nematic by interfering with the propagation of a single system director. As such, the "second" transition to a smectic phase (seen in the monocomponent systems) occurs without a global system director already in place, and the short-range clusters with both long and short axis alignment appear. The onset of this transition at $P^* \sim 1.6$ is higher than the equivalent transition to a smectic in a monocomponent system of 11-bead molecules, which occurs at $P^* \sim 1.3$.

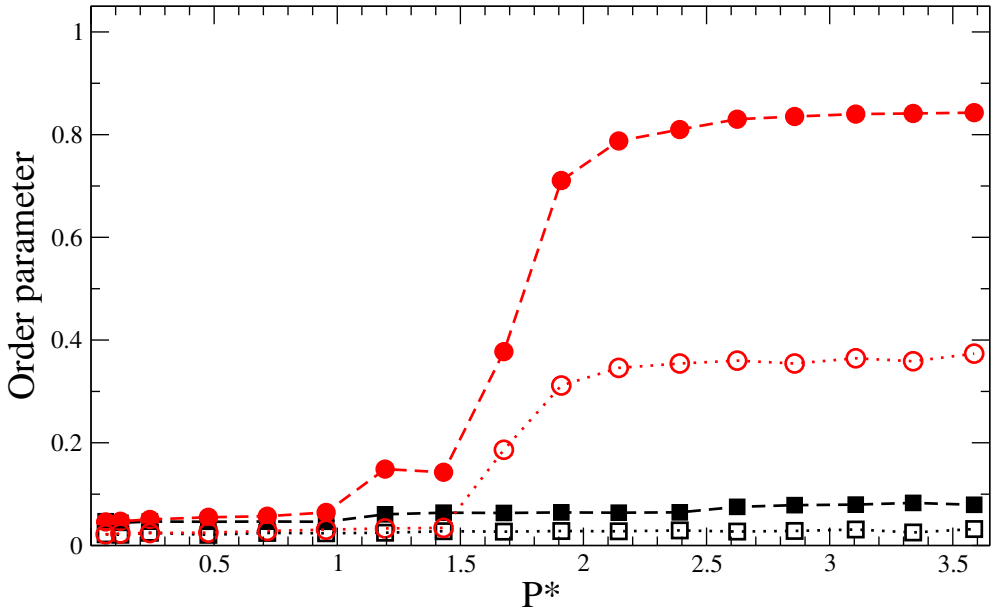

Figure 5.20: The uniaxial order parameter Q^2_{00} (solid symbols) and biaxial order parameter Q^2_{22} (hollow symbols) on compression, for a mixture of 512 11-bead molecules (red circles) and 512 5-bead molecules (black squares) with a common bend angle of $\theta = 140°$.

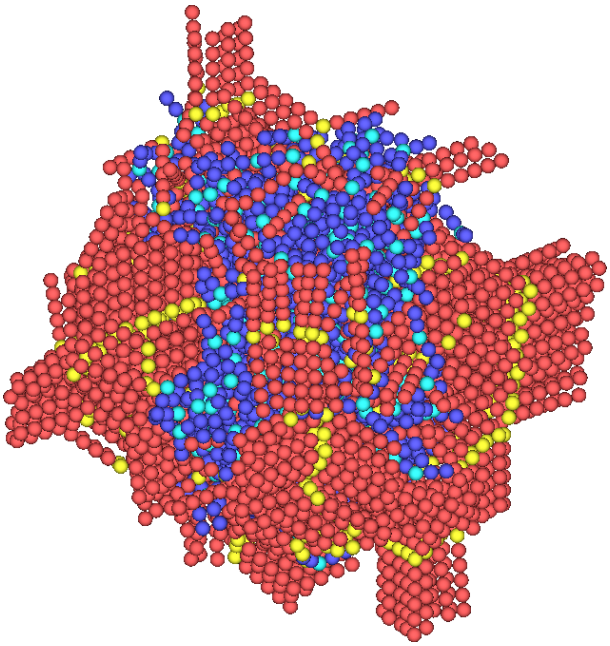

Figure 5.21: Snapshot at $P^* = 1.91$ from a compression run of 512 11-bead molecules (red-yellow) and 512 5-bead molecules (blue-cyan) with a bend angle of $\theta = 140°$.

5.3.2.3 $\theta = 130°$

The values for the order parameters Q^2_{00} and Q^2_{22} for binary mixtures of $\theta = 130°$, 11-bead and 5-bead molecules are much the same as for the $\theta = 140°$ molecules, and are shown in Fig. 5.22. This system also has a single obvious phase transition at $P^* \sim 1.6$ to short-range ordered clusters with no overall global alignment direction of the long axes.

The significantly higher final value of the Q^2_{00} order parameter for this system ($Q^2_{00} > 0.6$) relative to the $n_A = 11, n_B = 7, \theta = 130°$ systems in Sec. 5.3.1.3 ($Q^2_{00} < 0.4$) is due to the ease with which the two components separate. In the system containing 7-bead molecules, there are a significant number of 11-bead molecules that remain mixed with the shorter mesogens and bring the value of Q^2_{00} down. This is not the case in this system, where there are fewer "lone" molecules unattached to a cluster.

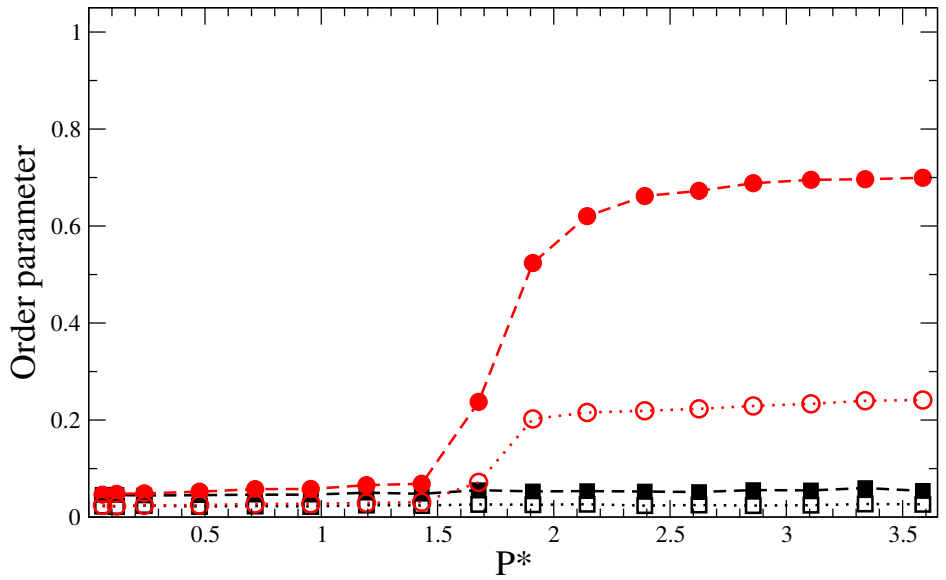

Figure 5.22: The uniaxial order parameter Q^2_{00} (solid symbols) and biaxial order parameter Q^2_{22} (hollow symbols) on compression, for a mixture of 512 11-bead molecules (red circles) and 512 5-bead molecules (black squares) with a common bend angle of $\theta = 130°$.

5.3.3 Summary

The complete set of Q_{00}^2 order parameters for all systems simulated in this section are presented in in Figs. 5.23 and 5.23 for the $n_A = 11, n_B = 7$ and $n_A = 11, n_B = 5$ binary mixtures respectively.

There are a number of interesting properties that can be observed from the results of these simulations. Firstly, the two components of the systems remain well-mixed on compression, in both the isotropic and the uniaxial nematic phases. When the isotropic–nematic transition occurs in the 11-bead molecules, the transition is induced simultaneously in the shorter molecules, despite occuring at a significantly lower pressure than in monocomponent systems. In addition, the uniaxial nematic phase is induced in systems that do not exhibit the phase at all in monocomponent simulations – specifically, we see this in our $n_A = 11, n_B = 7, \theta = 140^\circ$ and $n_A = 11, n_B = 5, \theta \geq 150^\circ$ simulations.

As the 11-bead molecules undergo a second transition from nematic to smectic, the two components of the system invariably demix. The shorter molecule then reverts to its typical phase behaviour as observed in monocomponent simulations. If the shorter molecule is able to maintain a uniaxial nematic phase by itself, then it remains aligned until its own independent nematic–smectic transition at a higher pressure (observed in the $n_A = 11, n_B = 7, \theta \geq 150^\circ$ simulations). If the shorter molecules lack a uniaxial nematic phase in monocomponent systems, but undergo a transition to a clustered phase (e.g. 7-bead molecules of $\theta \leq 140^\circ$), this transition is not observed and the shorter mesogens remain in the isotropic phase throughout.

The extra mobility added to the system by an isotropic phase of the shorter molecules assists significantly in the formation of well-organized smectic layers of the longer

molecules, rather than forming the half-offset smectic layers seen in monocomponent simulations of the 11-bead molecules. These offset layers remain for the $n_A = 11, n_B = 7, \theta \geq 150^\circ$ systems, where the nematic phase of the 7-bead molecules does not permit the same degree of movement. This extra freedom does not help with the lack of a global alignment director for systems of $\theta < 140^\circ$, 11-bead molecules, and the clustered phases with no global alignment director remain.

In terms of attempting to achieve a biaxial nematic phase, mixtures of two different lengths of molecule do not seem to help with the break-up of the smectic layering. The large difference in the monocomponent nematic–smectic transition pressures for molecules of two different sizes results in demixing when the first component transitions, and no "gaps" are opened up in the smectic layering as a result. In the next section, we will look at mixing together two molecules with different bend angles, which have much smaller differences in transition pressures and may experience improved mixing after the nematic–smectic transition.

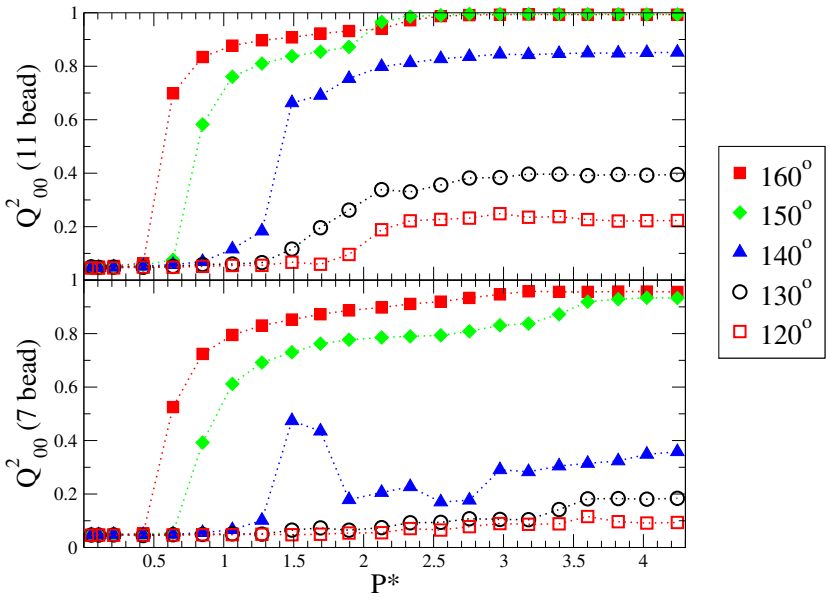

Figure 5.23: The change in the uniaxial order parameter Q^2_{00} with increasing pressure P^* for binary mixtures of 512 11-bead molecules (top) and 512 7-bead molecules (bottom). Legend values correspond to the mutual bend angle θ.

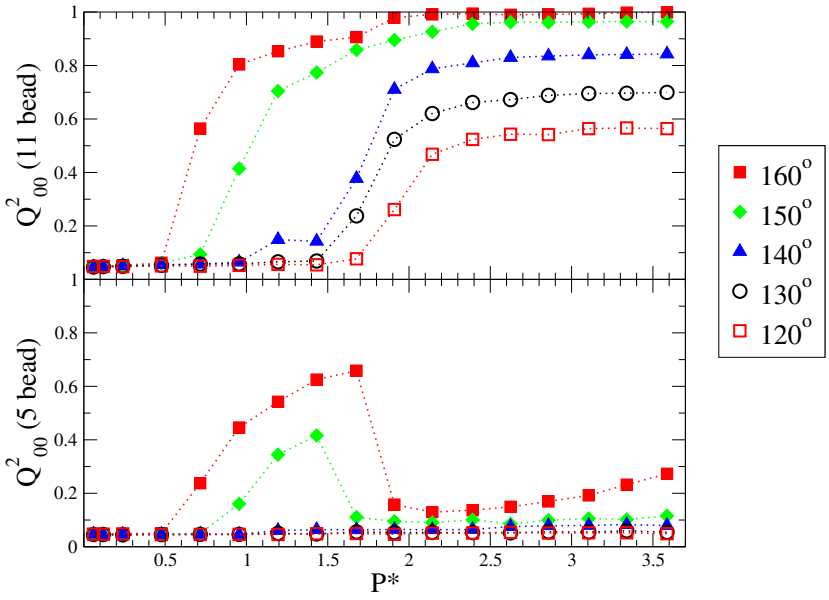

Figure 5.24: The change in the uniaxial order parameter Q^2_{00} with increasing pressure P^* for binary mixtures of 512 11-bead molecules (top) and 512 5-bead molecules (bottom). Legend values correspond to the mutual bend angle θ.

5.4 Mixtures of different bend angles

In this section, we present results for binary mixtures of molecules with different bend angles, θ_A and θ_B. The number of WCA potentials from which the molecules are constructed, n, will be fixed such that $n_A = n_B = 11$. The number of each type of molecule is fixed at $N_A = N_B = 512$ for all the simulations performed.

With the molecular size variation in Chapter 4, we were restricted to what we could simulate due to the increasing number of interacting potentials as the mesogen size is increased. The value of the molecular bend angle is a continuous variable and changing its value does not increase simulation complexity. Therefore the parameter space that can be sampled is effectively infinite. In Chapters 3 and 4 we restricted ourselves to bend angle steps of $5^\circ - 10^\circ$, but this also results in a large parameter space that is difficult to explore systematically.

In this section we present a number of results from an illustrative sampling of the available parameter space, in order to observe some of the characteristic of the interactions between mesogens with different bend angles.

5.4.1 Mixtures of $n = 11, \theta_A = 150^\circ, \theta_B = 130 - 145^\circ$

Compression runs were performed on a number of systems consisting of 1024 11-bead bent-core molecules, 512 with a bent angle of 150° and the remaining 512 with a bend angle of either 145°, 140° or 130°, depending on the system. These three values were chosen as to give a angle difference between the two components of 5°, 10° and 20° respectively. Pressure sweeps were performed at an initial barostat pressure of $P^* = 0.17$, and the pressure was increased in steps of $P^* \sim 0.17$.

The uniaxial order parameters Q_{00}^2 for the components of the three systems are shown in Fig. 5.25. All three plots show the signs of a pair of phase transitions. An isotropic–nematic transition occurs in the pressure window $0.52 < P^* < 0.69$ for the $\theta_B = 145°$ and $\theta_B = 140°$ systems, while the transition is slightly delayed to $0.69 < P^* < 0.87$ for the $\theta_B = 130°$ systems. A second transition then occurs at $1.21 < P^* < 1.39$, or $1.39 < P^* < 1.64$ for the $\theta_B = 130°$ systems, corresponding to the nematic–smectic transition.

For the $\theta_B = 145°$ and $140°$ mixtures, both these transition windows match the pressures at which phase transitions occur in $150°$ monocomponent systems, as shown in Table 3.1. As with the binary mixtures of different lengths in the previous section, the molecules with the higher monocomponent transition pressure (in this case, the narrower molecules) undergo the transitions simultaneously.

Unlike the systems where $n_A \neq n_B$, both components in the $\theta_B = 145°$ and $\theta_B = 140°$ simulations undergo a simultaneous nematic–smectic transition. Snapshots of these systems at $P^* = 1.56$ are given in Figs. 5.26a and 5.26b. These show that the systems remain well-mixed, and the offset smectic layers seen in the monocomponent systems return. While the difference in transition pressures between the two types of molecules is small enough to allow them to remain mixed and not phase separate, the change in bend angle is insufficient to prevent the appearance of the offset smectic layers.

The higher final values for the Q_{00}^2 order parameters compared to their monocomponent systems is due to a less pronounced "zig-zag" packing of the offset smectic layers (see Sec. 3.3.2). The two slightly different bend angles introduces a small amount of extra free space into the system in the smectic phase, and so the clusters are not forced into this configuration as strongly.

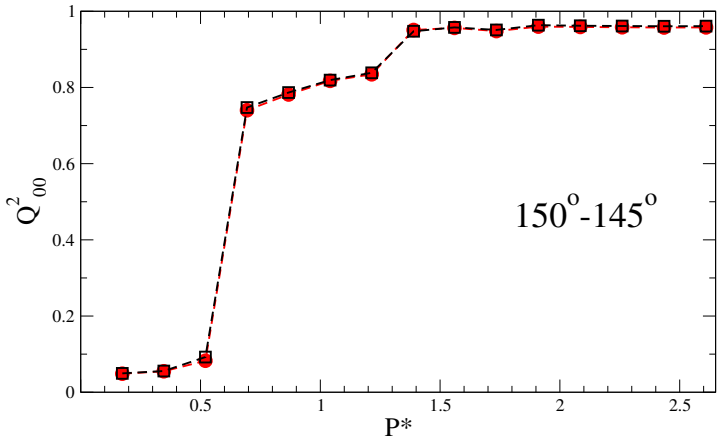

(a) $\theta_B = 145°$

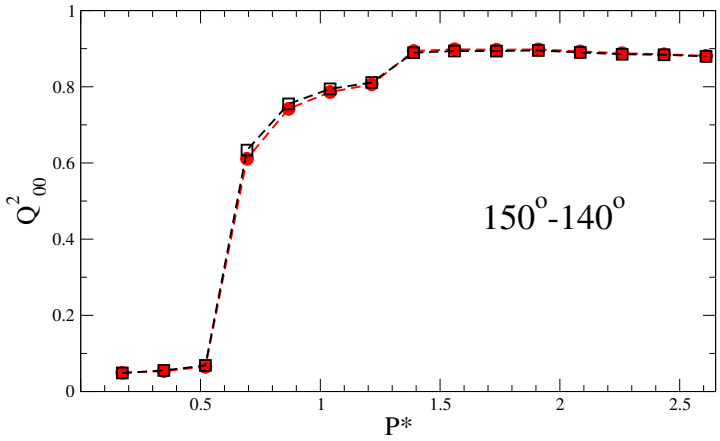

(b) $\theta_B = 140°$

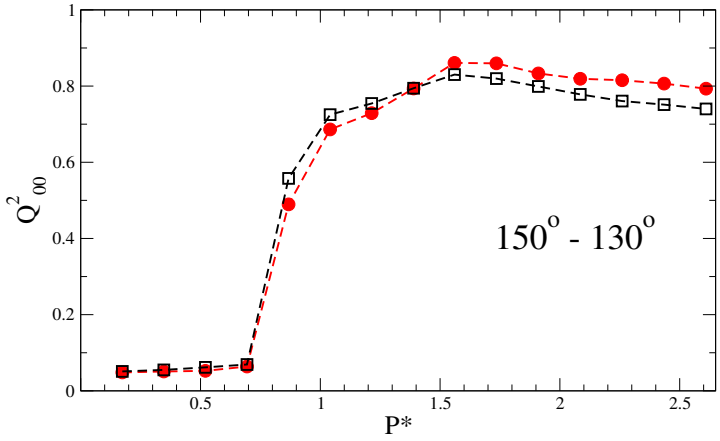

(c) $\theta_B = 130°$

Figure 5.25: The change in the uniaxial order parameter Q^2_{00} with increasing pressure P^* for binary mixtures of 11-bead molecules with different bend angles. The $\theta = 150°$ molecules are shown with red symbols, while the narrower molecules ($145°$, $140°$, $130°$) have black symbols in each plot.

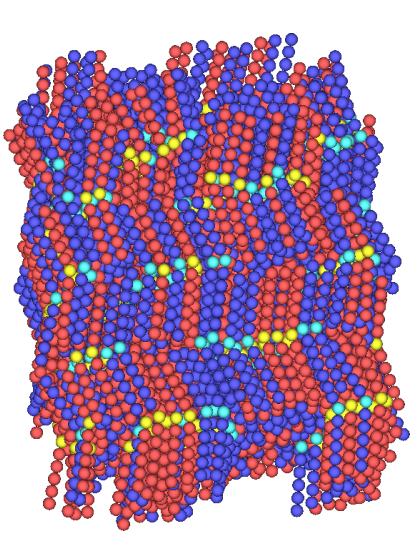

(a) $\theta_B = 145°$

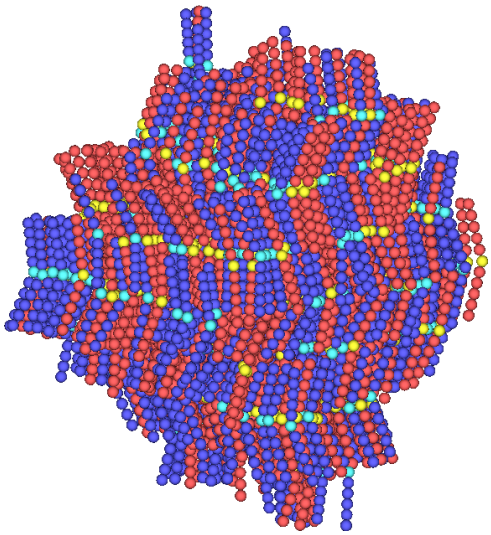

(b) $\theta_B = 140°$

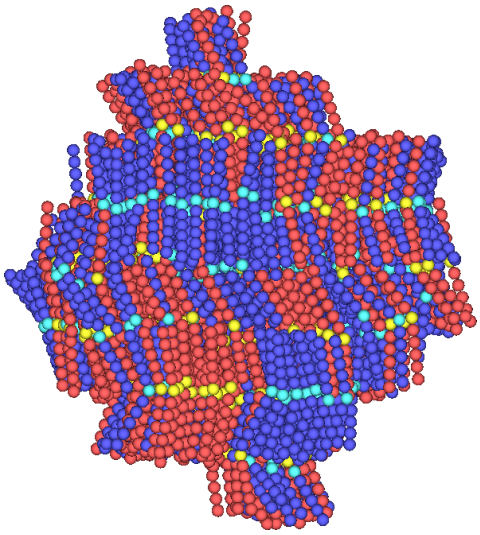

(c) $\theta_B = 130°$

Figure 5.26: Snapshots at $P^* = 1.56$ of binary mixtures of 512 11-bead $\theta_A = 150°$ molecules and (a) $\theta_B = 145°$, (b) $\theta_B = 140°$ and (c) $\theta_B = 130°$ molecules.

We now look at the results of the $\theta_B = 130°$ simulations. In a monocomponent system, 11-bead $130°$ molecules do not have a nematic phase, and the lack of a global director results in smectic-like clusters with no overall direction. We have also seen in Sec. 5.3.1.2 that if one component of a mixture undergoes a transition to a uniaxial nematic phase, it can induce the same phase in a mesogen which does not exhibit it in monocomponent simulations.

The Q^2_{00} order parameters for the $\theta_B = 130°$ simulations are shown in Fig. 5.26c. The presence of three distinct phases for both components shows that this induction of phases exists for mesogens with different bend angles too, with isotropic, nematic and smectic behaviour present for both components.

Unlike the results in Sec. 5.3.1.2, the $130°$ molecules do not return back to an isotropic state once the $150°$ molecules transition to a smectic phase. As monocomponent $130°$ molecules transition to a clustered phase at a similar pressure, they do not have the opportunity to "relax" back to isotropic and undergo their own transition. However, as they are already being held in nematic alignment, they also form an ordered smectic with offset layers. A snapshot of this system at $P^* = 1.56$, beyond this second transition, is shown in Fig. 5.26c. From the snapshot, we can also tell that the two components are not as well mixed as for the components separated by $10°$ and $5°$. There is a level of phase separation occuring, with significant numbers of similar-coloured central atoms clustering together.

5.4.2 Mixtures of $n = 11, \theta_A = 160°, \theta_B = 140°$

It is possible that the phase separation seen in the $\theta_A = 150°, \theta_B = 130°$ simulations is arising from two different causes. As well as there being a $20°$ difference

in the bend angles, the two mesogens in monocomponent systems exhibit different phase behaviour. Therefore, we also performed simulations on binary mixtures of $n = 11, \theta_A = 160°, \theta_B = 140°$. These two components also differ by $20°$, but both exhibit nematic and smectic behaviours in monocomponent simulations.

Compression runs were performed using 512 $\theta_A = 160°$ and 512 $\theta_B = 140°$ molecules from an initial pressure of $P^* = 0.17$ and a step size of 0.17. The uniaxial order parameters Q^2_{00} for each of the components are shown in Fig. 5.27, once again showing the expected three phases of isotropic, nematic and smectic phases. The transition windows are the same as those for the $\theta_A = 150°, \theta_B = 145°$ and $\theta_A = 150°$, $\theta_B = 140°$ systems in the previous section. The onset of nematic behaviour occurs at a slightly higher pressure than it occurs at in monocomponent $160°$ systems, $0.52 < P^* < 0.69$ compared to $P^* \sim 0.4$. The onset of smectic behaviour occurs in the pressure window $1.21 < P^* < 1.40$, which is below the onset of smectic behaviour for monocomponent $160°$ molecules but in line with the onset for $140°$ molecules. The nematic phase is therefore of some intermediate width between the two components.

A snapshot of the system at $P^* = 1.56$ in the smectic phase is presented in Fig. 5.28. As with the $\theta_A = 150°, \theta_B = 130°$ simulations, the formation of significant clusters of similar molecules indicates that the system is wanting to demix into two separate components, rather than remain in a fully mixed smectic phase.

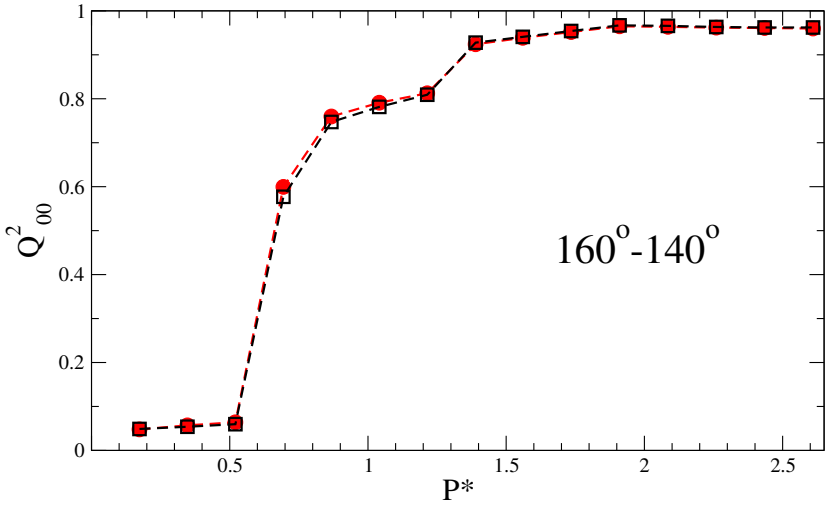

Figure 5.27: The change in the uniaxial order parameter Q^2_{00} with increasing pressure P^* for binary mixtures of 11-bead molecules. 512 molecules have a bend angle of $160°$ (red symbols), while another 512 have a bend angle of $140°$ (black symbols).

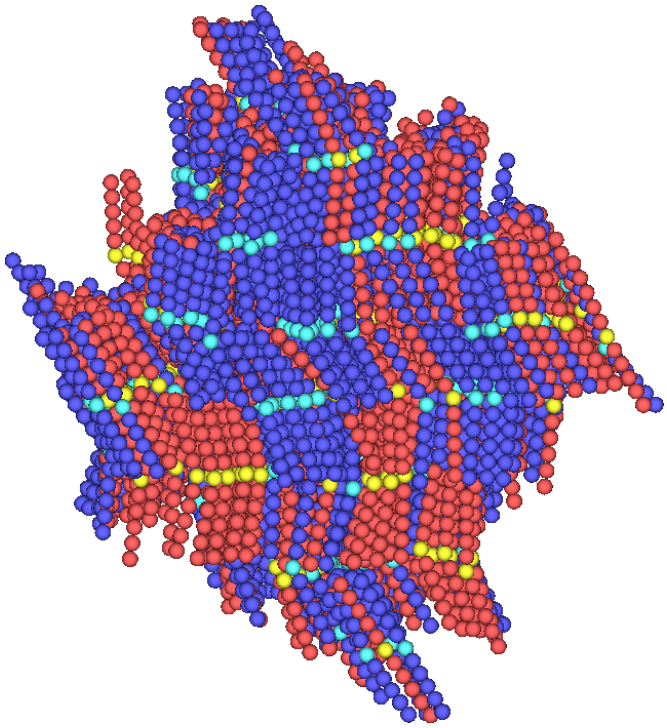

Figure 5.28: Snapshot at $P^* = 1.56$ from a compression run of a binary mixture of 512 11-bead $\theta_A = 160°$ molecules (red-yellow) and 512 11-bead $\theta_B = 140°$ molecules (blue-cyan).

5.4.3 Summary

In the previous section we examined the effects of mixing together two kinds of 11-bead molecules with a number of pairs of different bend angles. There are notable differences in the behavour of these systems compared to that of molecules with matching angles but different arm lengths.

Firstly, the phase separation of the two components is far less pronounced. For differences in bend angles of $5^\circ - 10^\circ$, both components remain well-mixed in the isotropic, uniaxial nematic and smectic phases. For differences of 20° phase separation begins to occur, although this is only observed as small groupings rather than complete demixing into two distinct regions rich in a single component. This was observed in both the $160^\circ - 140^\circ$ mixtures as well as the $150^\circ - 130^\circ$ mixtures.

As with the differing length molecules, the mixing of the two components can induce phase behaviour not seen in monocomponent systems. In the $150^\circ - 130^\circ$ mixtures, a uniaxial nematic is induced in the 130° component which is not seen in isolation. However, unlike the $n_A = 11, n_B = 7$ systems, the transition of the 150° molecules to the smectic-like phase does not lead to the 130° molecules returning to an isotropic phase. Instead, they too transition to the same smectic-like phase with offset layers. This is likely due to the proximity of the transitions of the two systems in isolation – by the time the 150° molecules have transitioned from a nematic to a smectic, the 130° molecules have also reached the pressure at which they undergo a transition. By being mixed with the 150° molecules and held in a uniaxial nematic phase, they already have a global director when they form their clustered phase, and can therefore transition to a smectic phase with long axis alignment.

Secondly, the effect of different bend angles seems to have little effect on the phase

behaviour. In all instances, the same offset smectic-like layering is observed as the final phase behaviour and the transition pressures are not significantly different from those observed for the wider molecules in monocomponent systems. As the difference between the two bend angles is increased, the transition from nematic to smectic is not as sudden, but the molecules also appear to preferentially demix. This is true for both the $150^\circ - 130^\circ$ and the $160^\circ - 140^\circ$ systems. The threshold of compatibility between the two bend angles is seemingly between $10^\circ - 20^\circ$, at least for the bend angle mixtures studied.

5.5 Conclusions

We have examined the effects on the liquid crystal phase behaviour of bent-core mesogen systems when two distinct components are present, either with the same bend angle and different molecular sizes, or with two equally sized molecules that have different bend angles.

For the systems of molecules of different sizes, the components remain well mixed in both the isotropic and uniaxial nematic phases. Mesogens that do not have a nematic phase in isolation exhibit one when mixed with a component that does. However, at the point where the first nematic–smectic transition occurs for either of the components, the two systems are seen to completely demix. As the longer molecules transition to a smectic phase, the extra mobility afforded to the system by the shorter molecules allows the smectic layers to rearrange and reorganize better, and the half-offset layering is reduced for the $\theta = 160^\circ$ systems, and absent for the $\theta = 140^\circ$ systems of $n_A = 11, n_B = 7$ molecules.

In cases where the shorter molecule would normally transition to a clustered phase with no uniaxial alignment, the separation of the components reduces the amount of space available and the clustering is supressed, with the shorter component remaining in the isotropic phase. This is seen for all of the $n_A = 11, n_B = 5$ systems, as well as the narrower bend angles for the $n_B = 7$ systems. The "clustering" behaviour is not supressed for the first molecule to transition, as seen in the $\theta = 130^\circ, n_A = 11, n_B = 7$ simulations.

The mixtures of two differently sizes molecues do not assist us in our attempts to find a biaxial nematic phase. The longer molecule still transitions to a smectic phase, and the shorter components preferentially demix rather than stay combined and produce

"gaps" in the layering. However, they do assist with the formation of better smectic layering. It would be interesting to study a variety of component ratios other than $50 : 50$ to see if the formation of better smectic layers can be improved with an increased number of small molecules. It would also be interesting to see whether the supression of the clustered behaviour of the short molecules ceases as their quantity increases.

Mixtures of molecules with the same size but differing bend angles show much greater success in remaining mixed through the isotropic, nematic and smectic phases. For bend angles of $5^\circ - 10^\circ$ similar phase behaviour is observed as it would be by the wider molecule in isolation. However, improved mixing is likely due to the fact that the molecules are not sufficiently different to significantly alter the resulting phase behaviour. As the bend angle difference is increased to 20°, the two components begin to separate. Therefore, there is likely a degree of tolerance for different bend angles while not affecting the phase behaviour or level of mixing.

In order to pursue this further, it would be very interesting to explore polydisperse systems with a wide range of bend angles, varying continuously with no jumps greater than 10°. Through having no large differences in bend angles, it may be possible to keep multiple repulsive molecules with very different angles mixed together, while incompatibility in their bend angles would open up spaces in the smectic layering.

Chapter 6

Conclusions

In this thesis we have comprehensively explored the liquid crystal phase behaviour that can be attained using a simple model of a bent-core mesogen, with a goal of generating a biaxial nematic. Our mesogenic model was constructed from a number of repulsive Weeks-Chander-Andersen potentials, arranged in a V-shape along two molecular "arms". The potentials were placed such that their centers were a distance σ apart and formed a bend angle of θ between the two arms, with 180° defining a straight rod. We studied the phase behaviour of systems of the molecules with a wide range of both internal bend angles and relative arm lengths. In addition, we investigated the effects of binary mixtures of molecules with either different bend angles or different arm lengths. All of our simulations were conducted by compressing initially isotropic systems using molecular dynamics simulation techniques.

In Chapter 3, we initially examined the phase behaviour of systems of bent-core mesogens constructed from 11 potentials at a wide variety of bend angles. We found that there were two distinct regions of phase behaviour, above and below a critical angle that lies in the range $130^\circ < \theta < 140^\circ$. For molecules with an internal bend angle

greater than this, isotropic, uniaxial nematic and smectic-like phases are seen as the systems are compressed, with a strong degree of polarization of the short axes of the molecules in the smectic phases. For smaller systems of 512 molecules, offset smectic layers were seen, where the "upper" arms of the molecules of one layer aligned with the "lower" arms of another layer. By reducing the pressure step size and increasing the number of molecules to 4096, these offset layers diappear and smectic A phases are generated. It is likely that these offset layers pay a relatively small free energy price, and the level of layer dislocations increases as the internal bend angles of the molecules become narrower.

For bend angles of $\theta \leq 130^\circ$, no global uniaxial alignment director was seen, and the systems preferentially formed small clusters with strong levels of alignment along both their long and short axes. Increasing the system size to 4096 molecules and reducing the size of the pressure steps did not help resolve any different phases. Upon attempting to melt the resulting configurations, a number of these clusters rotated to mutually align their long axes and form larger, smectic-like groupings. However, the systems transitioned back to an isotropic phase before a complete smectic phase could be seen.

Overall, these results match well with the phase diagram obtained by Lansac *et al.* [71] for hard spherocylinder dimers with L/D ratios of 5, in that there is no uniaxial nematic phase for systems with bend angles of $\theta < 135^\circ$. However, we do not see a clear isotropic–smectic transition for molecules narrower than this. It appears repeated decompression and recompression is required to generate a well-ordered smectic. Our simulations suggest that this isotropic–smectic phase cannot be found directly on compression.

We then extended our model in Chapter 4 to include the effects of changing the lengths

of the arms of our mesogenic model. We studied a similar range of bend angles as with our 11-bead simulations, but varied the number of beads from which the molecules were constructed to include 9-, 7- and 5-bead variants. As the size of the molecule was reduced to 9- and then to 7-bead models, the pressures required to induce uniaxial nematic phases increased dramatically. For molecules closer to 180°, the width of the uniaxial nematic phase broadened and the organization of the smectic phase into distinct layers was improved. No mesophases were seen at all for molecules consisting of 5 beads, regardless of bend angle. This fits with the observations made by Galindo *et al.* [95] on linear rods constructed of five Lennard-Jones potentials. As the size of the molecules was reduced, the angle at which the uniaxial nematic phase disappears was also seen to change, with the 7-bead molecules experiencing a loss of the phase in the $140^\circ < \theta < 150^\circ$ angle window.

In Chapter 5, we investigated the phase behaviour of binary mixtures of our bent-core mesogenic models. Our mixtures consisted of mesogens of either differing bend angles or differing molecule sizes. For molecules of different arm lengths but the same bend angle, we observed that the two components of a system will remain well mixed in the isotropic and uniaxial nematic phases. In addition, the longer molecule will induce a uniaxial nematic phase in the shorter molecule at a lower pressure than it would in isolation. The longer molecules can also induce nematic phases in molecules that would not experience them at all in monocomponent systems. As the pressure is increased further, the longer molecules transition to a smectic phase and the two components comprehensively demix.

If the shorter molecules are able to maintain a uniaxial nematic phase by themselves at this pressure, they too will undergo their own nematic–smectic phase transition. Otherwise the shorter molecules revert to an isotropic state and experience no further

mesophases. Instead they act as a liquid, allowing the longer molecules to move more freely and form more well-organized smectic layers. The extra fluiditiy does not help the formation of well-aligned smectic layers for 11-bead molecules of $\theta = 140°$, and the clustered behaviour with no overall global alignment director remains.

For binary mixtures of molecules with different bend angles, the mixing of the two types of mesogens is substantially improved for molecules with differences of up to $10°$, although no significantly different phase characteristics are seen. At bend angle differences of $20°$ for the 11-bead molecules, the two components begin to demix at the nematic–smectic phase transition.

6.1 Discussion and future work

We have successfully examined and characterized a large parameter space for repulsive bent-core mesogens under compression using molecular dynamics simulations. To our knowledge, we have also performed the first ever simulations of binary mixtures of bent-core molecules. Through this, we discovered intruiging phase behaviour that is very strongly linked to both the molecule size and the bend angle of the two individual components.

In addition to this, we have validated our model against previous Monte-Carlo based research. Therefore we are confident it can be used as a starting point for future molecular dynamics simulations exploring the kinetics of the phase behaviours and the mechanisms of the phase transitions.

Despite exploring a wide region of the available parameter space, our simulations did not reveal the presence of a biaxial nematic phase. This may be due to the difficulty in

maintaining the uniaxial nematic towards the 110° region, where the biaxial nematic phase has been predicted to exist by Tiexeira *et al.* [69] and Luckhurst [22]. In the hunt for the bent-core biaxial nematic, there are a number of potential avenues which would be interesting to explore in future research:

1. The theoretical predictions of the biaxial nematic at 110° are for $L >> D$, and our results have shown that the angle at which the uniaxial nematic phase is lost varies relatively slowly with molecule size. As such, it appears that much longer molecules would be needed to approach this angle. Simulation using sufficiently large quantities of linked spherical potentials are currently computationally infeasible. It may be possible to simulate very long molecules by reverting to spherocylinder dimer mesogens, and event-driven molecular dynamics may prove useful in this regard. However, such simulations would still require a huge number of molecules to sufficiently fill the space of the simulation cell, making the systems slow to run and leading to long equilibration times.

2. The lack of demixing in bent-core binary systems with bend angle differences of $5^\circ - 10^\circ$ may also prove fruitful. In a more polydisperse system, a entire continuum of different bend angles may help keep narrower molecules in a uniaxial nematic phase. If this can be done to induce nematic phases in molecules as narrow as 110° and beyond, very different phase behaviour may be seen, including plate-like nematics and the biaxial nematic. Larger systems would be required in order to simulate a sufficiently large spread of bend angles, but not vastly different from those conducted in previous chapters.

3. Given our comprehensive search of the available parameter space, it is conciev-able that the mesogenic model itself lacks the minimum characteristics needed for the formation of a biaxial nematic. The recent work by Jócefowicz and Longa [75] suggests a small degree of flexibility in the central bend angle may help in the formation of a biaxial nematic using bent-core molecules with a bend angle of $\approx 140^{\circ}$. By adding a small degree of flexibility to the core or even the arms of our mesogenic model, we may be able to delay the onset of smectic behaviour and obtain new phases – potentially including the biaxial nematic.

Final thought

With available computing resources growing exponentially year-on-year, there are always opportunities to simulate more and more complex systems of liquid crystals, including fully atomistic models. However, the ability to simulate increasingly large bulk systems of simplified mesogenic shapes will always be important in determining the essential ingredients needed for the formation of thermotropic liquid crystal phases.

Appendix A

Theoretical isotropic compressibility of soft-potential polymers

A.1 Derivation

The compressibility of a system of hard spheres is given as

$$Z = \frac{\beta P}{\rho} = 1 + \tfrac{2}{3}\pi\rho\sigma^3 g(\sigma) \tag{A.1}$$

where β is the thermodynamic value $1/kT$, P is the pressure, ρ is the number density, σ is the diameter of the sphere and $g(\sigma)$ is the pair correlation function at the point of contact [112]. Additionally, the modified Carnahan-Starling equation of state for spherical WCA potentials is given as

$$Z = \frac{1 + \eta + a\eta^2 - b\eta^3}{(1-\eta)^3} \tag{A.2}$$

where $\eta = \pi\rho\sigma^3/\,6$ is the packing fraction of the spheres, and a and b are the fitting constants $a = 3.597 \pm 0.087$ and $b = 5.84 \pm 0.18$ [64]. WCA spheres also have an an "effective hard-sphere diameter" based on the temperature of the system, which is given as

$$\sigma_{\text{eff}} = \frac{2^{1/6}}{(1+\sqrt{T})^{1/6}}. \tag{A.3}$$

If a polymer is constructed out of WCA potentials separated by σ_{eff} for the relevant temperature, we make the assumption that the point-of-contact pair correlation function is also valid for them, despite being soft.

By equating, $g(\sigma_{\text{eff}})$ can be approximated as

$$\begin{aligned} g(\sigma_{\text{eff}}) &= (Z-1)\,\frac{3}{2\pi\rho\sigma_{\text{eff}}^3} \\ &= \frac{4\eta + (a-3)\eta^2 + (1-b)\eta^3}{(1-\eta)^3} \cdot \frac{3}{2\pi\rho\sigma_{\text{eff}}^3} \\ &= \frac{4 + (a-3)\eta + (1-b)\eta^2}{4(1-\eta)^3}. \end{aligned} \tag{A.4}$$

From the SAFT theory of associating fluids [65], we know that the contribution to the Helmholtz free energy of a system from the association of spherical potentials into chains is given to a good approximation by

$$\beta A_{\text{chain}} = -N(m-1)\ln g(\sigma) \tag{A.5}$$

where N is the number of molecules and m is the number of potentials per molecule.

Taking the partial derivative with respect to volume gives

$$\begin{aligned}
\beta P_{\text{chain}} &= -\frac{\partial}{\partial V}\left[\beta A_{\text{chain}}\right] \\
&= -\frac{\partial \eta}{\partial V}\cdot\frac{\partial}{\partial \eta}\left[\beta A_{\text{chain}}\right] \\
&= \frac{\eta}{V}\cdot\left[-N(m-1)\frac{\partial}{\partial \eta}\ln g(\sigma)\right] \\
&= \frac{-N(m-1)\eta}{V}\cdot\frac{\partial}{\partial \eta}\left[\ln\left(\frac{4+(a-3)\eta+(1-b)\eta^2}{4(1-\eta)^3}\right)\right] \\
&= \frac{-N(m-1)\eta}{V}\left[\frac{a-3+2\eta(1-b}{4+(a-3)\eta+(1-b)\eta^2}+\frac{3}{1-\eta}\right].
\end{aligned} \tag{A.6}$$

Finally, using Wertheim pertubation theory [66], we can express the compressibility for the whole system as a sum of contributions from an ideal term, an excess contribution from the monomers, and the chain contribution

$$\begin{aligned}
\beta P &= \rho + \beta P_{\text{monomers}} + \beta P_{\text{chain}} \\
&= \rho + \beta(Z-1)\rho_{\text{monomers}} + \beta P_{\text{chain}} \\
&= \frac{N}{V} + \frac{Nm}{V}\left[\frac{4\eta+(a-3)\eta^2+(1-b)\eta^3}{(1-\eta)^3}\right] + \beta P_{\text{chain}}
\end{aligned} \tag{A.7}$$

where ρ_{monomers} is the number density of monomers and ρ is the number density of polymers, such that $\rho = \rho_{\text{monomers}}/m$. Finally,

$$\begin{aligned}
Z = 1 &+ m\left[\frac{4\eta+(a-3)\eta^2+(1-b)\eta^3}{(1-\eta)^3}\right] \\
&- (m-1)\eta\left[\frac{a-3+2\eta(1-b)}{4+(a-3)\eta+(1-b)\eta^2}+\frac{3}{1-\eta}\right]
\end{aligned} \tag{A.8}$$

A.2 Choice of fitting parameters a and b

In order to determine the most appropriate values for the fitting parameters a and b, Eqn. (A.8) was plotted against a selection of simulation data from Chapter 3. The hard-sphere values $a = 1, b = 1$ and the WCA values $a = 3.60, b = 5.84$ were tested, as well as the Carnahan-Starling equation for a fluid of hard sphere monomers. An example of these three curves is given in Fig. A.1, fitted to data obtained from a simulation run of 4096 11-bead bent-core molecules with an internal bend angle of $140°$.

From validating against multiple simulation runs, we found that the hard sphere values of $a = 1$ and $b = 1$ gave a very good fit, while the WCA fitting parameters $a = 3.60$ and $b = 5.84$ from Ref. [64] tend to slightly underestimate the isotropic liquid density. Meanwhile, the curve obtained for a simple Carnahan-Starling hard sphere monomer fluid severely underestimates the isotropic liquid densities. Therefore, we selected the fitting parameters of $a = 1$ and $b = 1$ for all of our bent-core mesogen analysis.

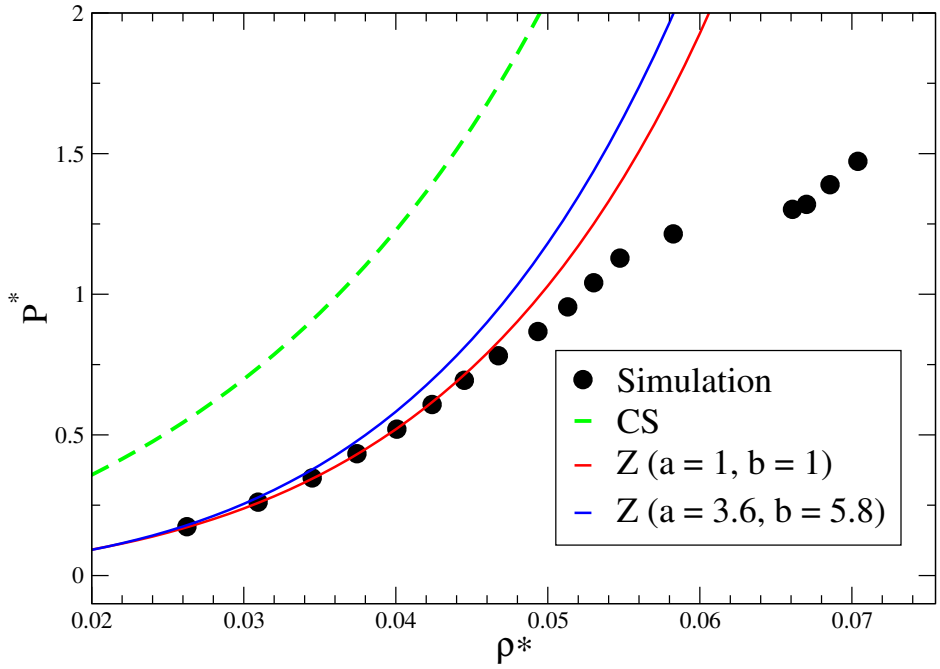

Figure A.1: The equation of state for 4096 11-bead bent-core molecules with a bend angle of 140° (black circles), fitted to three choices of theoretical liquid density curve. The Carnahan-Starling equation of state is shown in green, while the hard sphere and WCA fitting parameters for Eqn. (A.8) are shown in red and blue respectively.

Bibliography

[1] F. Reinitzer, Monatshefte für Chemie **9**, 421 (1888).

[2] D. Dunmur and T. Sluckin, *Soap, Science, and Flat-Screen TVs* (Oxford University Press, Oxford, UK, 2010).

[3] G. Friedel, Annales de Physique **18**, 273 (1922).

[4] P. de Gennes and J. Prost, *The Physics of Liquid Crystals*, 2 ed. (Oxford University Press, Oxford, UK, 1993).

[5] P. D. Duncan, M. Dennison, A. J. Masters, and M. R. Wilson, Physical Review E **79**, 031702 (2009).

[6] S. Hussan, W. Rowe, and G. J. T. Tiddy, in *Handbook of Applied Surface and Colloid Chemistry* (John Wiley & Sons, Chichester, UK, 2001), Chap. 21.

[7] D. Fazio *et al.*, Journal of Materials Chemistry **11**, 2852 (2001).

[8] G. W. Gray and S. M. Kelly, Journal of Materials Chemistry **9**, 2037 (1999).

[9] S. Singh and D. Dunmur, *Liquid Crystals Fundamentals* (World Scientific, Singapore, 2002).

[10] D. Lundstrom and J. Yilbar, Experimental Material Physics: Liquid Crystal Materials, Lecture notes from the KTH Royal Institute of Technology, 1998.

[11] M. J. Freiser, Physical Review Letters **24**, 1041 (1970).

[12] C. Tschierske and D. J. Photinos, Journal of Materials Chemistry **20**, 4263 (2010).

[13] G. Luckhurst, Nature **430**, 413 (2004).

[14] R. Berardi, L. Muccioli, and C. Zannoni, Journal of Chemical Physics **128**, 024905 (2008).

[15] L. J. Yu and A. Saupe, Physical Review Letters **45**, 1000 (1980).

[16] J. Malthete, H. T. Nguyen, and A. M. Levelut, Journal of the Chemical Society, Chemical Communications **20**, 1548 (1986).

[17] S. Chandrasekhar, B. R. Ratna, B. K. Sadashiva, and V. N. Raja, Molecular Crystals and Liquid Crystals **165**, 123 (1988).

[18] K. Praefcke *et al.*, Liquid Crystals **7**, 589 (1990).

[19] F. P. Nicoletta, G. Chidichimo, A. Golemme, and N. Picci, Liquid Crystals **10**, 665 (1991).

[20] S. M. Fan *et al.*, Chemical Physics Letters **204**, 517 (1993).

[21] J. R. Hughes *et al.*, Journal of Chemical Physics **107**, 9252 (1997).

[22] G. R. Luckhurst, Thin Solid Films **393**, 40 (2001).

[23] G. R. Luckhurst, Angewandte Chemie International Edition **44**, 2834 (2005).

[24] L. A. Madsen, T. J. Dingemans, M. Nakata, and E. T. Samulski, Physical Review Letters **92**, 145505 (2004).

[25] H. Takezoe and Y. Takanishi, Japanese Journal of Applied Physics **45**, 597 (2006).

[26] Y. Mastsunaga and S. Miyamoto, Molecular Crystals and Liquid Crystals **237**, 311 (1993).

[27] T. Akutagawa, Y. Matsunaga, and K. Yasuhara, Liquid Crystals **17**, 659 (1994).

[28] T. Niori *et al.*, Journal of Materials Chemistry **6**, 1231 (1996).

[29] G. Pelzl, S. Diele, and W. Weissflog, Advanced Materials **11**, 707 (1999).

[30] M. B. Ros, J. L. Serrano, M. R. de la Fuente, and C. L. Folcia, Journal of Materials Chemistry **15**, 5093 (2005).

[31] J. Etxebarria and M. B. Ros, Journal of Material Chemistry **18**, 2919 (2008).

[32] R. A. Reddy and C. Tschierske, Journal of Materials Chemistry **16**, 907 (2006).

[33] N. Metropolis *et al.*, Journal of Chemical Physics **21**, 1087 (1953).

[34] M. N. Rosenbluth and A. W. Rosenbluth, Journal of Chemical Physics **22**, 881 (1954).

[35] B. J. Alder and T. E. Wainwright, Journal of Chemical Physics **31**, 459 (1959).

[36] B. J. Alder and T. E. Wainwright, Journal of Chemical Physics **27**, 1208 (1957).

[37] W. W. Wood and J. D. Jacobson, Journal of Chemical Physics **27**, 1207 (1957).

[38] D. Frenkel and B. Smit, *Understanding Molecular Simulation* (Academic Press, London, UK, 1996).

[39] M. P. Allen and D. J. Tildesley, *Computer Simulation of Liquids* (Oxford University Press, Oxford, UK, 1990).

[40] L. Verlet, Physical Review **159**, 98 (1967).

[41] G. Dahlquist and A. Bjork, *Numerical methods* (Prentice-Hall, New Jersey, USA, 1974).

[42] R. P. Feynman, R. B. Leighton, and M. Sands, *The Feynman Lectures on Physics, Volume 1* (Addison-Wesley, Boston, USA, 1963).

[43] W. C. Swope, H. C. Andersen, P. H. Berens, and K. R. Wilson, Journal of Chemical Physics **76**, 637 (1982).

[44] H. Goldstein, *Classical mechanics* (Addison-Wesley, Massachusetts, USA, 1980).

[45] M. P. Allen, Liquid Crystals **8**, 499 (1990).

[46] D. Fincham and B. J. Ralston, Journal of Chemical Physics **84**, 4535 (1986).

[47] T. F. Miller *et al.*, Journal of Chemical Physics **116**, 8649 (2002).

[48] J. P. Ryckaert, G. ciccotti, and H. J. C. Berendsen, Journal of Computational Physics **23**, 327 (1976).

[49] H. C. Andersen, Journal of Computational Physics **52**, 24 (1983).

[50] H. J. C. Berendsen *et al.*, Journal of Chemical Physics **81**, 3684 (1984).

[51] D. J. Evans and O. P. Morriss, Computer Physics Reports **1**, 297 (1983).

[52] S. Nose, Journal of Chemical Physics **81**, 511 (1984).

[53] W. G. Hoover, Physical Review A **31**, 1695 (1984).

[54] S. Melchionna, G. Ciccotti, and B. L. Holian, Molecular Physics **78**, 533 (1993).

[55] W. Smith, T. R. Forester, and I. T. Todorov, *The DL_POLY_2 User Manual* (STFC Daresbury Laboratory, Warrington, UK, 2009).

[56] M. N. Bannerman, L. Lue, and L. V. Woodcock, Journal of Chemical Physics **132**, 084507 (2010).

[57] B. D. Lubachevsky, Journal of Computational Physics **94**, 255 (1991).

[58] M. Marin, D. Risso, and P. Cordero, Journal of Computational Physics **109**, 306 (1993).

[59] M. Marechal, A. Cuetos, B. Martinez-Haya, and M. Dijkstra, Journal of Chemical Physics **134**, 094501 (2011).

[60] J. M. Haile, *Molecular Dynamics Simulations* (John Wiley & Sons, New York, USA, 1997).

[61] M. J. Mandell, Journal of Statistical Physics **15**, 299 (1976).

[62] S. C. McGrother, D. C. Williamson, and G. Jackson, Journal of Chemical Physics **104**, 6755 (1996).

[63] N. F. Carnahan and K. E. Starling, Journal of Chemical Physics **51**, 635 (1969).

[64] D. M. Heyes and H. Okumura, Journal of Chemical Physics **124**, 164507 (2006).

[65] W. G. Chapman, K. E. Gubbins, G. Jackson, and M. Radosz, Fluid Phase Equilibria **52**, 31 (1989).

[66] M. S. Wertheim, Journal of Chemical Physics **87**, 7323 (1987).

[67] P. J. Camp, M. P. Allen, and A. J. Masters, Journal of Chemical Physics **111**, 9871 (1999).

[68] A. T. Gabriel, T. Meyer, and G. Germano, Journal of Chemical Theory and Computation **4**, 468 (2008).

[69] P. I. C. Teixeira, A. J. Masters, and B. M. Mulder, Molecular Crystals and Liquid Crystals **323**, 167 (1998).

[70] G. R. Luckhurst, C. Zannoni, P. L. Nordio, and U. Segre, Molecular Physics **30**, 1345 (1975).

[71] Y. Lansac, P. K. Matil, N. A. Clark, and M. A. Glaser, Physical Review E **67**, 011703 (2003).

[72] R. Memmer, Liquid Crystals **29**, 483 (2002).

[73] S. J. Johnston, R. J. Low, and M. P. Neal, Physical Review E **65**, 051706 (2002).

[74] W. Jozefowicz and L. Longa, Molecular Crystals and Liquid Crystals **478**, 871 (2007).

[75] W. Jozefowicz and L. Longa, Molecular Crystals and Liquid Crystals **545**, 1428 (2011).

[76] G. V. Paolini, G. Ciccotti, and M. Ferrario, Molecular Physics **80**, 297 (1993).

[77] A. Dewar and P. J. Camp, Physical Review E **70**, 011704 (2004).

[78] J. Pelaez and M. R. Wilson, Physical Review Letters **97**, 267801 (2006).

[79] B. R. Acharya, A. Primak, and S. Kumar, Physical Review Letters **92**, 145506 (2004).

[80] J. D. Weeks, D. Chandler, and H. C. Andersen, Journal of Chemical Physics **54**, 5237 (1971).

[81] D. Ben-Amotz and D. R. Herschbach, Journal of Physical Chemistry **94**, 1038 (1990).

[82] W. Smith and T. R. Forester, Journal of Molecular Graphics **14**, 136 (1996).

[83] L. Onsager, Annals of the New York Academy of Sciences **51**, 575 (1949).

[84] J. Vieillard-Baron, Molecular Physics **28**, 809 (1974).

[85] M. A. Cotter and D. E. Martire, Journal of Chemical Physics **52**, 1909 (1970).

[86] A. Stroobants, H. N. W. Lekkerkerker, and D. Frenkel, Physical Review A **36**, 2929 (1987).

[87] J. A. C. Veerman and D. Frenkel, Physical Review A **41**, 3237 (1990).

[88] P. Bolhuis and D. Frenkel, Journal of Chemical Physics **106**, 666 (1997).

[89] E. de Miguel, L. F. Rull, M. K. Chalam, and K. E. Gubbins, Molecular Physics **74**, 405 (1991).

[90] E. de Miguel, Molecular Physics **15**, 2449 (2002).

[91] E. de Miguel and C. Vega, Journal of Chemical Physics **117**, 6313 (2002).

[92] J. T. Brown, M. P. Allen, E. M. del Rio, and E. de Miguel, Physical Review E **57**, 6685 (1998).

[93] C. Vega, C. McBride, and L. G. MacDowell, Journal of Chemical Physics **115**, 4203 (2001).

[94] A. Perera and F. Sokolic, Molecular Physics **88**, 543 (1996).

[95] A. Galindo *et al.*, Journal of Chemical Physics **120**, 3957 (2004).

[96] G. Cinacchi, L. de Gaetani, and A. Tani, Physical Review E **71**, 031703 (2005).

[97] R. Alben, Journal of Chemical Physics **59**, 4299 (1973).

[98] Y. Rabin, W. E. McMullen, and W. M. Gelbart, Molecular Crystals and Liquid Crystals **89**, 67 (1982).

[99] A. Stroobants and H. N. W. Lekkerkerker, Journal of Physical Chemistry **88**, 3669 (1984).

[100] P. Palffy-Muhoray, J. R. de Bruyn, and D. A. Dunmur, Journal of Chemical Physics **82**, 5294 (1985).

[101] R. Hashim, G. R. Luckhurst, F. Prata, and S. Romano, Liquid Crystals **15**, 283 (1993).

[102] A. G. Vanakaras, A. F. Terzis, and D. J. Photinos, Molecular Crystals and Liquid Crystals **362**, 67 (2001).

[103] A. Cuetos, A. Galindo, and G. Jackson, Physical Review Letters **101**, 237802 (2008).

[104] J. J. Hunt *et al.*, Journal of the American Chemical Society **123**, 10115 (2001).

[105] A. Stroobants, Physical Review Letters **69**, 2388 (1992).

[106] A. Stroobants, Condensed Matter **6**, A285 (1994).

[107] R. van Roij and B. Mulder, Physical Review E **54**, 6430 (1996).

[108] G. Cinacchi, L. Mederos, and E. Velasco, Journal of Chemical Physics **121**, 3854 (2004).

[109] A. G. Vanakaras, M. A. Bates, and D. J. Photinos, Physical Chemistry Chemical Physics **5**, 3700 (2003).

[110] E. van den Pol *et al.*, Liquid Crystals **37**, 641 (2010).

[111] S. Belli, A. Patti, M. Dijkstra, and R. van Roij, Physical Review Letters **107**, 148303 (2011).

[112] J. P. Hansen and I. R. McDonald, *Theory of Simple Liquids* (Accademic Press, Massachusetts, USA, 2006).